BREAKING IN: MECHANISMS OF HUMAN METAPNEUMOVIRUS FUSION AND ENTRY

By

Reagan Josephine Greene Cox

Dissertation

Submitted to the Faculty of the

Graduate School of Vanderbilt University

in partial fulfillment of the requirements

for the degree of

DOCTOR OF PHILOSOPHY

in

Microbiology and Immunology

December, 2012

Nashville, Tennessee

Approved:

Christopher Aiken

Borden Lacy

Earl Ruley

Roy Zent

John Williams

To the man who holds my hand and my heart,
my beloved husband, David.

ACKNOWLEDGEMENTS

This work was financially supported by Public Health Service grants AI-56170, AI-73697, AI-85062, and T32 AI-7611 from the National Institute of Allergy and Infectious Diseases, and T32 CA-9682 from the National Cancer Institute. Additional support was provided by the Elizabeth B. Lamb Center for Pediatric Research, a P.E.O. Scholar award from the Philanthropic Educational Organization, and Vanderbilt CTSA grant UL1 RR-24975-01 from NCRR/NIH. The Vanderbilt Medical Center Flow Cytometry Shared Resource is supported by the Vanderbilt Ingram Cancer Center (NIH P30 CA-68485) and the Vanderbilt Digestive Disease Research Center (NIH DK-58404). I thank all these funding sources for their support.

First, I would like to thank my mentor John Williams. When I interviewed at Vanderbilt University for the IGP, others viewed me as a risky student because of my non-academic scientific background. However, John saw me as the perfect Ph.D. candidate because of my diverse research experience, and in his easy-going manner he reassured me that Vanderbilt was the place for me. It was not surprising that I found myself back in his laboratory at the end of my rotations. John's guidance and commitment to my growth as a scientist ensured that I receive the best graduate training possible. His enthusiasm, leadership, and passion are all qualities that make him an excellent mentor and scientist. John has shown undying faith in my abilities, and his constant encouragement has allowed me to develop into a better teacher, an independent thinker, and a confident scientist. I thank him for believing in me, challenging me, encouraging me, and supporting me.

The Williams laboratory is an exciting and supportive place to train. Each laboratory member has contributed to my scientific development and I cannot thank them enough for their friendship, scientific advice, suggestions, critiques, and daily encouragement. I thank the lovely, Sharon Tollefson for the wisdom that she has generously shared with me for years and stellar technical support. I thank Monika Johnson for technical assistance and providing me with amazing baked goods! "Team VLP" has my gratitude for all the mouse work that I could not have completed without their support. I extend special thanks to John Erickson for helping me with immunology experiments and his efforts to improve my writing (if only I could learn from his perfect example). Finally, I thank my lab buddy, Andrew Hastings, for his optimism, patience, eclectic taste in music, and all the years of laughter.

I would like to extend my heartfelt gratitude to Dr. James Crowe, Jr. and all the members of the Crowe laboratory for adopting me. It is not easy being the first graduate student in a lab, but Mohammed Aiyegbo, Dr. Natalie Thornberg, Dr. Thomas Utley, Dr. Mike Lindquist, Dr. Fyza Shaikh, Dr. Bryan Briney, and Frances House supported me through my formative years and have been great friends. I especially thank Fyza, without whom I would have been lost. Many of my experiments would not have been possible without the Crowe lab fluorescence plate reader, which they graciously let me commandeer for hours, sometimes days.

I thank the Department of Pathology, Microbiology and Immunology, the former Department of Microbiology and Immunology, and the Graduate Education Committee for the Graduate Program in Microbiology and Immunology for their dedication to training students. I especially thank my former department chair, Dr. Jacek Hawiger, for

his generous support of me and my research. I would also like to thank the Chappell, Crowe, Denison, and Dermody labs for their help, reagents, and friendship.

I had the pleasure to work with wonderful collaborators at Vanderbilt. I thank Dr. Melanie Ohi, Brent Livesay, and Melissa Chambers for their advice, technical guidance, and providing training on the electron microscope. Drs. Terry Dermody and Bernardo Mainou have been valued mentors, given considerable time, shared reagents, and provided a number of ideas for my work. I also thank Dr. Melissa Farrow and Dr. Borden Lacy for kindly providing siRNAs, technical advice, and structural modeling assistance.

I would like to thank my thesis committee for steering my graduate studies. I thank Dr. Chris Aiken, my committee chair, for his advice, encouragement, and the rigor he brought to my scientific endeavors. I thank Dr. Earl Ruley for his refreshing honesty, zest for scientific discovery, and for helping me to become an effective communicator. I am grateful to Dr. Roy Zent for his invaluable advice, support, and for always seeing the bigger picture. I thank Dr. Borden Lacy for her quiet leadership, helpful suggestions, and constant encouragement. Borden is the perfect example of how a brilliant woman scientist can balance a family and a successful career. I was fortunate to learn from her example.

Many scientific mentors have challenged and inspired me to be the scientist I am today. I am indebted to Drs. Anton Schreiner, Stefan Franzen, and David Shultz who provided me with a solid, quantitative chemistry background and encouraged me to find my own scientific path. I thank my industry mentors, Dr. Meg Thompson, Jonathan M. White, Dr. Dennis Lambert, and the late, Dr. Tom Matthews, for believing in me as a young scientist, pushing me to achieve, giving me research projects that were

"beyond my years", and teaching me to aim high and work hard. They all know that 80-hour workweeks are normal.

I am forever indebted to my family for their love and support. I thank them for all the sacrifices they have made so I could pursue my dreams. My mother was my first and best teacher. She has always encouraged me to use my intelligence to benefit mankind. There are no words to express my gratitude for her example of how to be a wife, mother, and succeed in an ambitious career. I thank my father for raising me to believe that I could do anything *because* I was a woman and for his encouragement to always follow my dreams. I inherited my independence, courage and passion from my mother and my strength, grit and "never say die" attitude from my father. These personality traits are priceless in the everyday life of a scientist! I also thank my loving sister, Rheanne Bumgarner, for years of support. My life would not be complete without the love and support given to me by my best friend, Brooke Caudill, for whom I am very grateful. I thank my second parents, Bud and Elizabeth Cox, for their support, as well as the love and light they bring to my life. I am also thankful for my son, Jon, who has taught me to laugh at myself and learn from my mistakes.

My graduate studies would not have been possible without my loving husband, David. He is my champion and my rock. I thank him for his support and unwavering love, all the sacrifices he has made for me, and for his belief in me and my dreams. I regret that my graduate studies have kept me from spending more time with my husband and son. However, "my boys" never made me feel like they were neglected, although I am sure they must have felt that way at times. Win or lose…we do it together, and there is no other place I would rather be than holding their hands.

TABLE OF CONTENTS

LIST OF TABLES

LIST OF FIGURES

LIST OF ABBREVIATIONS

AMPV	Avian metapneumovirus
ANOVA	Analysis of variance
BSA	Bovine serum albumin
CHO	Chinese hamster ovary
DAPI	4’,6-diamidino-2-phenylindole
DiH2O	Deionized water
ELISA	Enzyme-linked immunosorbent assay
ER	Endoplasmic reticulum
F	Fusion protein
FACS	Fluorescence-activated cell sorting
FBS	Fetal bovine serum
G	Glycoprotein
GAG	Glycosaminoglycans
GAPDH	Glyceraldehyde-3-phosphate dehydrogenase
H	Hour
HIV	Human immunodeficiency virus
HMPV	Human metapneumovirus
HRSV	Human respiratory syncytial virus
IC_{50}	50% inhibitory concentration
M	Matrix protein
MAB	Monoclonal antibody

MIN	Minute
PBS	Phosphate-buffered saline
PCR	Polymerase chain reaction
PFU	Plaque forming unit
PIV5	Parainfluenza virus 5
PVDF	Polyvinylidene fluoride
R18	Octadecyl rhodamine B chloride
RAE	Arginine-Alanine-Glutamate
RGD	Arginine-Glycine-Aspartate
RGE	Arginine-Glycine-Glutamate
RT-PCR	Reverse transcription polymerase chain reaction
SD	Standard deviation
SEM	Standard error of the mean
SH	Short hydrophobic protein
VLP	Virus-like particle
VSV	Vesicular stomatitis virus

CHAPTER I

INTRODUCTION

Thesis Overview

The experiments described in this thesis were designed to elucidate how the human metapneumovirus fusion protein initiates virus entry. In Chapter I, I provide a brief background on human metapneumovirus (HMPV), the proposed mechanism of HMPV entry, the HMPV fusion protein structure, and a family of cell surface proteins called integrins, which we have shown are cellular receptors for HMPV. In Chapter II, I present our findings that RGD-binding integrins promote HMPV infection. In Chapter III, I describe new assays and tools that I developed to study HMPV attachment and fusion. In Chapter IV, I examine the role of RGD-binding integrins during HMPV entry. I show that the HMPV fusion protein mediates entry via an interaction with RGD-binding integrins, confirming that integrins serve as receptors for HMPV during virus attachment to human bronchial epithelial cells. Chapter V describes my studies designed to elucidate the site of HMPV virus-cell fusion. I demonstrate that HMPV fusion occurs with intracellular vesicles after virus particles are internalized into cells. My data indicate that fusion pore formation does not occur at the cell surface and suggest that HMPV enters cells via a mechanism that is distinct from other well-studied paramyxoviruses. In Chapter VI, I summarize my thesis studies and offer potential future experiments for the continuation of this work.

Human Metapneumovirus (HMPV) Background

Human metapneumovirus (HMPV) was first isolated in 2001 in the Netherlands (van den Hoogen et al., 2001). Dutch investigators discovered an unknown virus in respiratory secretions collected from young children with lower respiratory illness. Virus-infected cell supernatants were examined by electron microscopy and found to contain pleiomorphic virus particles measuring 150 to 600 nm, with spike-like envelope projections of 13 to 17 nm (Schildgen et al., 2011). PCR and sequence analysis revealed a single-stranded, negative-sense RNA genome with close resemblance to avian metapneumovirus (AMPV), an avian virus that causes serious respiratory disease in chickens and turkeys (Cook, 2000). Based upon virion morphology and genome organization, HMPV was classified as the first human member of the *Metapneumovirus* genus, in the subfamily *Pneumovirinae* of the paramyxovirus family (van den Hoogen et al., 2002; van den Hoogen et al., 2001).

HMPV is a ubiquitous respiratory pathogen that has been circulating in human populations undetected for decades. The original report detected HMPV-specific antibodies in archived human sera from the 1950s (van den Hoogen et al., 2001) and HMPV has been detected by RT-PCR in specimens from 1976 (Williams et al., 2004b). Phylogenetic analysis of multiple HMPV gene sequences suggests that HMPV diverged from an avian metapneumovirus (AMPV-C) between 200-300 years ago (de Graaf et al., 2008; Yang et al., 2009).

HMPV is a leading cause of lower respiratory infection in infants and children worldwide (Boivin et al., 2003; Dollner et al., 2004; Ebihara et al., 2004; Esper et al., 2004; Foulongne et al., 2006; Mackay et al., 2006; McAdam et al., 2004; Mullins et al.,

2004; Peiris et al., 2003; van den Hoogen et al., 2003; Williams et al., 2004b; Williams et al., 2006). HMPV is also associated with severe disease in immunocompromised hosts or persons with underlying conditions (Englund et al., 2006; Larcher et al., 2005; Madhi et al., 2003; Pelletier et al., 2002; Vicente et al., 2004; Williams, 2005; Williams et al., 2005a). HMPV causes a clinical spectrum of illness from upper airway infection to severe lower respiratory tract infections (e.g. bronchiolitis and pneumonia) (Brodzinski and Ruddy, 2009; Williams et al., 2004b). HMPV pathogenesis is similar to human respiratory syncytial virus (hRSV), another leading cause of lower respiratory infection in children; HMPV causes inflammation, sloughing, and necrosis of the bronchiolar epithelium (Loughlin and Moscona, 2006). Experimental studies in nonhuman primates and small animal models (hamsters, cotton rats, and mice) indicate that HMPV replicates in the upper and lower respiratory tract epithelium and demonstrate no evidence of viral dissemination, indicating a distinct tissue tropism for HMPV which is consistent with clinical illness observed during human infection (Hamelin et al., 2006; Kuiken et al., 2004; Williams et al., 2005b).

The HMPV virion is similar to other paramyxoviruses. The viral lipid bilayer is derived from the plasma membrane of infected cells during virus egress, as virions bud from the infected cell surface. HMPV matrix (M) protein lines the inner leaflet of the viral lipid bilayer, and virions contain three integral membrane surface glycoproteins, the fusion (F), glycoprotein (G), and short hydrophobic (SH) proteins (Fig. 1-1). The envelope contains a helical ribonucleoprotein (RNAP) complex consisting of nucleoprotein (N), phosphoprotein (P), matrix 2 protein (M2), large polymerase protein (L), and the single-stranded, negative-sense RNA genome. The HMPV genome ranges in

length from 13,281 to 13,387 nucleotides, and contains 8 genes with 9 open reading frames (Fig. 1-2).

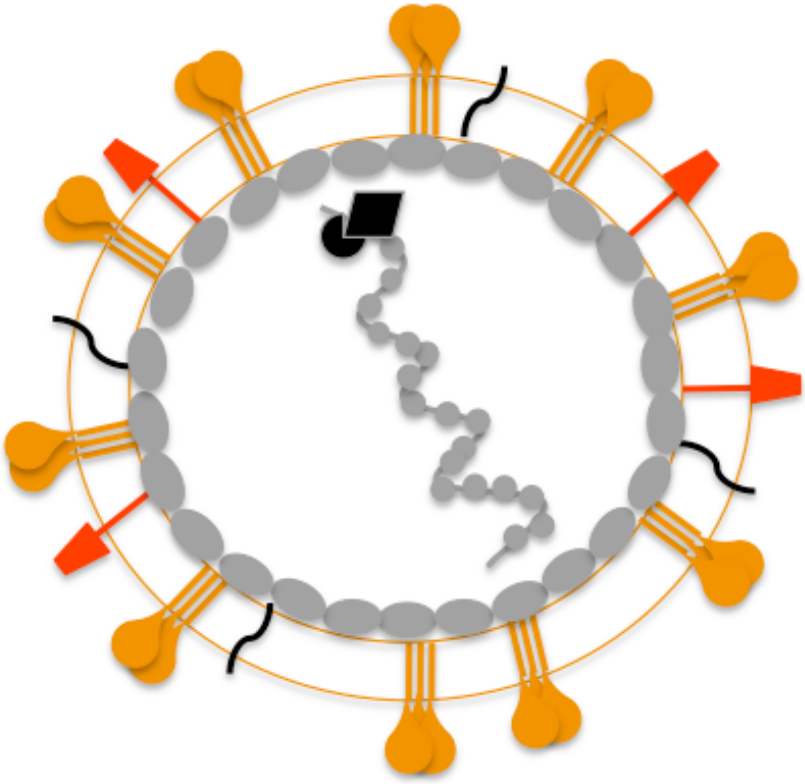

Fig. 1-1. Schematic representation of an HMPV virion.
The fusion (orange), attachment (red), and short hydrophobic (black) glycoproteins are depicted at the virion surface. The matrix protein (gray ovals) lines the inner leaflet of the virus membrane. Encapsidated within the viral envelope is the RNAP complex consisting of helical, genomic RNA wrapped by the nucleoprotein (N), the viral RNA-dependent, RNA polymerase (L), phosphoprotein (P), and matrix 2 protein (M2).

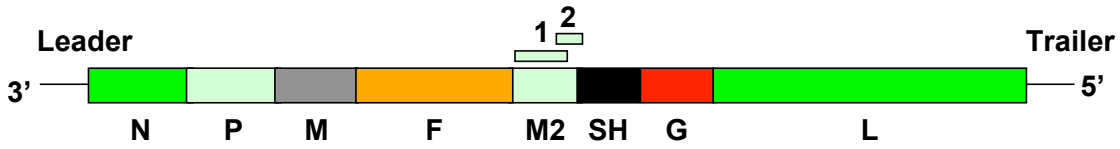

Fig. 1-2. Schematic representation of the HMPV genome.
The negative-sense, single stranded HMPV genome contains 8 genes: N, P, M, F, M2, SH, G and L. The M2 gene contains 2 overlapping reading frames, 1 and 2 that code for the viral M2-1 and M2-2 proteins. Two non-coding regions, a 3' leader sequence and a 5' trailer sequence, serve as promoter regions for viral transcription and replication. Not to scale.

HMPV Replication

HMPV infection is initiated by viral surface glycoproteins that attach to cellular receptors and mediate virus membrane fusion with cellular membranes. After the virus and cell membranes merge, the viral RNAP complex is delivered into the cell's cytoplasm where virus transcription begins. The viral RNA-dependent RNA polymerase, attached to the incoming RNAP complex, produces viral mRNA transcripts that are translated into viral proteins. After sufficient viral proteins accumulate within the infected cell, the RNAP serves as a template for positive-sense genomic intermediates that then serve as a template for progeny negative-sense RNA genomes. The viral glycoproteins (F, G, and SH) are translated on the rough endoplasmic reticulum, where they become membrane anchored and glycosylated. F, G and SH proteins traffic through the secretory pathway, and require additional glycan modification in the Golgi apparatus before they are delivered to the surface of the infected cell. The virus M protein assembles underneath the viral glycoproteins at the cell surface and RNAP complexes are recruited to assembly sites. Assembled progeny virions bud from the infected cell surface, resulting

in new enveloped virus particles that are capable of infecting other cells. Fig. 1-3 shows an illustration of the virus lifecycle.

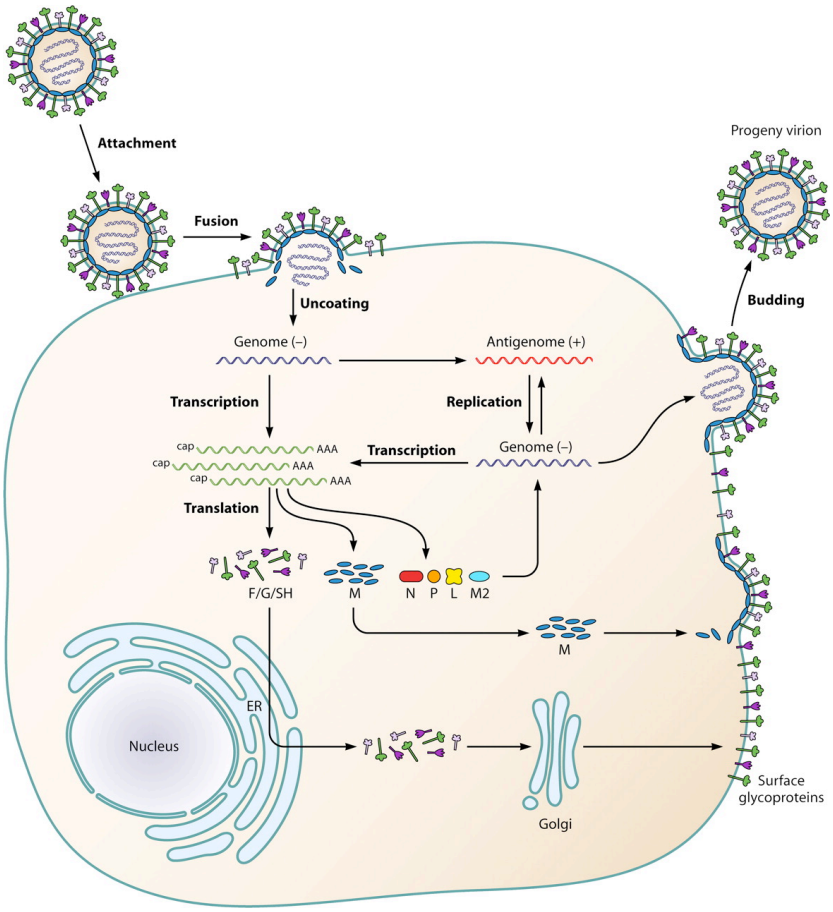

Fig. 1-3. Schematic representation of the HMPV lifecycle.
The HMPV virion attaches to receptors on the cell surface, where virus-cell membrane fusion is proposed to occur. Following fusion of the virus and cell membranes, the viral ribonucleoprotein complex is delivered into the cytoplasm. Next, the HMPV genome is transcribed into viral mRNAs, which are translated into proteins. HMPV surface glycoproteins F, G and SH are translated by host ribosomes on the endoplasmic reticulum (ER), trafficked from the ER to the Golgi apparatus, and delivered to the surface of the HMPV-infected cell. A switch occurs from virus transcription to virus replication, resulting in progeny negative-sense RNA genomes that are coated with the viral N protein and the viral proteins that collectively function as an RNA-dependent RNA polymerase (L, P and M2). All virion components are trafficked to the cell surface where they assemble into progeny virions that bud from the infected cell. Image reproduced from CLINICAL MICROBIOLOGY REVIEWS, 2011, 24(4):734-754.

HMPV Entry

Most paramyxoviruses use two viral glycoproteins to facilitate virus entry—an attachment protein, called HN, H or G (depending on the virus), and a fusion (F) protein. Indeed, elegant studies on paramyxoviruses in the subfamily *Paramyxovirinae* have demonstrated that viral attachment and fusion are mediated by two individual viral proteins that act in concert during virus entry (reviewed in (Lamb, 1993)). For the *Paramyxovirinae*, F is capable of catalyzing membrane fusion only in the presence of the attachment protein. For example, Sendai and human parainfluenza viruses require both a hemagglutinin/ neuraminidase (HN) protein that binds sialic acid receptors on the cell surface and the F protein to catalyze membrane fusion during virus entry (Bagai and Lamb, 1995; Connolly et al., 2009; Horvath et al., 1992; Russell et al., 2003; Takimoto et al., 2002). Investigators have elucidated specific regions of the viral HN proteins that serve as molecular switches to regulate viral fusion (Bose et al., 2011; Krishnan et al., 2009; Mahon et al., 2011; Melanson and Iorio, 2004; Melanson and Iorio, 2006; Porotto et al., 2003; Tanabayashi and Compans, 1996; Tsurudome et al., 1995; Wang et al., 2004), and viral fusion is thought to be triggered by HN interactions with the cell surface (McGinnes and Morrison, 2006; Porotto et al., 2007; Yao et al., 1997). Although thought to be rare in nature, F proteins for these viruses can mutate in a manner that allows a relaxed requirement for the HN protein during F-mediated fusion (Markwell et al., 1985; Paterson et al., 2000).

Measles virus expresses a hemagglutinin (H) attachment protein that interacts with CD46 or signaling lymphocyte activation molecule (SLAM) receptors on the host cell surface (Navaratnarajah et al., 2009; Tatsuo et al., 2000; Yanagi, 2001). Like the

paramyxoviruses described above, receptor engagement is coupled to fusion activity (Iorio and Mahon, 2008; Lee et al., 2008; Plemper et al., 2002; Smith et al., 2009). Receptor binding by H is required to activate F-mediated fusion (Lee et al., 2008; Navaratnarajah et al., 2009; Plemper et al., 2002; Wild et al., 1991). Measles viruses lacking the H protein are not viable (Roberto Cattaneo, personal communication). The newly identified Nipah and Hendra viruses also utilize proteinaceous receptors. These paramyxoviruses express a glycoprotein (G) protein that binds ephrin-B2 on target cells (Bonaparte et al., 2005; Negrete et al., 2005). Like measles, G-mediated attachment is coupled to F activation and required for fusion activity (Aguilar et al., 2009; Bishop et al., 2007; Smith et al., 2009; Whitman and Dutch, 2007).

The current model for paramyxovirus entry is based upon studies of viruses in the *Paramyxovirinae* subfamily. The proposed model is a stepwise process where 1) the attachment protein binds to cellular receptors, 2) the bound attachment protein directly interacts with and transmits a signal to the F protein, 3) the F protein becomes activated to undergo structural changes, 4) F refolds from a prefusion to postfusion structural conformation, resulting in the merging of the viral membrane with the plasma membrane, and 5) the genome is delivered into the cytoplasm from a fusion pore created at the cell surface. However, membrane fusion for paramyxoviruses in the *Pneumovirus* subfamily is unique in that F drives fusion in the absence of a separate viral attachment protein. The pneumoviruses incorporate three surface glycoproteins that could potentially facilitate entry: F, SH, and G. The first indication that pneumovirus entry may not absolutely depend upon all surface glycoproteins was the identification of a live, cold-passaged human respiratory syncytial virus (hRSV) strain (cp-52) that had a large deletion

spanning most of the SH and G coding sequences but replicated efficiently in Vero cells (Karron et al., 1997). Thus, in the absence of SH and G, hRSV was infectious and capable of replicating to high titer *in vitro*, although cp-52 replication was severely attenuated *in vivo* in both animals and humans (Karron et al., 1997). Subsequent studies with hRSV engineered without the SH and G genes have confirmed that hRSV F is sufficient for virus entry in cell culture, but replication is attenuated in animal models of infection (Feldman et al., 2000; Kahn et al., 1999; Schlender et al., 2003; Techaarpornkul et al., 2001; Techaarpornkul et al., 2002; Teng et al., 2001; Widjojoatmodjo et al., 2010). The invention of reverse genetics for HMPV has enabled researchers to rescue viruses engineered to express the F protein in the absence of G and/or SH, and define the individual contributions of each protein for virus entry. Deletion of the SH gene from HMPV did not alter viral growth in cell culture or animal models of infection (Biacchesi et al., 2005; Biacchesi et al., 2004), confirming that the SH protein does not serve a role in virus entry. HMPV lacking both G and SH replicated efficiently in cell culture (Biacchesi et al., 2004) and in both the upper and lower respiratory tracts of hamsters after intranasal inoculation (Biacchesi et al., 2004) although the virus was attenuated *in vivo.* HMPV lacking G was capable of infecting African green monkeys but peak virus titers were reduced six-fold and 3,200-fold in the upper and lower respiratory tract, respectively (Biacchesi et al., 2005).

The fact that both hRSV and HMPV viruses lacking the G and SH genes are infectious indicates that the F proteins from these pneumoviruses can perform the necessary functions for virus entry, i.e. attachment and fusion. However, the G protein is clearly important for virus fitness *in vivo*. Current evidence suggests that pneumovirus G

proteins help tether virus particles to the cell surface, and are likely important for strengthening particle adhesion and concentrating virions on the cell surface. Techaarpornkul et al. demonstrated that hRSV G is required for optimal virus attachment to the cell surface, but not for virus fusion and entry as the F protein alone is sufficient for efficient virus fusion with cultured cells (Techaarpornkul et al., 2001). HRSV and HMPV G have been shown to bind adhesion molecules on the cell surface such as heparan sulfate or glycosaminoglycans (GAGs) (Hallak et al., 2000; Krusat and Streckert, 1997; Thammawat et al., 2008). Pretreatment of HMPV with soluble heparin inhibits infection, and recombinant G protein binds to heparin-agarose columns and cells in a GAG-dependent manner (Thammawat et al., 2008). Thus, HMPV G is capable of binding cell surface GAGs and may contribute to virus attachment; however, because G is dispensable for viral entry, it is not absolutely required for the membrane fusion activity of F during the virus entry process. Furthermore, transient transfection of HMPV F is sufficient to induce cell-cell fusion, and co-expression of the G protein does not significantly enhance cell-cell fusion (Schowalter et al., 2006). This evidence coupled with the observation that HMPV lacking the G protein is infectious suggests that the G protein is not a critical component of the HMPV fusion machinery.

As noted, HMPV diverged from the avian pneumovirus, AMPV-C (de Graaf et al., 2008; Yang et al., 2009). HMPV does not replicate in birds and evidence of AMPV infection has not been detected in humans (van den Hoogen et al., 2001). The switch in virus tropism appears to be due to the attachment function of the F protein. In cell culture, HMPV expressing only F (HMPVΔGΔSH) binds to the cell surface with the same efficiency as wild type virus (Chang et al., 2012b). Moreover, HMPV F confers species

specificity of infection, as F was found to be primarily responsible for the difference in the ability of AMPV-C and HMPV to infect quail fibroblast (QT6) cells (de Graaf et al., 2009). Further, the F2 subunit (and not the G protein) of both hRSV (Schlender et al., 2003) and HMPV (de Graaf et al., 2009) have been shown to confer species-specific infection of cells. This evidence strongly indicates that HMPV F interacts with cell surface receptors.

Thus, HMPV F is necessary and sufficient for membrane fusion and capable of mediating entry without an additional attachment protein, in contrast to the firmly established model for most paramyxoviruses that absolutely require two viral proteins. To be sufficient for virus entry, HMPV F must be able to attach to cellular receptors and this attachment should activate F-mediated membrane fusion. How HMPV F mediates both attachment to cellular receptors and membrane fusion has been the focus of my thesis studies.

HMPV F protein

All paramyxovirus F proteins are class I fusion proteins that due to the conservation of conserved structural domains are thought to mediate fusion via the same global mechanism (reviewed in (Lamb and Jardetzky, 2007)). HMPV F is a trimeric, type I membrane glycoprotein. A schematic of the HMPV F protein structure is shown in Fig. 1-4. Each HMPV F monomer must be proteolytically cleaved to convert the inactive precursor, F0, into a fusion-competent, disulfide-linked F1/F2 heterodimer. The monobasic, consensus cleavage site (PRQSR) is a trypsin-like cleavage motif, which is cleaved after the final Arg residue. For most cell types, cell surface HMPV F is expressed

in the F0 precursor form. In cell culture, F protein cleavage occurs when trypsin is added to the cell medium. Indeed, HMPV grows poorly (or not at all) unless trypsin in added to virus growth medium during virus propagation in cell culture (Biacchesi et al., 2004; Tollefson et al., 2010; van den Hoogen et al., 2001). Trypsin treatment of HMPV F expressing cells is also required for cell-cell fusion activity (Schowalter et al., 2006). *In vivo*, cleavage is likely mediated by extracellular proteases such as TMPRSS2 (Shirogane et al., 2008) or mini-plasmin (Murakami et al., 2001) expressed in the respiratory tract of infected humans. HMPV F cleavage activates the protein by creating a new F1 N-terminus, the fusion peptide (FP), which is inserted into target cell membranes during the fusion process. Two heptad repeat (HR) regions are located in the F1 subunit; HRA is adjacent to the FP and HRB is adjacent to the transmembrane (TM) domain.

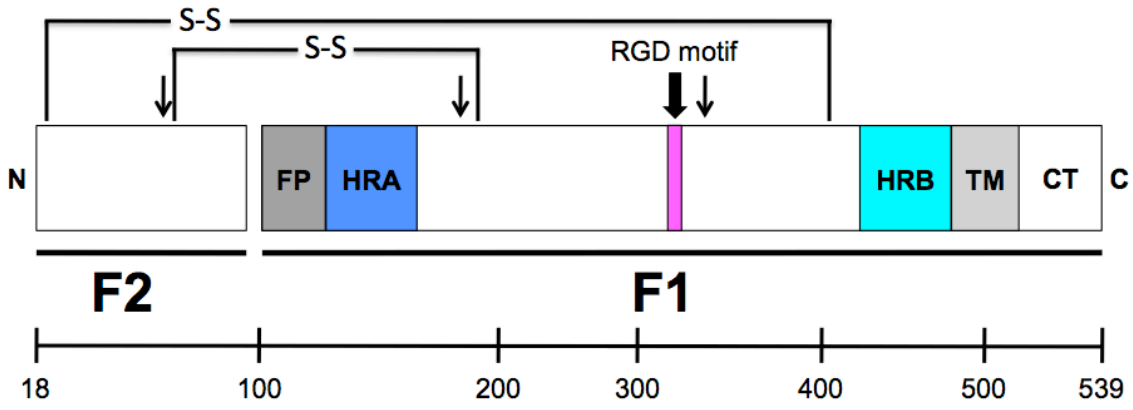

Fig. 1-4. Schematic representation of the cleaved HMPV fusion protein.
The mature, proteolytically cleaved HMPV F protein contains 522 amino acids, with 82 residues in the F2 subunit and 440 residues in the F1 subunit, which includes a large extracellular domain, an ~23-amino acid transmembrane domain, and a cytoplasmic tail of 25 residues. FP = fusion peptide; HRA = heptad repeat A; HRB = heptad repeat B; TM = transmembrane domain; CT = cytoplasmic tail. The approximate location of a conserved RGD motif (residues 329-331) is indicated as a magenta box. Arrows indicate the three N-linked glycosylation sites. The location of two disulfide bonds that connect the F1 and F2 protein subunits are shown. (Scale bar, amino acids.)

During fusion, a metastable, prefusion conformation of F refolds into a highly stable postfusion conformation. During the prefusion-to-postfusion transition, the HRA and HRB form trimeric coiled-coils that rearrange to fold into a highly stable six-helix bundle that drives the formation of a fusion pore between the virus and cell membranes. Formation of the six-helix bundle is irreversible and is directly linked to membrane merging, as peptides mimicking the heptad repeats are capable of blocking membrane fusion (Deffrasnes et al., 2008; Miller et al., 2007; Russell et al., 2001).

Crystal structures for the parainfluenza virus 5 (PIV5) prefusion F (Yin et al., 2006) and the hRSV postfusion F (Swanson et al., 2011) have been determined and are shown in Fig. 1-5A. Three discrete domains, DI (orange), DII (red) and DIII (blue), have been colored to indicate how the linear sequence of amino acids is arranged in the tertiary structure of the prefusion and postfusion F proteins. The HRA domain (light blue) changes significantly in both secondary structure and location, and the F head domain becomes more compact, during the prefusion-to-postfusion F transition (reviewed in (Lamb and Jardetzky, 2007)). During my thesis studies, we collaborated with Dr. Ted Jardetzky at Stanford University to determine the structure of the HMPV F protein. Ted's postdoctoral fellow, Xiaolin Wen, solved a crystal structure of HMPV F in complex with a neutralizing antibody (DS7 Fab) and I was a co-author on the recently published manuscript (Wen et al., 2012). The HMPV F structure was solved as a monomer, and is depicted in Fig. 1-5B. The HMPV F DIII domain is similar to the prefusion PIV5 F protein but overall the HMPV F structure resembled the hRSV postfusion F (Wen et al., 2012).

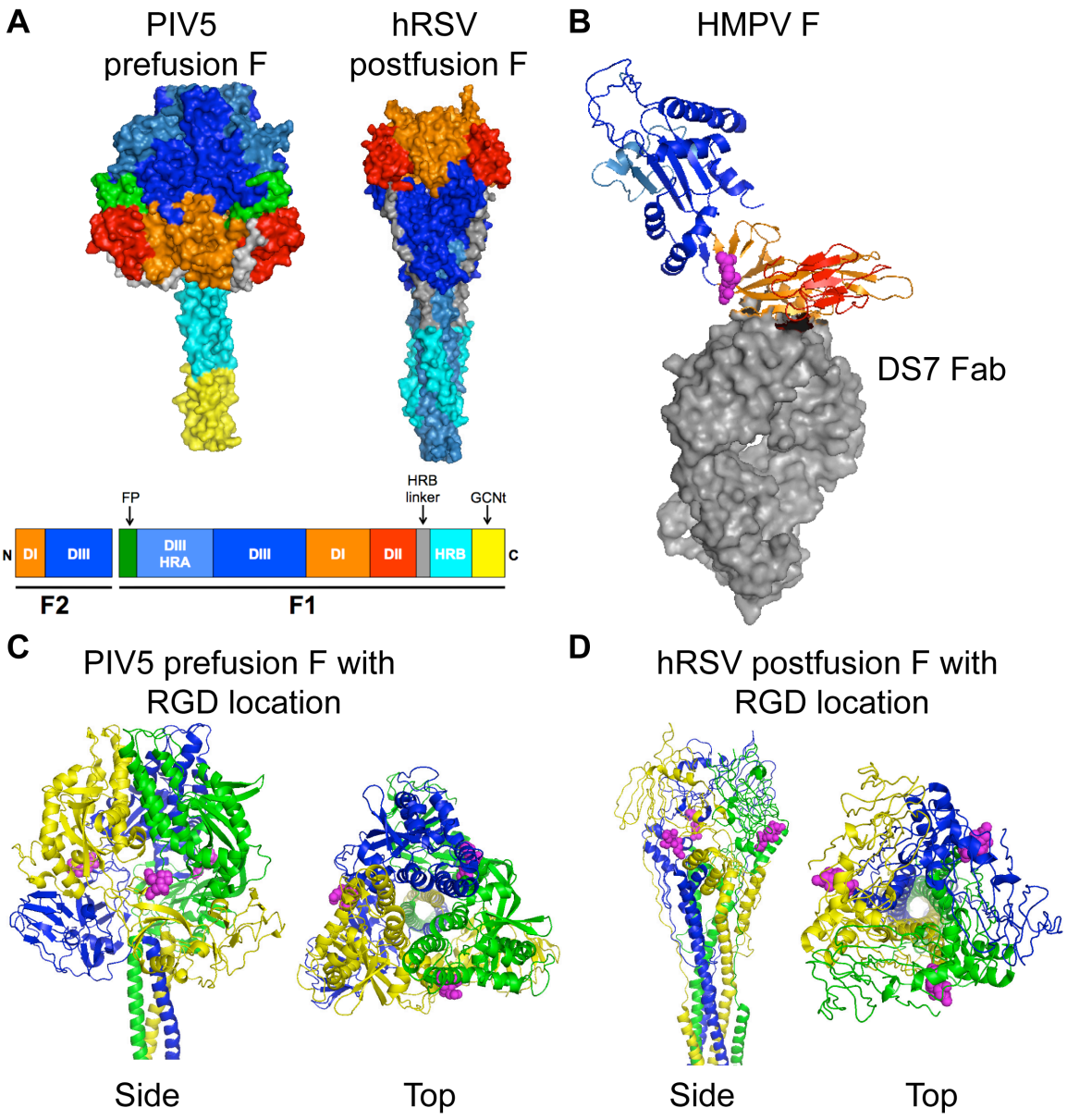

Fig. 1-5. Structures of paramyxovirus F proteins.
(A) Structures of the prefusion conformation of the PIV5 F trimer and the postfusion conformation of the hRSV F trimer are shown. A schematic of the F protein color-coded by structural domain is shown below the structures. DI domain is shown in orange, DII domain is shown in red, and DIII domain is shown in blue (HRA in light blue). HRB is shown in cyan and the HRB linker domain in gray. The fusion peptide (shown in green) for prefusion PIV5 F was not solved in the hRSV F structure. The GCNt domain (shown in yellow) was added to the PIV5 F trimer for crystallization. (B) HMPV F in complex with a neutralizing antibody (DS7 Fab, shown as gray surface). DI, DII, and DIII coloring is the same as in (A). The conserved RGD motif is shown as magenta spheres. (C and D) Side and top views of the prefusion PIV5 F trimer (C) or the postfusion hRSV F trimer (D) are shown with the homologous residues to HMPV F-RGD indicated by magenta spheres. Each F monomer is shown in blue, yellow, or green.

Paramyxovirus F proteins mediate fusion in a pH-independent manner (Lamb, 2007), and commonly induce fusion of cultured cells at neutral pH resulting in syncytium formation during virus infection. Surprisingly, the first report of HMPV F-mediated cell-cell fusion activity suggested that HMPV F required low pH for activation (Schowalter et al., 2006). Schowalter et al. determined that HMPV F required both trypsin treatment, to mediate proteolytic processing, and low pH pulses for fusion activity of the A2 genotype strain CAN97-83 (Schowalter et al., 2006). A follow-up study by Herfst et al. suggested that the low-pH-induced fusion phenotype of HMPV strain CAN97-83 was not indicative of the fusion activity requirement for all HMPV strains (Herfst et al., 2008). HMPV isolates have been categorized into four genotypes: A1, A2, B1 and B2. Herfst et al. demonstrated that HMPV F-mediated cell-cell fusion for most A2 strains and all B genotype strains was pH-independent; however, fusion by a prototype A1 strain (NL001) was enhanced by pH 5 pulses (Herfst et al., 2008). A mutagenesis approach was used to determine that the presence of a Gly residue at position 294 was a key determinant of the low-pH-induced fusion phenotype for HMPV A strains, but inserting the Gly_{294} residue into F proteins of the B genotype did not confer pH sensitivity (Herfst et al., 2008). I compared the sequences of more than 1000 published full-length and partial HMPV F sequences from isolates collected around the world to determine the frequency of the residue present at position 294. Most HMPV strains encode a Glu residue at position 294, 5.9% encode a Gly (59 of 1005), and rarely a Lys residue is found at this position in the sequence (15 of 1005). The diversity in the actual amino acid at position 294 is largely found in lineage A viruses, as only 11 genotype B viruses were found to have a Lys residue in lieu of the conserved Glu residue. The lack of HMPV F proteins with the low-

pH sensitive Gly_{294} suggests that exposure to low pH is not a general requirement for fusion activity. Thus, the general trigger that activates HMPV F to drive the membrane fusion process is still not known. I hypothesized that F binding to cell surface receptors triggered HMPV fusion and tested this hypothesis during my thesis studies (observations described in Chapters IV and V).

HMPV F contains a conserved RGD motif

HMPV F amino acid sequences are highly conserved, falling into two major lineages (A and B), each with two subgroups (1 and 2), which exhibit a mean of ~96% identity (van den Hoogen et al., 2004; Yang et al., 2009). A study in 2004 comparing 64 partial F gene sequences from the United States, Canada, Peru, France, Israel, Republic of South Africa, Australia, and the Netherlands confirmed that HMPV isolates circulating around the world encode F proteins from the A1, A2, B1, and B2 genetic lineages (Boivin et al., 2004). Distinct canonical amino acid differences are present between major subgroups, and polymorphic variations tend to cluster in discrete regions (Boivin et al., 2004; Yang et al., 2009). Amino acid identity within and between subgroups is higher than nucleotide identity, suggesting structural or functional constraints on F protein diversity. A study comparing 85 full-length F gene sequences collected over a 20-year period from the United States (all isolated in Tennessee), Canada, Japan, and the Netherlands suggested that there was no progressive genetic drift over time, and the genetic lineages were stable over time in circulating viruses in a population of children with respiratory illnesses (Yang et al., 2009).

Before I began my thesis studies, my mentor had compared full-length F gene sequences from 71 clinical isolates of HMPV collected worldwide over a 20-year period and discovered an invariant arginine-glycine-aspartate (RGD) motif at residues 329–331 in the HMPV F1 subunit. The RGD motif, along with 5 N- and 16 C-terminal flanking residues, was strictly conserved, regardless of genetic lineage and despite diversity in other regions of the F gene (Cseke et al., 2009). The RGD sequence is present at residues 329-331 in all F gene sequences that have been studied to date, unique to HMPV F among human paramyxovirus fusion proteins, and absent in all published hRSV F sequences. The RGD motif is located in DI of the HMPV F protein and is shown in Fig. 1-5B as magenta spheres. Based upon homology, the predicted location of the RGD motif is also shown on the PIV5 prefusion (Fig. 1-5C, magenta spheres) and the hRSV postfusion (Fig. 1-5D, magenta spheres) F trimer structures. The presence of the invariant RGD motif led us to speculate that integrins function as receptors for HMPV.

RGD-binding integrins

Integrins are heterodimeric integral membrane proteins composed of one α and one β subunit. Several integrins (αVβ1, αVβ3, αVβ5, αVβ6, αVβ8, α5β1, α8β1 and αIIbβ3) bind proteins with RGD motifs, such as fibronectin and vitronectin. Integrins are adhesion receptors that bind extracellular proteins to modulate cell behavior and survival. Integrins associate with cytoskeletal proteins, adaptors, and kinases via the cytoplasmic tails of the α and β subunits, allowing them to transduce bidirectional signals between the intra- and extra-cellular environments (Hynes, 2002). The intimate link between integrins and cell signaling cascades, as well as endosomal sorting pathways, makes them a

desirable receptor for mammalian viruses. Several viruses including adenovirus, hantavirus, herpesvirus, picornavirus, and reovirus utilize integrins during entry, either as attachment or internalization receptors (reviewed in (Stewart and Nemerow, 2007)). For example, the RGD-binding integrin αVβ3 mediates hantavirus attachment and internalization (Raymond et al., 2005), while adenoviruses attach to cells by binding the coxsackie adenovirus receptor (CAR) and utilize various RGD-binding integrins for internalization (Davison et al., 2001; Wickham et al., 1993).

RGD-binding integrins are expressed on the surface of all nucleated mammalian cells. Three different RGD-binding integrin heterodimers (αVβ5, αVβ6, and αVβ8) are expressed on airway epithelial cells in healthy adults (reviewed in (Sheppard, 2003)). Of these, αVβ6 is constitutively expressed at low levels in uninjured epithelium but expression is upregulated in the lung in response to injury and inflammation (Breuss et al., 1995; Weinacker et al., 1995). While α5β1 is generally not expressed in healthy adult airway epithelial cells, expression is induced during lung cell injury (Pilewski et al., 1997; Roger et al., 1999) and the integrin is apically exposed in dedifferentiated respiratory epithelial cells during epithelium repair following injury (Roger et al., 1999). Thus, RGD-binding integrins are expressed on the surface of human respiratory epithelial cells where they may bind to HMPV F during infection. A primary objective of my thesis research was to determine whether HMPV F binds to RGD-binding integrins during virus entry and if F binding to integrins triggers fusion.

CHAPTER II

RGD-BINDING INTEGRINS PROMOTE HMPV INFECTION

Introduction

Proteinaceous cellular receptors have been identified for some paramyxoviruses, including measles virus (Dorig et al., 1993; Tatsuo et al., 2000), Nipah virus, and Hendra virus (Bonaparte et al., 2005; Negrete et al., 2005). Sialylated cell-surface proteins serve as receptors for other paramyxoviruses, such as parainfluenza virus (Moscona, 2005; Villar and Barroso, 2006). For all paramyxoviruses identified to date, the G or H/HN protein, rather than the F protein, is the receptor-binding moiety. When my dissertation research began, receptors for HMPV had not been reported. However, other investigators had shown that HMPV F was sufficient for virus attachment and fusion (Biacchesi et al., 2005; Biacchesi et al., 2004), suggesting that F may interact with distinct cell surface receptors during virus docking.

The invariant arginine-glycine-aspartate (RGD) motif within the F extracellular domain led us to hypothesize that RGD-binding integrins served as receptors for HMPV. Our initial experiments were designed to elucidate whether integrins were required for HMPV infection. In this section, I show that the divalent chelator, EDTA, which reduces integrin-ligand binding, diminished HMPV infectivity but had no effect on the closely related paramyxovirus, hRSV. Linear peptides containing an RGD motif reduced HMPV infection in a dose-dependent manner, but peptides with an RGE motif had no significant effect. Function-blocking integrin monoclonal antibodies (mAbs), specific to several

integrin subunits, inhibited HMPV infection, but not hRSV. Further, while transfection of human αV and β1 integrin subunits into poorly permissive Chinese hamster ovary (CHO) cells conferred HMPV infectivity, siRNA treatment to reduce αV and β1 integrin subunit expression in highly permissive human bronchial epithelial cells significantly reduced HMPV infection. Finally, recombinant F protein bound specifically to permissive cells, and mutation of the F protein RGD motif abolished binding. Collectively, these data provide strong evidence that the HMPV F protein engages RGD-binding integrins during infection.

When I began my dissertation research in the Williams laboratory, Gabriella Cseke, a former graduate student, and Melissa Maginnis, a former graduate student in Terry Dermody's laboratory, had completed several experiments described in this chapter (Figures 2-1, 2-2 and 2-6). I acknowledge their work and intellectual contributions to the conclusions drawn from results presented in this chapter. My experiments were both new experiments (Figures 2-3, 2-4 and 2-5) and experiments designed to contribute additional controls for previous experiments (Figure 2-7). I also acknowledge Ms. Sharon Tollefson for technical assistance with virus infectivity assays.

Materials and Methods

Cells and viruses. BEAS-2B (ATCC CRL-9609) and LLC-MK2 (ATCC CCL-7) cells were maintained in Opti-MEM I (Invitrogen) containing 2% fetal bovine serum (FBS), 2 mM L-glutamine, 50 μg/mL gentamicin and 2.5 μg/mL amphotericin B. CHO cells were maintained in DMEM/F12 medium (Invitrogen) supplemented to contain 10% FBS, glutamine, and antimicrobials above. The HMPV strain, TN/96–12, a genotype A1 virus,

which is a clinical isolate passaged 8 times in LLC-MK2 cells before this study, was used for all experiments. Virus was propagated in LLC-MK2 cells maintained in serum-free LLC-MK2 growth medium with 5 μg/mL trypsin (Invitrogen) as described (Williams et al., 2005b). hRSV strain A2 was cultivated as described for growth of HMPV. Both HMPV and hRSV had a titer of 1 x 10^6 pfu/mL by plaque titration using LLC-MK2 cell monolayers.

Peptides and antibodies. Linear GRGDSP and GRGESP peptides were purchased from American Peptide. Polyclonal anti-HMPV antibody was generated by infecting guinea pigs twice intranasally with 10^5 pfu of sucrose-gradient-purified HMPV. This anti-HMPV antibody has low nonspecific background, does not cross-react with other viruses by immunofluorescence or immunoblotting, and detects recombinant HMPV F protein with high sensitivity (Cseke et al., 2007; Williams et al., 2005b). Function-blocking human integrin-specific mAbs MAB2021Z (αv; clone AV1), MAB1957Z (β3; clone 25E11), and MAB1976Z (αvβ3; clone LM609) were purchased from Millipore (formerly Chemicon). Function-blocking human integrin-specific mAbs AIIB2 (β1) and BIIG2 (α5) were obtained from the Developmental Studies Hybridoma Bank at the University of Iowa. Human JAM-A-specific mAb J10.4 was provided by Charles Parkos (Liu et al., 2000). Function-blocking human α2-specific mAb 6F1 was provided by Richard Bankert (Chen et al., 1991).

Immunostaining assay of viral infection. Confluent monolayers of cells grown in 48-well plates were washed twice with Dulbecco PBS solution. Dilutions of EDTA,

peptides, or antibodies were prepared in serum-free OptiMEM medium, and 75 µL of each dilution or medium alone was added to wells in triplicate. Cells were incubated at 37°C for 90 min, followed by incubation at 4°C for 30 min. Cells were adsorbed with HMPV at a multiplicity of infection of 60 pfu per well and incubated at RT for 60 min (adsorption) and 37°C for 60 min (internalization), with occasional rocking. Cells were washed twice with Dulbecco PBS solution and incubated in 0.5 mL cell growth medium at 37°C for 24 h. Cells were fixed in formalin at RT for 1 h, washed with diH2O, and incubated with blocking buffer (5% dried milk, 0.05% Tween in PBS solution) at 37°C for 30 min. Cells were incubated with polyclonal guinea pig anti-HMPV antibody in blocking buffer at 37°C for 2 h, washed, and incubated with an HRP-conjugated goat anti-guinea pig IgG antibody (Southern Biotech) at 37°C for 2 h. Cells were washed, incubated with TrueBlue peroxidase substrate (Kirkegaard and Perry Laboratories) at room temperature for 10 min, washed, and air-dried. Infected cells were visualized and enumerated with a dissecting microscope.

Subcloning of integrin constructs used for transfection. A cDNA encoding human αv integrin (Fitzgerald et al., 1987) cloned into the BamHI and XbaI site of pcDNA-1neo (Invitrogen) was excised by digestion and sub-cloned into pcDNA3.1+ (Invitrogen) using complementary restriction enzyme sites. A cDNA encoding human β1 integrin cloned into the EcoRI and XhoI sites of pBluescript SK (ATCC) was excised by digestion and sub-cloned into complementary restriction enzyme sites of pcDNA3.1+. Integrin expression plasmids were sequenced to confirm fidelity of cloning.

Transfection of human integrin cDNA. Cells grown in 24-well plates were transfected with either empty vector (pcDNA3.1+) or plasmids encoding human integrin constructs using TransFectin reagent (Bio-Rad). Cells were incubated for 24 to 48 h to allow receptor expression before adsorption with HMPV for infectivity studies.

Knockdown of integrin expression with siRNA. BEAS-2B cells were grown in 24-well plates to achieve 90% confluency on day of transfection. Cells were mock-transfected, or transfected with integrin-specific or control siRNAs (Qiagen AllStars Negative Control siRNA) using HiPerFect reagent (Qiagen). After 48 h incubation, cells were either harvested for determination of cell-surface integrin expression by flow cytometry or adsorbed with HMPV or hRSV for infectivity experiments.

HMPV F protein binding assay. The HMPV F protein RGD motif was changed to RGE using site-directed mutagenesis (Stratagene, Quikchange II). WT and RGE mutant HMPV F ectodomain (FΔTM) constructs were purified as described (Cseke et al., 2007). LLC-MK2 cells and CHO cells were detached from plates and pelleted by centrifugation. Cells (2 to 3 x 10^5/mL) were resuspended in PBS/1% FBS (FACS buffer), pelleted, and washed with FACS buffer. Cells were resuspended in 0.2 mL FACS buffer with 10 μg of purified HMPV FΔTM and incubated at 4°C for 1 h with rocking. Cells were centrifuged, the supernatant removed, and cells were incubated with anti-HMPV polyclonal guinea pig serum in 0.2 mL FACS buffer at 4°C for 30 min. Cells were pelleted, washed twice, and stained with AlexaFluor 568-conjugated goat anti-guinea pig IgG secondary antibodies (Molecular Probes) in 0.2 mL FACS buffer at 4°C for 30 min. Cells were

resuspended in FACS buffer and analyzed by flow cytometry using a LSRII flow cytometer (BD Biosciences). F protein binding was quantified by setting the M1 gate region at the first decade of fluorescence in all experiments and enumerating the percentage of cells contained within this gate.

Statistical analysis. Means of replicate experiments, each performed in triplicate, were compared by using an unpaired, 2-tailed Student's *t* test assuming unequal variance. *P* values < 0.05 were considered statistically significant.

Results

EDTA and RGD-specific peptides reduce HMPV infectivity. In many cases, integrin-ligand interactions are dependent on divalent cations, including Ca^{2+} and Mg^{2+} (Hynes, 2002). Attachment of integrin-dependent viruses to RGD-binding integrins is diminished by the divalent cation chelator EDTA (Bergelson et al., 1993; Hynes, 2002; Summerford et al., 1999; Wang et al., 2003; Williams et al., 2004a). We tested the effect of EDTA on HMPV binding and infection of cells using a quantitative immunostaining assay. The closely related paramyxovirus, hRSV, which lacks an RGD motif in its analogous F protein, was used as a control. Rhesus monkey kidney epithelial (LLC-MK2) cells, which are permissive for infection by both HMPV and hRSV, were incubated with increasing concentrations of EDTA before adsorption with either HMPV or hRSV (Fig. 2-1A). EDTA blocked HMPV infection in a dose-dependent manner but had no effect on hRSV infectivity at any concentration tested. The cell monolayer began to detach at EDTA concentrations greater than 2.5 mM; however, HMPV infection was not detected in the

remaining adherent cells. hRSV-infected cells were present at EDTA concentrations >2.5 mM in numbers that appeared similar to those following treatment with lower EDTA concentrations. We conclude that EDTA exerts a specific inhibitory effect on HMPV, supporting a role for integrins during HMPV infection.

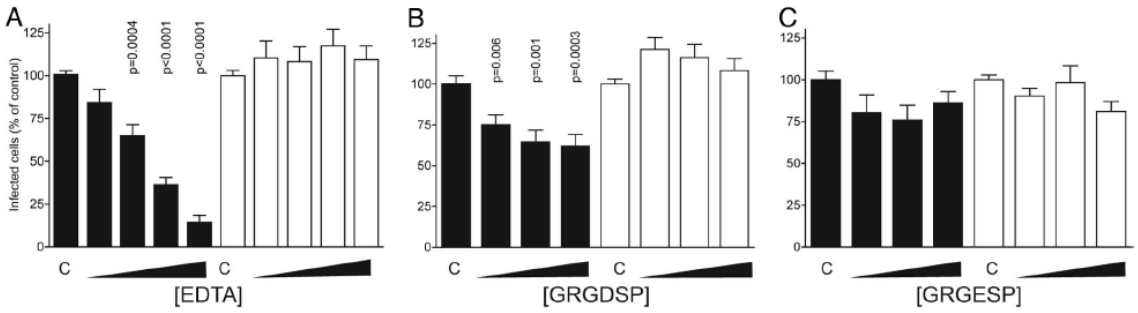

Fig. 2-1. EDTA and linear RGD peptides inhibit infection by HMPV but not hRSV. LLC-MK2 cells were treated with increasing concentrations of (A) EDTA (0.3 mM, 0.6 mM, 1.25 mM, and 2.5 mM), (B) linear peptide GRGDSP (0.15 µM, 0.3 µM, and 0.6 µM), or (C) linear peptide GRGESP (0.15 µM, 0.3 µM, and 0.6 µM) before adsorption with HMPV (black bars) or hRSV (white bars). Infected cells were identified by indirect immunostaining for viral antigen. Black triangles represent increasing EDTA or peptide concentration. C indicates untreated controls. Results are expressed as the mean percentage of infected cells following inhibitor treatment compared with the mean percentage of infected control cells for at least three independent experiments performed in triplicate. Error bars = SEM. Only *P* values < 0.05 (Student's *t* test) are shown.

To determine whether the RGD tripeptide motif is required for HMPV infection, we incubated LLC-MK2 cells with the integrin binding peptide, GRGDSP, and the control peptide, GRGESP, before virus adsorption. Treatment of cells with GRGDSP resulted in dose-dependent inhibition of HMPV infectivity (Fig. 2-1B), with ~45% inhibition observed at a concentration of 0.6 μM, whereas the control GRGESP peptide had a minimal, non-significant effect (Fig. 2-1C). Neither peptide produced statistically significant inhibition of hRSV infection (Fig. 2B and C), suggesting a specific effect of the GRGDSP peptide on infection by HMPV. Although the inhibitory effect of the linear GRGDSP peptide is modest, the magnitude of the infectivity blockade approximates that achieved in studies of other viruses known to engage integrins (Akula et al., 2002; Guerrero et al., 2000; Jackson et al., 2002; Pulli et al., 1997; Williams et al., 2004a).

αv and β1 integrin-specific antibodies reduce HMPV infectivity. To identify integrins required for HMPV infection, we screened mAbs directed against the specific RGD-binding integrins expressed by LLC-MK2 cells for the capacity to inhibit HMPV infection. Cells were incubated with antibodies specific for RGD-binding integrin subunits alone or in combination, adsorbed with either HMPV or hRSV, and scored for infection by immunostaining (Fig. 2-2 A and B). Antibodies specific for αv and β1 integrin subunits displayed the greatest inhibition of HMPV infectivity, with an αv-specific antibody demonstrating ~55% inhibition and a β1-specific antibody demonstrating ~40% inhibition. Using a combination of αv and β1 integrin-specific antibodies resulted in ~80% inhibition. Antibodies specific for αvβ3 and α5β1 integrins exhibited 35% and 30% inhibition, respectively, whereas α5 and β3 integrin-specific

antibodies had a minimal, non-significant effect. Thus, antibodies directed against either αv or β1 integrin significantly inhibit HMPV infection. Control antibodies specific for α2 integrin and junctional adhesion molecule-A (JAM-A) had no effect at any concentration tested (Fig. 2-2A and C). Importantly, none of the integrin-specific or control antibodies had any significant effect on the infectivity of hRSV (Fig. 2-2B). The degree of inhibition of HMPV infection by αv and β1 integrin-specific antibodies was dose-dependent (Fig. 2-2C), providing further evidence that the inhibition of HMPV infection results from integrin blockade. RGD-binding integrin α and β subunits form an interface within the heterodimeric protein that binds the tripeptide RGD motif. Thus, integrin function-blocking antibodies that block individual subunits will inhibit binding of several different RGD-integrin heterodimers, e.g. a β1-specific antibody blocks adhesion of α5β1, α8β1, and αVβ1 integrins. Therefore, the additive inhibitory effect of αv and β1 integrin-specific antibodies (Fig. 2-2A and C) suggests that multiple RGD-binding integrins are required for HMPV infection. Based upon the antibodies used in these experiments, it appears that HMPV utilizes α5β1, αvβ3, and other integrin heterodimers containing the αv integrin subunit during infection of LLC-MK2 cells.

I repeated the integrin blockade experiments described above to confirm that HMPV infection of human bronchial epithelial (BEAS-2B) cells also depends upon RGD-binding integrins. I hypothesized that if HMPV F were capable of binding to different integrin heterodimers, I might observe different results when integrins on the surface of BEAS-2B cells were blocked during HMPV infection. HMPV infection of BEAS-2B cells was significantly inhibited in the presence of function-blocking antibodies directed against αV, α5, and β1 integrin subunits (Fig. 2-3). While blockade of

αvβ5 resulted in ~30% reduced infectivity, blocking αvβ3 had no effect on HMPV infection of BEAS-2B cells. Combination blockade of αv subunits with either α5 or β1 integrin subunits resulted in 90% reduced HMPV infectivity. These data suggest that a cell surface interaction between HMPV and various RGD-binding integrins is required for HMPV infectivity, and that HMPV F can utilize different RGD-integrin heterodimers during infection.

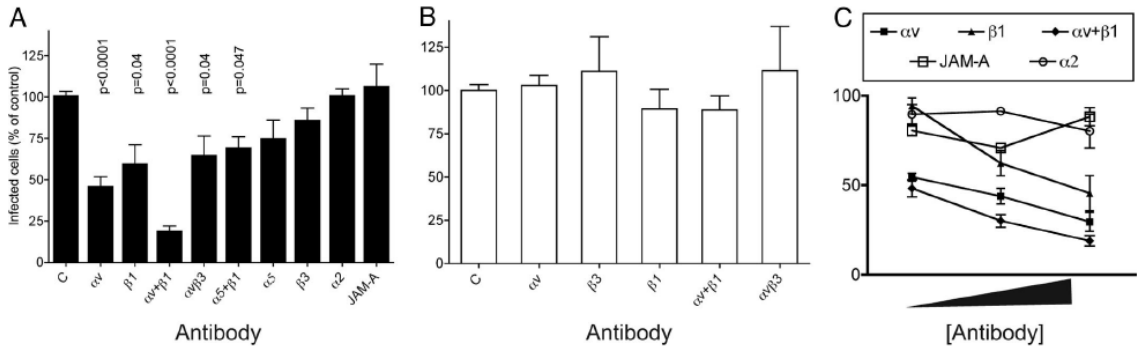

Fig. 2-2. Integrin function-blocking antibodies inhibit HMPV infection.
LLC-MK2 cells were incubated with the integrin function-blocking or control antibodies shown before adsorption with either HMPV (A, black bars) or hRSV (B, white bars). Infected cells were identified by indirect immunostaining. C indicates untreated controls. (C) LLC-MK2 cells were preincubated with increasing concentrations of the antibodies shown, adsorbed with HMPV, and scored for infection by indirect immunostaining. Black triangle represents increasing antibody concentration. Results are expressed as the mean percentage of infected cells following antibody treatment compared with the mean percentage of infected control cells for at least three independent experiments performed in triplicate. Error bars = SEM. Only *P* values < 0.05 (Student's *t* test) are shown. Antibody concentrations in A and B: αv (7.5 μg/mL); β1 (4 μg/mL); αvβ3 (20 μg/mL); α5 (2 μg/mL); β3 (20 μg/mL); α2 (20 μg/mL); and JAM-A (20 μg/mL). Antibody concentrations in C: JAM-A (5, 10, and 20 μg/mL), α2 (5, 10, and 20 μg/mL), αv (3.75, 7.5, and 15 μg/mL), and β1 (1, 2, and 4 μg/mL).

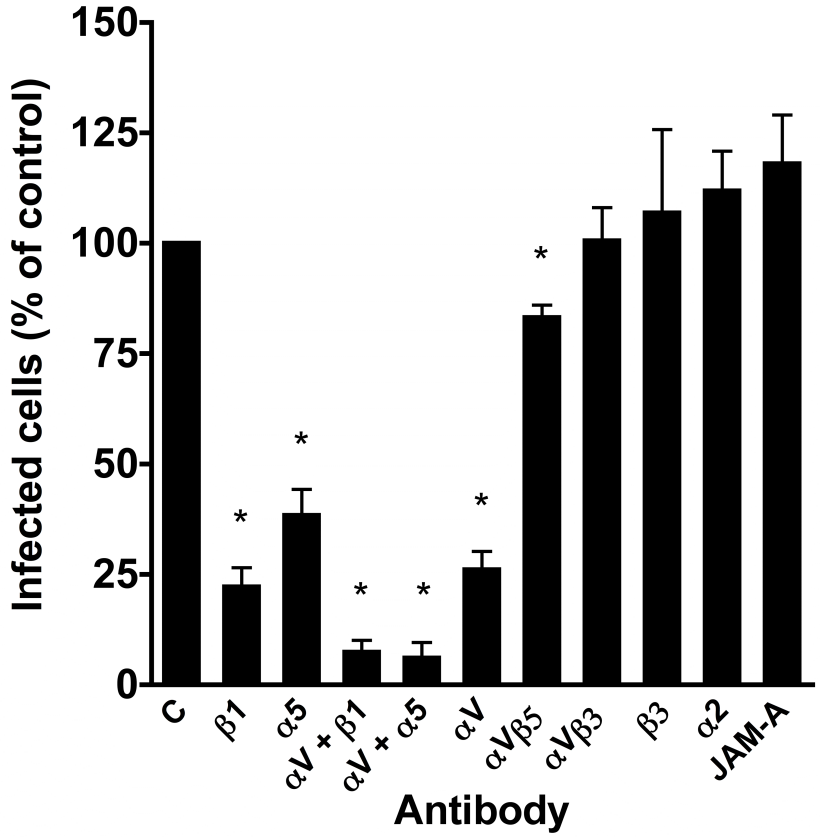

Fig. 2-3. RGD-binding integrins promote HMPV infection of BEAS-2B cells. BEAS-2B cells were incubated with integrin function-blocking or control antibodies before adsorption with HMPV. Infected cells were identified by indirect immunostaining. C indicates untreated control. Results are expressed as the mean percentage of infected cells following antibody treatment compared with the mean percentage of infected control cells for at least three independent experiments performed in triplicate. Error bars = SEM. *, $P < 0.05$ (Student's *t* test). Antibody concentrations: αv (40 μg/mL), β1 (12.5 μg/mL), αvβ3 (40 μg/mL), αvβ5 (40 μg/mL), α5 (14 μg/mL), β3 (40 μg/mL), α2 (40 μg/mL), and JAM-A (20 μg/mL).

Reduced expression of αv and β1 integrins decreases HMPV infectivity. To determine whether diminished integrin expression limits HMPV infection, I transfected BEAS-2B cells with siRNAs specific for αv, β1, or both integrin subunits to reduce integrin expression before HMPV or hRSV binding. Transfection with these siRNAs reduced cell-surface expression of αv and β1 integrins in the majority of the cells (Fig. 2-4), although a small subset of cells appeared to exhibit increased β1 integrin surface expression (Fig. 2-4D and F). As controls, mock transfection or transfection with nonspecific siRNA did not diminish cell-surface expression of αv or β1 integrin. The siRNA-transfected cells were adsorbed with HMPV or hRSV and scored for infectivity by immunostaining. The αv and β1 integrin-specific siRNAs decreased HMPV infectivity by 26% and 35%, respectively (Fig. 2-4G). Transfection of cells with both αv and β1 integrin-specific siRNA exhibited the most potent inhibitory effect, reducing infection by ~65% (Fig. 2-4G, black bar). In contrast, mock transfection or transfection of cells with nonspecific control siRNA did not affect HMPV infection. Consistent with results of experiments using integrin-specific antibodies, none of the transfected siRNAs (control or integrin-specific) inhibited hRSV infectivity (Fig. 2-4H). In fact, we detected an increase in hRSV-infected cells following treatment with integrin-specific siRNAs. We speculate that this effect is attributable to altered cell morphology or cytoskeletal rearrangements that serve to promote hRSV infection (Kallewaard et al., 2005).

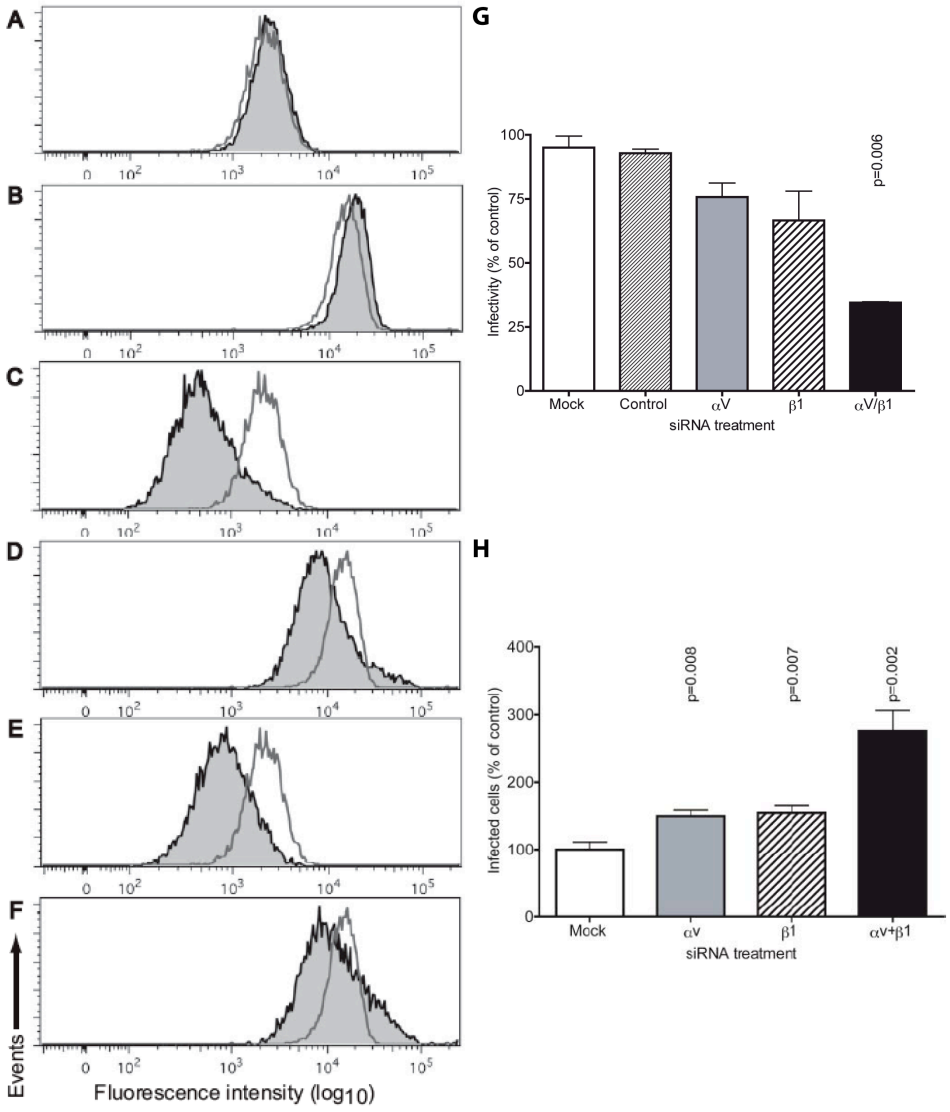

Fig. 2-4. Reduced expression of RGD-binding integrins decreases HMPV infectivity. (A-F) Reduction of cell surface integrin expression by siRNA. BEAS-2B cells were transfected with non-specific control siRNA or siRNAs specific for αV, β1, or both integrin subunits. Cells were stained 48h after siRNA transfection for surface expression of integrins. Open histograms indicate non-transfected cells. Shaded histograms indicate siRNA transfected cells. (A) non-specific control siRNA; stained for αV integrin. (B) non-specific control siRNA; stained for β1 integrin. (C) αV-specific siRNA; stained for αV integrin. (D) β1-specific siRNA; stained for β1 integrin. (E) αV- and β1-specific siRNA; stained for αV integrin; (F) αV- and β1-specific siRNA; stained for β1 integrin. (G and H) siRNA-treated cells were inoculated with either HMPV (G) or hRSV (H) and infected cells were identified after 24h by indirect immunostaining. Results are expressed as the mean percentage of infected cells following siRNA treatment compared with the mean percentage of infected control cells for at least three independent experiment performed in triplicate. Error bars = SEM.

BEAS-2B cells transfected with integrin-specific siRNAs had, on average, less integrin expression, but the level of αV and β1 integrin expression on the cell surface was heterogeneous and variable. Thus, I sought to determine whether the relative level of integrin expression correlated with HMPV infectivity. I repeated the above experiments, but stained HMPV-infected cells for analysis by flow cytometry. I transfected cells with either a non-specific control siRNA (control) or a combination of αV- and β1-specific siRNAs, inoculated cells with HMPV at a multiplicity of infection of 1 pfu/cell, and after 24 h stained the cell surface for αV integrin expression, β1 integrin expression, and HMPV F expression (a marker for HMPV infection). Based upon cell surface expression of αV and β1 integrin subunits, I defined three populations of cells that represented different levels of RGD-binding integrin expression (Fig. 2-5A). The first cell population was defined as αVhi/β1hi, and contains cells with normal high expression levels of both integrin subunits. The second cell population was defined as αVhi/β1lo, and represents a small subset of cells in the control siRNA treated cells, but the majority of cells in the integrin-specific siRNA treated cells. The third cell population was defined as αVlo/β1lo, and only contained a substantial number of cells after integrin-specific siRNA treatment (Fig. 2-5A). I observed a strong correlation between HMPV infectivity and RGD-binding integrin expression (Fig. 2-5B). In the control cells, ~50% of αVhi/β1hi cells and ~85% of αVhi/β1lo cells were infected. However, siRNA-mediated reduction in β1 expression (αVhi/β1lo), or reduced expression of both αV and β1 (αVlo/β1lo), resulted in significantly less HMPV-infected cells (85% versus 56% and 41%, respectively). Furthermore, HMPV preferentially infected cells with higher levels of αV and β1 expression. Compared to αVhi/β1hi cells present in the same well, αVlo/β1lo cells were

~50% less likely to be infected ($p = 0.005$). The additive effect from loss of both αV and β1 integrin subunit expression further supports our evidence that multiple integrin heterodimers (containing either αV or β1 subunits) promote HMPV infection. Therefore, reducing cell-surface expression of RGD-binding integrins with either the αv or β1 subunit reduces the efficiency of HMPV infection.

Transfection of αv and β1 integrins enhances HMPV infectivity. Chinese hamster ovary (CHO) cells are poorly permissive for HMPV infection. Following adsorption at equivalent multiplicity of infection, 80% fewer CHO cells are infected by HMPV compared with LLC-MK2 cells (Fig. 2-6, light gray vs. white bars). To complement the loss-of-function experiments described thus far, we tested whether transfection of CHO cells with cDNAs encoding human αV or β1 integrin subunits alters the infectivity of HMPV. Expression of human αV or β1 integrin subunits in CHO cells substantially increased the efficiency of HMPV infection (Fig. 2-6). Expression of αV integrin increased HMPV infection by 2-fold, and expression of β1 integrin increased infection by 3-fold. The increased efficiency of HMPV infection of human integrin-transfected CHO cells was inhibited by preincubation with αV and β1 integrin function-blocking antibodies (Fig. 2-6). Thus, human αV and β1 integrin expression enhances the efficiency of HMPV infection of CHO cells, and blockade of these integrins reduces the magnitude of this effect.

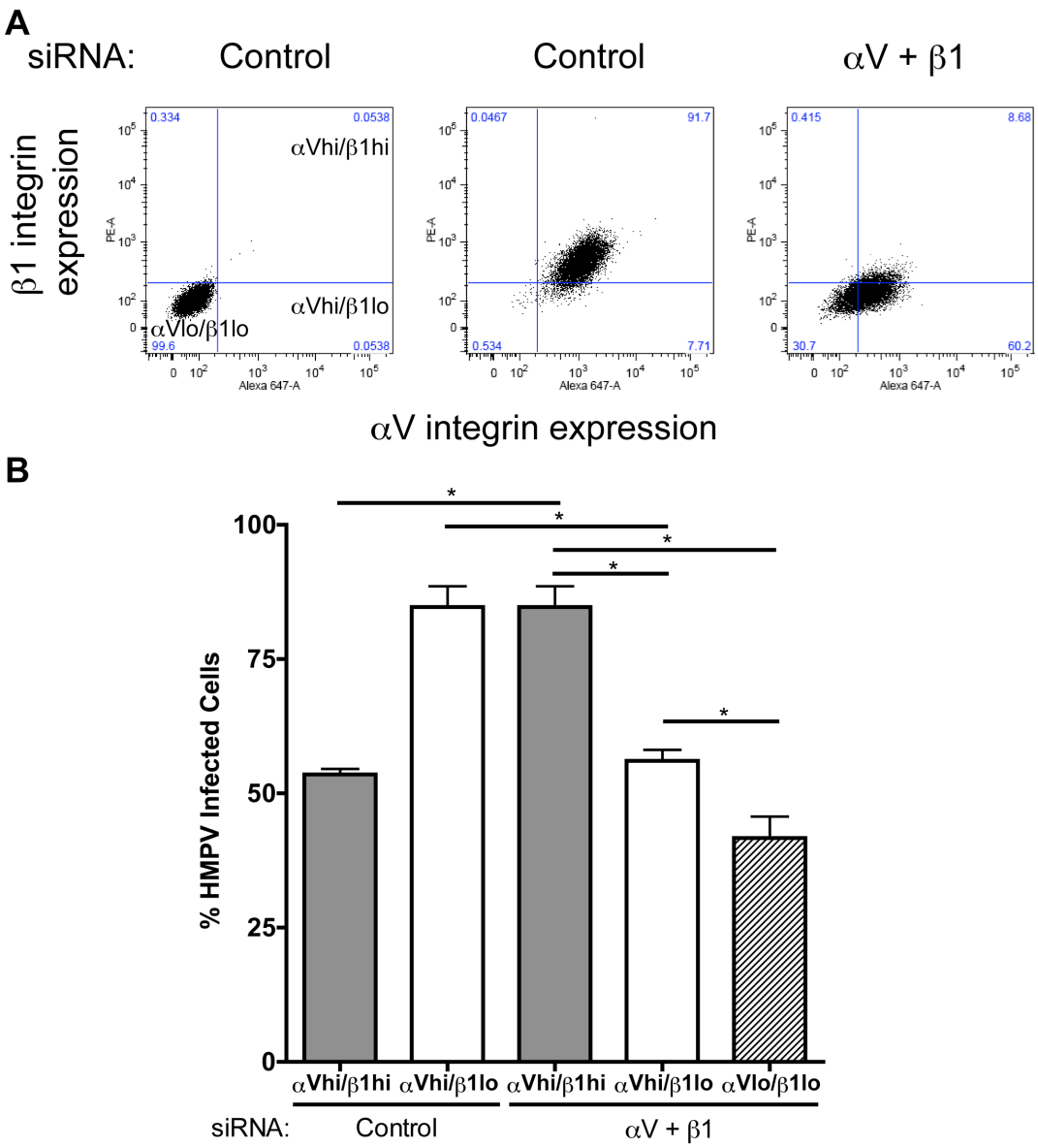

Fig. 2-5. HMPV preferentially infects cells with higher RGD-binding integrin expression.
(A) Reduction of cell surface integrin expression by siRNA. BEAS-2B cells were transfected with non-specific control siRNA (Control) or siRNAs specific for both αV and β1 integrin subunits. Cells were infected with HMPV 48h after siRNA transfection, and stained for surface expression of integrins and HMPV F 24h after infection. Representative flow cytometry dot plots showing the relative surface expression of αV integrin (x-axis) and β1 integrin (y-axis) are shown with the gates used to define three populations of cells that have different levels of integrin expression. Left panel represents unstained cells used to define αVhi/β1hi, αVhi/β1lo, and αVlo/β1lo gates. (B) HMPV infection rates of the different populations of cells defined by the gates shown in (A). Results are expressed as the mean percentage of infected cells in each gate for three biological replicates; Error bars = SEM. *, $P < 0.05$ (Student's *t* test).

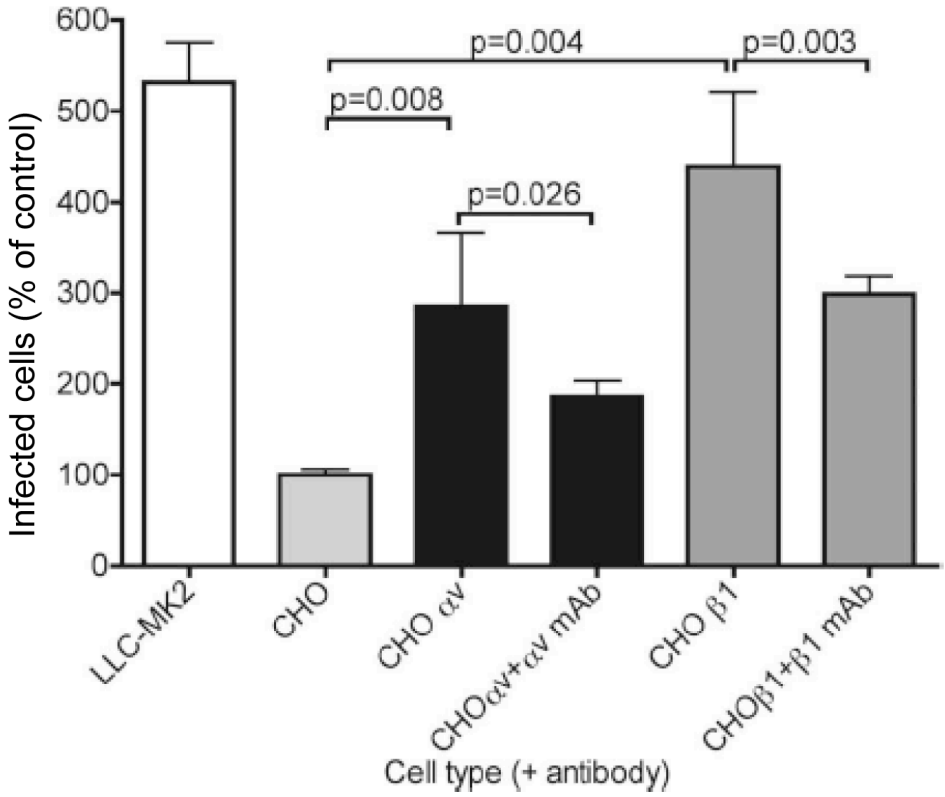

Fig. 2-6. Transfection of αv and β1 integrins enhances HMPV infectivity.
CHO cells were transfected with expression plasmids encoding either human αV (CHO αV) or human β1 (CHO β1) integrin, with and without additional incubation with function-blocking antibodies specific for human αV (CHO αV + αV mAb) or human β1 (CHO β1 + β1 mAb), before adsorption with HMPV. Surface expression of human αV or β1 integrin was confirmed by flow cytometry (data not shown). Infected cells were identified by indirect immunostaining. Results are expressed as the mean percentage of infected cells following transfection of integrin cDNA compared with the mean percentage of infected control cells for at least three independent experiments performed in triplicate. Error bars = SEM. Only *P* values < 0.05 (Student's *t* test) are shown.

Binding of HMPV F protein to LLC-MK2 cells is mediated by the RGD motif.

To determine whether a soluble fragment of HMPV F protein is capable of binding to permissive cells, LLC-MK2 cells were incubated with FΔTM protein, and binding was detected by flow cytometry. In contrast to LLC-MK2 cells incubated with primary and secondary antibodies alone (Fig. 2-7A, LLC panel), LLC-MK2 cells incubated with FΔTM protein and stained using HMPV-specific antibody showed a significant increase in fluorescence, indicating that FΔTM is capable of binding these cells (Fig. 2-7A, F panel). As a critical specificity control, a mutant form of FΔTM protein in which the RGD motif was altered to Arg-Gly-Glu (RGE) demonstrated significantly less binding to LLC-MK2 cells (Fig. 2-7A, F RGE panel). Furthermore, wild type FΔTM protein showed minimal binding to CHO cells (Fig. 2-7A, CHO panel), suggesting that the limited infection of CHO cells by HMPV is attributable to diminished interactions of F with a cell-surface receptor. To quantify F protein binding to cells, we calculated the percentage of cells contained within identical gates of the flow cytometric profiles. Percent binding as determined by fluorescence intensity differed significantly between CHO cells incubated with FΔTM protein, LLC-MK2 cells incubated with buffer alone or mutant F-RGEΔTM, and LLC-MK2 cells incubated with FΔTM protein (Fig. 2-7B). Thus, soluble F protein binds to cells expressing human αV and β1 integrin subunits in a manner dependent on the RGD motif.

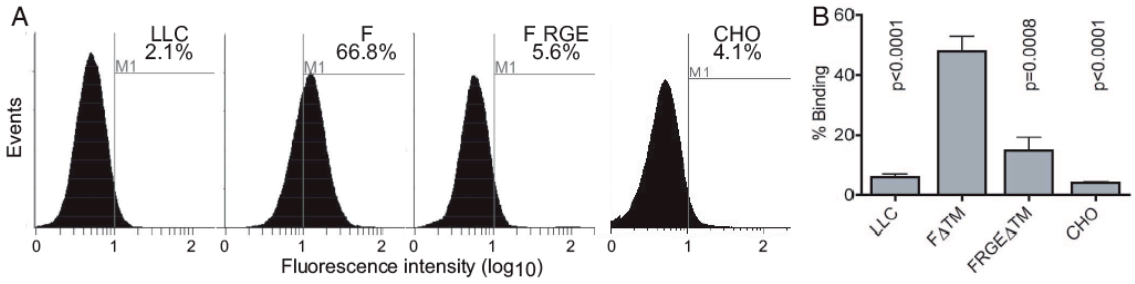

Fig. 2-7. HMPV F protein binding to LLC-MK2 cells is mediated by the RGD motif. (A) LLC-MK2 cells were incubated with buffer alone (LLC), FΔTM protein (F), or RGE mutant FΔTM protein (F RGE) or CHO cells were incubated with FΔTM protein (CHO). Cells were stained with guinea pig anti-HMPV antibody and AlexaFluor-568 anti-guinea pig Ig and analyzed by flow cytometry. (B) The results are presented as the mean percentage of events within the gate region (M1) indicative of binding from four independent experiments conducted as in (A). The M1 gate region was set at the first decade of fluorescence for all experiments. Error bars represent the SEM. Only *P* values < 0.05 (Student's *t* test) are shown.

Discussion

The HMPV F protein contains an RGD motif that is absolutely conserved, along with 5 N- and 16 C-terminal flanking residues, among 71 clinical isolates collected over a 20-year period throughout the world. The observed sequence conservation suggests that this region serves an important biological function in HMPV infection, as F is the major antigenic target and subject to variation in other domains (Bastien et al., 2003; Biacchesi et al., 2003; Ishiguro et al., 2004). The structure of HMPV F has recently been elucidated, and the RGD sequence is solvent-exposed, as predicted based upon homology to other paramyxovirus F protein structures (Lamb et al., 2006; Miller et al., 2007; Wen et al., 2012). Thus, the tripeptide motif is exposed on the surface of HMPV F where it could potentially interact with integrin receptors present on the cell surface. Treatment of cells with EDTA, which inhibits integrin function, potently decreased HMPV infectivity while showing no effect on infection by hRSV. Furthermore, RGD peptides inhibited HMPV at sub-micromolar concentrations, whereas RGE peptides had a minimal effect that was not statistically significant. The degree of inhibition was modest, but it is noteworthy that similar levels of inhibition for other viruses often require millimolar concentrations of peptide (Akula et al., 2002; Guerrero et al., 2000; Jackson et al., 2002; Pulli et al., 1997; Williams et al., 2004a).

Integrin-specific function-blocking mAbs exhibited potent inhibition of HMPV infection, with antibodies specific for αv and β1 integrin subunits showing the greatest effect, both independently and in combination. The additive effect of combination blockade suggests that integrin heterodimers containing αV or β1 subunits collectively promote HMPV infection of both LLC-MK2 and BEAS-2B cells. Taken together, our

results suggest that HMPV infection depends upon α5β1 and integrin heterodimers containing the αv subunit, which may vary based upon cell type as αvβ3 appears to be important for HMPV infectivity in LLC-MK2 cells but not BEAS-2B cells. The specific αv heterodimers may include αvβ3, αvβ5 (confirmed for BEAS-2B cells), αvβ6, αvβ8, and/or αvβ1. Importantly, the results suggest that HMPV infection is promoted by multiple RGD-binding integrins that appear to serve a redundant role during virus infection. Such is the case with foot-and-mouth-disease virus, which preferentially utilizes αvβ3 integrin as a receptor but is also capable of using αvβ1 and αvβ6 (Berinstein et al., 1995; Jackson et al., 2002; Jackson et al., 2000; Retta et al., 2001).

Further evidence for the utilization of RGD-binding integrins by HMPV comes from complementary approaches to alter the expression of αv and β1 integrin subunits. Diminished surface expression of both molecules by RNA interference resulted in significant inhibition of HMPV infection. Importantly, control siRNA had no effect on either integrin expression or HMPV infectivity. Moreover, the integrin-specific siRNAs tested here did not inhibit hRSV infectivity, suggesting that dampened HMPV growth is not attributable to a nonspecific effect of siRNA treatment (Retta et al., 2001). A small number of siRNA-treated cells exhibited increased surface expression of β1 integrin, possibly via dysregulation of integrin homeostatic networks, altered β1 integrin mRNA transcription, or β1 integrin pairing with alternate α subunits (Koistinen and Heino, 2002; Retta et al., 2001). Therefore, we may have underestimated the effect of siRNA-mediated knockdown of integrin expression on HMPV infection. In concordance with the siRNA experiments, transient transfection of CHO cells with human αv or β1 integrin allowed HMPV to infect these poorly permissive cells. Despite expressing hamster αv and β1

integrins (Bretscher, 1989; Brown and Juliano, 1988; Giancotti and Ruoslahti, 1990; Wang and Bergelson, 1999), CHO cells are poorly permissive for HMPV infection. Our observations suggest that the hamster integrin subunits partner with the human integrin subunits to provide partial complementation of HMPV infectivity. Thus, it is possible that species-specific integrin expression is a host-range determinant for HMPV.

Recombinant HMPV F protein bound specifically to LLC-MK2 but not to CHO cells, an effect that was abrogated by mutation of the RGD motif to RGE. Although we have not demonstrated direct binding of virus or F protein to an integrin heterodimer, our data strongly suggest that the F protein interacts directly with RGD-binding integrins. Results reported here do not define the precise step in HMPV infection mediated by RGD-binding integrins, although we hypothesize that integrins serve as receptors for F during virus entry. As most of the experiments we performed measured viral protein expression in infected cells, an alternative possibility is that integrin expression increases viral transcription and translation rather than mediating attachment or cell entry. However, the F ectodomain protein binding data demonstrate that F binding to cells is RGD-dependent. Based on the established function of integrins as receptors for other viruses, we favor a role for integrins in initiating the process of infection. For the analogous HIV class I fusion protein, gp120/gp41, binding to primary receptor (i.e., CD4) and co-receptor (i.e., CCR5) triggers the conformational changes associated with virus-cell membrane fusion (Chan and Kim, 1998), an event that occurs rapidly (Carr and Kim, 1993; Gallo et al., 2006). Influenza virus HA-mediated fusion occurs within endosomes and is triggered by low pH (Carr and Kim, 1993). Paramyxovirus fusion is thought to occur at the cell surface at neutral pH (Colman and Lawrence, 2003). We

speculate that HMPV F protein binding to RGD-binding integrins initiates the conformational changes that lead to fusion at either of these sites.

Our results indicate that RGD-binding integrins are required for efficient HMPV infection. Blockade of cell-surface RGD-binding integrins inhibits HMPV infectivity, and expression of αv or β1 integrin subunits allows nonpermissive cells to be infected. The HMPV F protein binds specifically to cells, and alteration of the RGD motif abolishes this interaction. Collectively, these data suggest that RGD-binding integrins are functional HMPV receptors, serving as receptors for the fusion protein. These findings extend the widening role of integrins as receptors for intracellular microbial pathogens and provide potential therapeutic targets for HMPV.

CHAPTER III

DEVELOPMENT OF ASSAYS TO MEASURE HMPV BINDING AND FUSION

Introduction

When I began my thesis research in the Williams laboratory, I was very interested in understanding how the HMPV F protein mediated membrane fusion. Specifically, I sought to elucidate whether binding to integrins induced conformational changes in the F protein that promoted refolding, initiated fusion, and led to virus entry. However, there were no established assays to test these important questions. Investigating HMPV entry presented methodological challenges because both attachment and fusion are necessary for virus entry; therefore, a complete understanding of virus entry required assays that quantify binding and measure fusion.

I spent several years developing methods to test HMPV fusion. My initial efforts involved developing a cell-cell fusion assay, similar to assays that others in the field were using to measure F-mediated fusion. Despite promising preliminary results, it became clear that the HMPV F proteins I was using did not strongly promote cell-to-cell fusion. I tested several different measures of content-mixing with similar (poor) results before I decided to switch directions and investigate particle-based assays. I thought that a particle-based assay would have a few advantages over a cell-cell fusion assay because i) a particle-based assay would allow me to quantify virus binding whereas a cell-cell fusion assay does not, ii) particle-based fusion assays allow measurement of both fusion kinetics and fusion extent while cell-cell fusion assays only detect differences in fusion

extent, and iii) particle fusion would provide a direct measure of virus-cell fusion, reflecting the actual virus entry process. After testing several different assays that again produced poor results, I decided to test a methodology that was pioneered by Dick Hoekstra in the 1980s (Hoekstra et al., 1984). Hoekstra's approach was to load virus particles with a self-quenching fluorescent dye and measure changes in fluorescence that occurred during virus-cell membrane fusion. This methodology, described in detail in this chapter, provided me with dynamic assays to study HMPV binding and fusion. Because this methodology has not been used extensively to study paramyxovirus fusion and had never been utilized to study HMPV fusion, I think that a detailed description of the assay development is warranted.

During my efforts to develop an HMPV fusion assay, I sought assistance from many colleagues. I am particularly grateful to Dr. Christopher Aiken for generously assisting me with a pseudovirus approach and a senior scientist in his laboratory, Jiong Shi, who provided me with reagents, guidance, and completed experiments for me. Although the approach we tested was not successful, it was these studies that led me to explore developing HMPV virus-like particles (VLPs) as a research tool. The development of HMPV VLPs and their utility in the study of HMPV binding and fusion will also be discussed in this chapter.

Materials and Methods

Design of R18-labeled virus particles. Enveloped virus particles can be fluorescently labeled via three strategies: packaging a fluorescent molecule inside the virion, covalently conjugating a fluorophore to structural proteins in the virion, or incorporating a

fluorescent dye into the virion's lipid bilayer. Octadecyl rhodamine B chloride (R18) (Fig. 3-1) is a lipophilic dye that can insert a long alkyl chain into the outer lipid layer of a virus particle. R18 molecules are capable of incorporating into virus particles at concentrations that are high enough to self-quench the fluorescent probe (Hoekstra et al., 1984; Pedroso de Lima et al., 1992; Razinkov et al., 2001; Srinivasakumar et al., 1991).

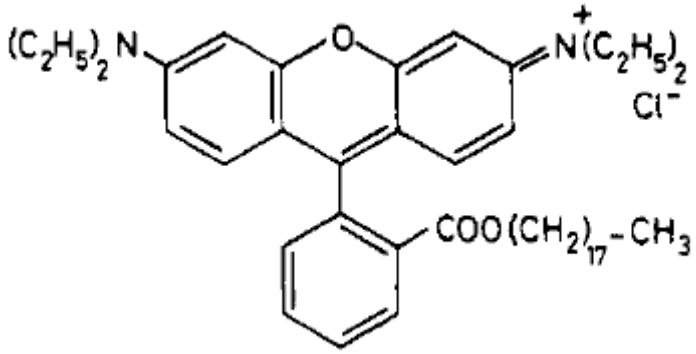

Fig. 3-1. Structure of Octadecyl Rhodamine B chloride (R18).

To label HMPV with R18, I modified a method used by Hoekstra et al. (Hoekstra et al., 1984). First, I purified HMPV through a 20% sucrose cushion via ultracentrifugation at 100,000 x g for 90 min at 4°C and resuspended the white virus pellet into a buffered (pH 7.4) solution containing 0.1 M $MgSO_4$, 50 mM HEPES, and 150 mM NaCl. I determined the total viral protein concentration of the solution, and added R18 dissolved at 10 mM in ethanol to the purified virus suspension at 20 nmol R18 per mg total virus protein for 1h at room temperature. When an ethanolic solution of R18

is added to the suspended virus particles, the amphiphilic R18 dye spontaneously incorporates into the virus membrane (Hoekstra et al., 1984). To remove any unincorporated dye, I pelleted the reaction mixture through a discontinuous 20/60% sucrose gradient by ultracentrifugation at 100,000 x g for 90 min at 4°C. The R18-labeled virus was pink by visible light and pelleted to the 20/60% sucrose interface. R18 incorporated into virus particles in a quenched state, because adding detergent to R18-labeled HMPV resulted in a 6-fold increase in R18 fluorescence. Attempts to label HMPV with higher concentrations of R18, e.g. 40 to 160 nmol R18 per mg of total virus protein, resulted in free unincorporated dye that was difficult to remove from the purified virus by ultracentrifugation, substantial virus particle aggregation during the labeling reaction, and viruses with altered plaque phenotypes after purification. Thus, I concluded that 20 nmol R18 per mg of virus protein was the best labeling condition. R18-labeled HMPV (R18-MPV) had equivalent titers to HMPV preparations prepared in parallel with equivalent volumes of ethanol without R18. Typical virus titers of 1×10^6 to 5×10^8 pfu/mL were achieved depending upon the volume of virus that was R18-labeled and purified.

Development of HMPV binding assay. I used the R18-labeled virus particles to develop a fluorescence-based assay to quantify HMPV binding independently of fusion and infection. To measure binding, R18-MPV was bound to cells, the unbound particles were washed away, the cells were solubilized in detergent, and R18 fluorescence (excitation, 544 nm; emission, 590 nm) was measured using a SpectraMax M5 (Molecular Devices) plate reader. R18-MPV binding resulted in a dose-dependent

increase in fluorescence intensity that directly correlated with infectivity (Fig. 3-2), confirming that the assay measured productive virus binding to human bronchial epithelial (BEAS-2B) cells. Furthermore, the R18 signal measured in the binding assay directly correlated with the amount of cell-associated HMPV F protein after virus binding, as detected by Western blot analysis (Fig. 3-3).

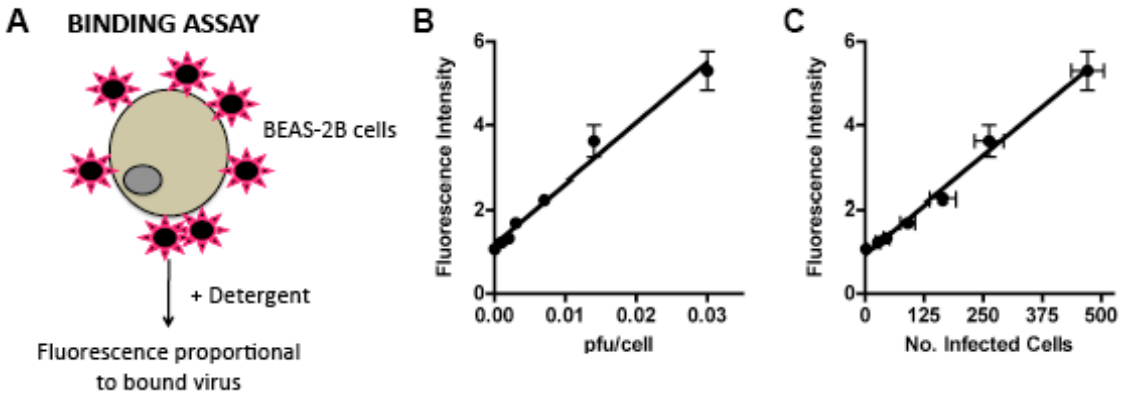

Fig. 3-2. A fluorescence-based assay to quantify HMPV binding.
(A) Schematic of HMPV binding assay. R18-MPV was bound to cells on ice to prevent virus fusion. Adding detergent chemically dequenched the R18 dye associated with virus membranes, resulting in measurable fluorescence proportional to the amount of virus bound to cells. (B) R18-MPV binding to human bronchial epithelial (BEAS-2B) cells results in a linear increase in fluorescence (slope = 144.1 ± 8.8; r^2 = 0.9817). Binding was measured as fluorescence of cell-bound virus after addition of 1% Triton X-100. Results are means ± standard errors of the means (SEM) for three independent experiments performed in triplicate. (C) R18-MPV binding correlates with infectivity (slope = 0.009 ± 0.0004; r^2 = 0.9910). R18-MPV binding was assessed as for panel B; identical wells were incubated at 37°C in culture medium, and HMPV-infected cells were identified by indirect immunostaining and enumerated at 24 h postbinding. Results are means ± SEM for three independent experiments performed in triplicate.

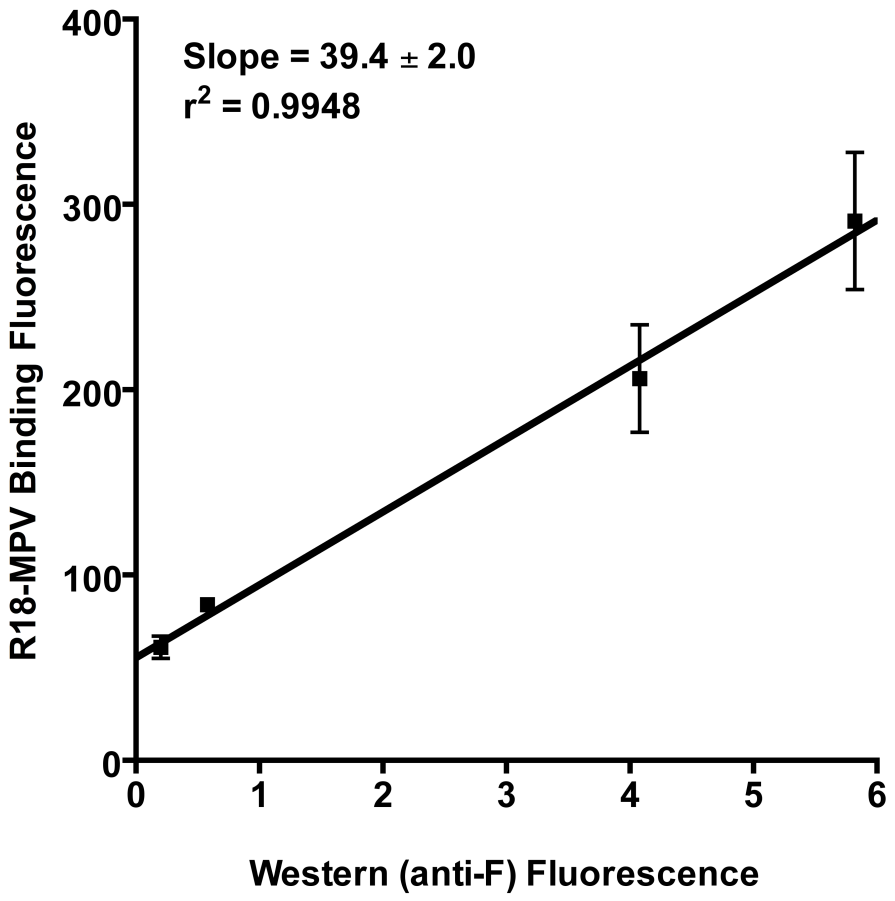

Fig. 3-3. Fluorescence intensity of R18-MPV binding correlates with HMPV F associated with cells postbinding.
Serial dilutions of R18-MPV were bound to cells on ice to prevent virus fusion. Triplicate wells were analyzed for R18 fluorescence by adding detergent and measuring R18 fluorescence intensity (y-axis). Cells in four replicate wells were solubilized in cell lysis buffer and analyzed by Western blot analysis. Proteins were separated by SDS-PAGE, transferred to PVDF membranes, and immunoblotted for HMPV F with an F-specific mAb and Cy5-conjugated secondary antibody. Membranes were washed with PBS and dried. Bands were imaged and quantified using an Odyssey infrared imaging system (Li-Cor). The fluorescence intensity of the F band from the Western blot analysis is shown on the x-axis.

To confirm the specificity of the binding assay, I tested whether R18-MPV binding could be inhibited with HMPV-specific antiserum or unlabeled virus. Neutralizing HMPV-specific antiserum inhibited R18-MPV binding in a dose-dependent manner (Fig. 3-4A). Increasing amounts of antibody were capable of blocking R18-MPV binding, with the highest dose inhibiting binding by ~75%. These results suggest that the R18 fluorescence signal detected with the binding assay is specifically due to virus particles binding to the cell surface. R18-MPV binding was also significantly inhibited by unlabeled HMPV (Fig. 3-4B). R18-MPV binding decreased in a dose-dependent manner when increasing numbers of unlabeled HMPV competed for binding sites on the cell surface. An inhibition of ~70% was achieved when 28-fold more unlabeled particles were mixed with the R18-labeled virus during binding. These results confirm that R18-MPV competes for the same receptor sites on the cell surface as unlabeled virus.

Collectively, the experiments described in this section confirm that the new binding assay accurately reflected the extent of HMPV binding to the cell surface. Furthermore, specific inhibitors of HMPV binding are capable of inhibiting the R18 fluorescence signal measured by the binding assay. Thus, the R18-MPV binding assay can be used to identify regions of the F protein that are necessary for virus binding and screen for inhibitors of HMPV binding.

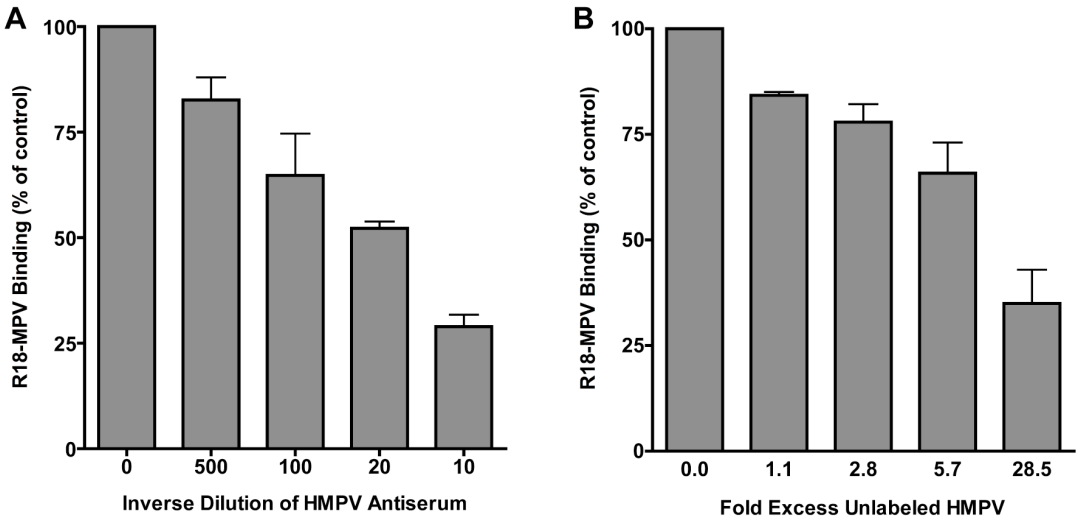

Fig. 3-4. R18-MPV binding is inhibited by HMPV-specific neutralizing antiserum and unlabeled virus.

(A) Neutralizing HMPV-specific antiserum inhibits R18-MPV binding in a dose-dependent manner. R18-MPV was incubated with serial dilutions of a potent anti-HMPV antiserum for 30 min at room temperature. Virus-antiserum mixtures were added to suspension 293-F cells in triplicate in a 96-well plate. Virus was allowed to bind for 1 h on ice before cells were washed twice with ice-cold PBS to remove unbound virus. Binding was measured as fluorescence of cell-bound virus after addition of 1% Triton X-100. Results (mean ± SD) for a representative experiment are shown. (B) R18-MPV was mixed with increasing amounts of unlabeled, sucrose-purified HMPV. Virus mixtures were added to suspension 293-F cells in triplicate in a 96-well plate. Virus was allowed to bind for 1 h on ice before cells were washed twice with ice-cold PBS to remove unbound virus. Binding was measured as fluorescence of cell-bound virus after addition of 1% Triton X-100. Results (mean ± SD) for a representative experiment are shown. The fold excess of unlabeled virus was based upon plaque titers of R18-MPV and unlabeled HMPV.

Development of HMPV fusion assay. I also used the R18-labeled virus particles to develop a fluorescence-based assay to quantify HMPV fusion. The principle of the R18-MPV fusion assay is based upon the self-quenching properties of R18. When inserted into the viral membrane at high concentrations, R18 fluorescence self-quenches. When R18-MPV fuses with an unlabeled cell membrane, the R18 dye redistributes into the target cell membrane resulting in a relief of self-quenching (R18 dequenching) that results in increased fluorescence that can be measured quantitatively. By adding detergent, at the end of the experiment, the remaining R18 probe is chemically dequenched and the fluorescence intensity reflects the total amount of R18 dye associated with the virus membrane. Thus, percent R18 dequenching can be calculated at any time during the fusion assay according to the following equation:

$$\% \text{ R18 dequenching} = 100 \times (F - F_0)/(F_d - F_0),$$

where F is fluorescence, F_0 is fluorescence at t = 0 min, and F_d is fluorescence after the addition of Triton X-100 (at the end of the experiment).

To measure fusion, I incubated cells with R18-MPV at 4°C, washed away unbound virus, added fresh cell culture medium (without phenol red), and incubated cells at 37°C, monitoring R18 fluorescence in real time. I tested the fusion assay in either 48- or 96-well plates, and confirmed that either adherent or suspended cells could be used to obtain fluorescence measurements. The plate-based format allowed for kinetic measurement of fluorescence intensity (excitation, 544 nm; emission, 590 nm) using a plate reader equipped with temperature control. I tested various plate reader settings and found that top-read and bottom-read fluorescence readings generated equivalent R18 dequenching curves during R18-MPV fusion with cells. HMPV fusion kinetics were

similar when monitored in either clear 48-well plates or black (opaque) transparent-bottom 96-well plates, indicating that cross talk between adjacent wells did not significantly affect fluorescence readings for this assay. Fig. 3-5 shows a schematic of the fusion assay (Fig. 3-5A) and representative results from a typical fusion experiment (Fig. 3-5B). R18-MPV fluoresced at a steady, low intensity in the absence of cellular membranes (Fig. 3-5B, gray diamonds); however, R18 fluorescence intensity dynamically increased when R18-MPV was bound to the surface of human embryonic kidney (293F) cells (Fig. 3-5B, black circles). After a brief delay, HMPV fusion occurred with steady kinetics for the first 90 min and the fusion rate slowed after 2 h, reaching a plateau around 4 h.

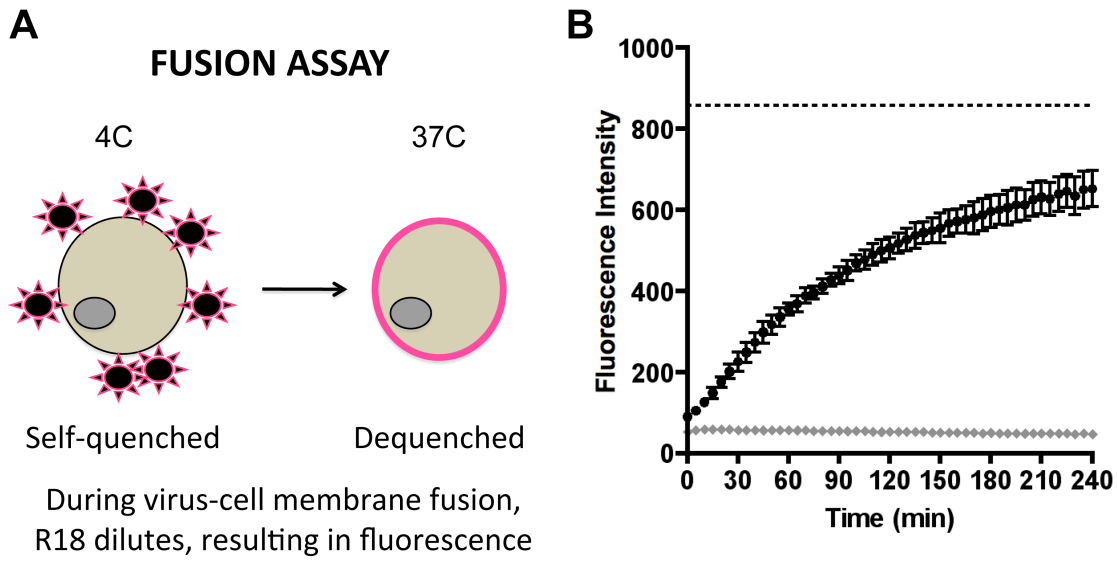

Fig. 3-5. HMPV fusion assay.
(A) Schematic of the HMPV fusion assay. (B) Representative fusion experiment. R18-MPV was adsorbed to the surface of suspension 293-F cells, the unbound virus washed away, and R18 fluorescence was monitored at 37°C in a 96-well plate for 4 h with measurements taken every 5 min. R18 fluorescence was measured for R18-MPV only (gray diamonds) or R18-MPV bound to 293 cells (black circles), demonstrating that fluorescence intensity increases only in the presence of target cell membranes. The hashed line represents total fluorescence of R18-MPV after the addition of 1% Triton X-100, maximal fluorescence intensity achievable. Results (mean ± SD) for triplicate wells are shown.

In principle, transfer of R18 from the virus membrane into an unlabeled cell membrane can occur during membrane fusion or via passive transfer of dye from virus to cell membrane. Various control experiments excluded the possibility that R18 dequenching in the HMPV fusion assay resulted from passive dye redistribution. First, heat inactivated R18-MPV does not fuse with cells. Paramyxovirus fusion proteins can be artificially triggered to refold into an inactive postfusion structure by heat (Bissonnette et al., 2006), such that heating virus at temperatures of 60 to 75°C results in inactivated particles that are no longer capable of mediating membrane fusion and infection. When HMPV is heated at 75°C for 15 min, the virus particles are completely inactivated and no longer infect cells. I heated R18-MPV at 75°C for 15 min and tested whether the virus could mediate fusion. I found that heat inactivated R18-MPV could bind to the cell surface, but not fuse with human bronchial epithelial (BEAS-2B) cells, even at high multiplicities of inoculation (Fig. 3-6). When heat inactivated R18-MPV was incubated with cells, R18 fluorescence intensity did not increase appreciably over time. Addition of detergent at the end of the experiment resulted in a 6-fold increase in fluorescence intensity (Fig. 3-6, indicated by arrow), confirming that the R18-MPV bound to cells remained in a quenched state during the 4 h experiment. This increase in fluorescence is precisely the level of quenching achieved during R18-labeling of HMPV. These results suggest that active HMPV fusion is required to observe increased R18 fluorescence intensity during the experiment, as observed in Fig. 3-5B. Further, the results argue against the possibility that R18 dye passively redistributes into cell membranes during the experimental time course.

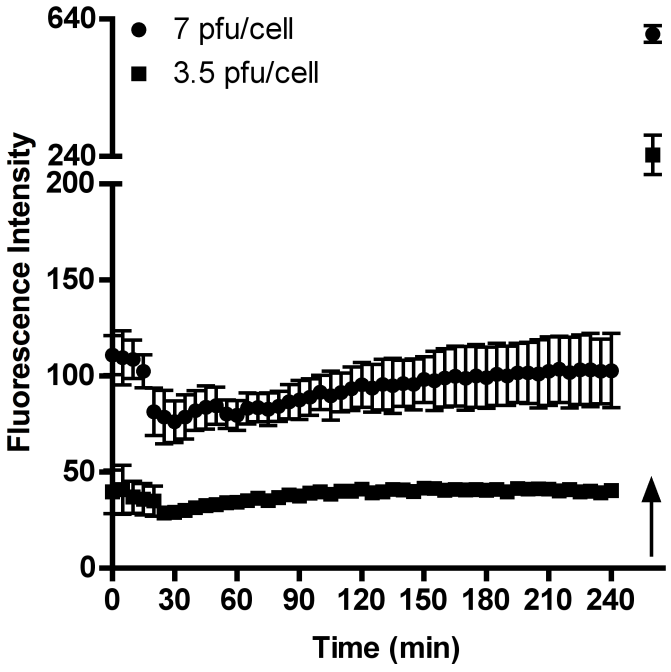

Fig. 3-6. Heat-inactivated R18-MPV binds to the surface of adherent cells, but does not mediate membrane fusion.
R18-MPV was heat inactivated at 75°C for 15 min and cooled to room temperature. Heat inactivated R18-MPV was incubated with adherent BEAS-2B cells at 3.5 pfu/cell (squares) or 7 pfu/cell (circles) on ice for 1 h to allow virus binding, and the unbound virus was washed away. R18 fluorescence was monitored at 37°C in a 96-well plate for 4 h with measurements taken every 5 min. Triton X-100 was added to cells (final concentration of 1%) at the time point indicated by the arrow and a final fluorescence reading was measured. Error bars represent standard deviation for triplicate measurements in a representative experiment.

Two other lines of evidence suggest that the increase in R18 fluorescence intensity I observed in the R18-MPV fusion experiments was due to active virus fusion, rather than passive dye transfer. First, I tested the capacity of HMPV-specific antiserum, one that recognizes the F protein but did not inhibit infection and another that recognizes F but potently neutralized infection (Fig. 3-7C), to inhibit R18-MPV fusion. I found that the neutralizing antiserum inhibited R18-MPV fusion in a dose-dependent manner (Fig. 3-7A), while the non-neutralizing antiserum did not inhibit R18-MPV fusion (Fig. 3-7B). The ability to inhibit R18-MPV fusion directly correlated with antiserum inhibition of infectivity, which would be expected if the fusion assay measures active virus-cell fusion required for virus entry and productive infection. These results demonstrate that R18-MPV does not fuse in the presence of neutralizing antiserum, and this can be accurately measured with the R18-dequenching-based fusion assay. I also tested whether unlabeled HMPV could compete with R18-MPV and inhibit fusion. I found that unlabeled HMPV could inhibit R18-MPV fusion in a dose-dependent manner (Fig. 3-8). These results indicate that increased R18 fluorescence observed in the fusion assay results from active virus fusion and can be diminished in the presence of unlabeled HMPV particles that are competing for binding sites on the cell surface.

Collectively, these experiments confirm that the R18-MPV fusion assay is measuring virus fusion. They do not exclude the possibility that R18 could be passively transferring into cell membranes too; however, the majority of the increase in R18 signal observed during the incubation of R18-MPV with cells at 37°C appears to reflect HMPV-to-cell fusion. Thus, the R18-MPV fusion assay can be used to identify regions in the F

protein that are critical for fusion activity, as well as screen for potential inhibitors of HMPV fusion.

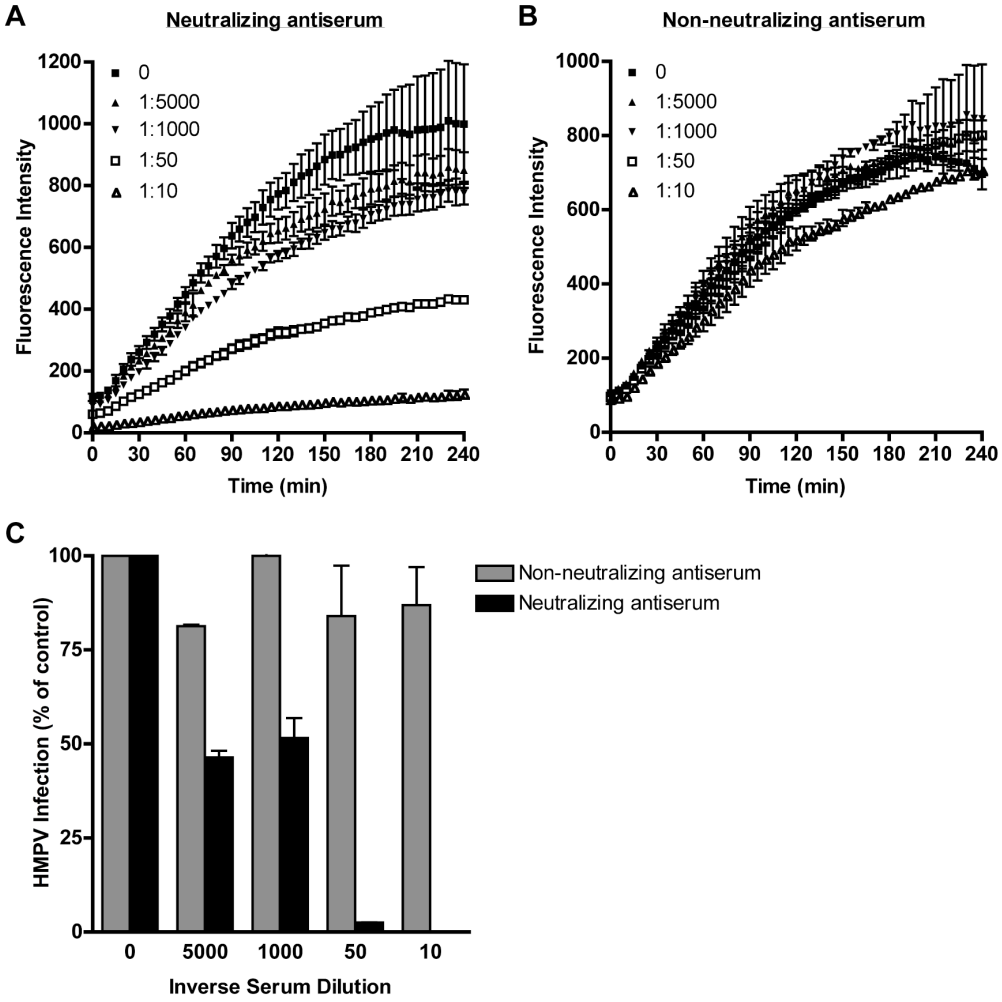

Fig. 3-7. R18-MPV fusion is inhibited by neutralizing antiserum but not by F-binding, non-neutralizing antiserum.
(A-B) R18-MPV was incubated with serial dilutions of either a potent anti-HMPV antiserum (A) or a non-neutralizing antiserum specific to HMPV F (B) for 30 min at room temperature. Virus-antiserum mixtures were allowed to bind suspension 293-F cells for 1 h on ice before cells were washed twice with ice-cold PBS and resuspended in fusion media in 96-well plates. R18 fluorescence for triplicate wells was monitored for 4 h at 37°C. Results (mean ± SD) for a representative experiment are shown.
(C) The ability of HMPV-specific antiserum to inhibit fusion correlates with neutralization of HMPV infection. R18-MPV was incubated with serial dilutions of antisera, as above, before infection of adherent BEAS-2B cells. At 24 hours postinfection, infected cells were identified by indirect immunostaining. Results from two independent experiments performed in triplicate are shown as mean ± SEM.

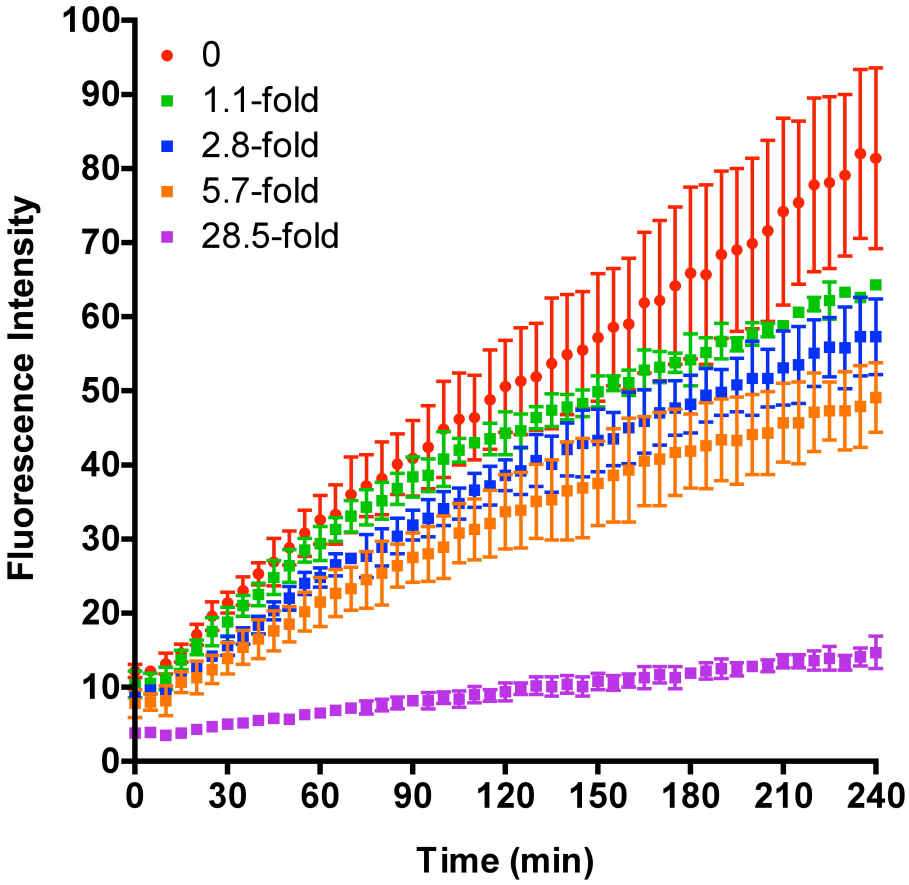

Fig. 3-8. R18-MPV fusion is inhibited by unlabeled HMPV in a dose-dependent manner.
R18-MPV was mixed with increasing amounts of unlabeled, sucrose-purified HMPV. Virus mixtures were added to suspension 293-F cells in triplicate in a 96-well plate. Virus was allowed to bind for 1 h on ice before cells were washed twice with ice-cold PBS and then resuspended in fusion media. Plates were transferred to a pre-heated plate reader (37°C) and R18 fluorescence was monitored for 4 h. Results (mean ± SD) for a representative experiment are shown. The fold excess of unlabeled virus relative to R18-MPV, based upon plaque titers of R18-MPV and unlabeled HMPV, is indicated in the legend.

Development of HMPV virus-like particles (VLPs). The particle-based binding and fusion assays provided excellent methods to study virus-cell interactions that occur during HMPV entry. However, engineering viruses with mutations in the F protein is not only technically challenging but has a high probability of failure because mutating regions of the F protein that are essential for function commonly results in significant defects to virus growth in culture. Moreover, the plasmid we currently use to rescue engineered HMPV encodes all the surface glycoproteins (F, G, and SH), while I sought to investigate F function in the absence of other surface proteins. In an effort to study the function of the HMPV F protein, in the absence of the viral attachment (G) protein, I developed a system where I could generate virus-like particles (VLPs) with only the F protein. VLPs bud from cells into the extracellular medium (supernatant), contain virus structural proteins including viral attachment and/or fusion proteins, but lack virus genome and are thus non-replicating particles.

Previous studies have shown that the contributions of viral structural proteins to virus particle formation differ widely among paramyxoviruses (reviewed in (Harrison et al., 2010)) and I found no reports of HMPV VLPs in the literature. Thus, I first explored which HMPV structural proteins (F, M, N, and/or P) were required to form VLPs by transient expression of viral proteins in cells. I chose to produce VLPs in suspension 293-F cells because these cells i) have a high transfection efficiency, ii) express large amounts of plasmid-encoded proteins, iii) grow to very high densities (>3 x 10^6 cells/mL) without a loss in cell viability, iv) propagate readily in serum-free medium allowing me to supplement the medium with trypsin that is required to process the HMPV F protein, and v) were previously used to generate the recombinant F ectodomain protein used in

binding experiments described in Chapter II. In my initial experiments, I transfected plasmids encoding HMPV F, F and M, or F, M, N and P proteins into 293-F cells and collected the cell supernatant at 72 h posttransfection. Following immunoprecipitation of the supernatants with an F-specific antibody, I separated the immune complexes by SDS-PAGE and detected M or F protein by Western blot (Fig. 3-9). FΔTM protein was used as a positive control for the immunoprecipitation, and was detected in the Western blot (Fig. 3-9, FΔTM lane). HMPV F protein was also detected in the VLP producer cell supernatants at comparable levels, regardless of M, N, or P protein expression. The majority of the F protein was in the F0 precursor form, as expected because I did not add trypsin to the culture medium during VLP production. In contrast, HMPV F in virus particles is predominantly in the F1, cleaved, form due to trypsin treatment during virus propagation (Fig. 3-9, MPV lane). Unfortunately, the M protein was only detected in virus particles, and could not be detected in the F-specific immunoprecipitations. Thus, it was unclear whether I was generating VLPs or F protein was simply being released into the supernatant. However, these results were encouraging and led me to focus on whether F and M proteins were sufficient to build HMPV VLPs.

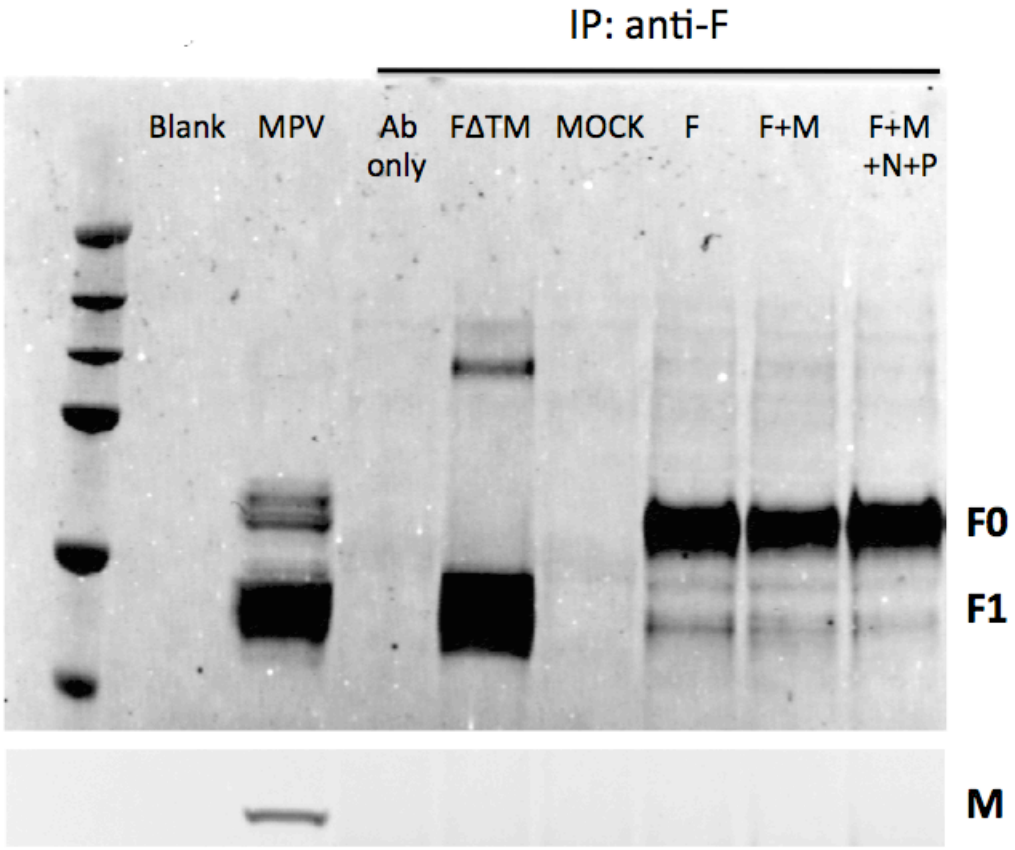

Fig. 3-9. HMPV F protein is released from F-expressing cells into the supernatant. 293-F cells (3 x 10^7 cells; 1 x 10^6 cells/mL) were transfected with 60 µg of plasmid using 60 µL 293fectin reagent. Four conditions were tested: Mock (no plasmid), F (pcDNA3.1-F [60 µg], F + M (pcDNA3.1-F and pcDNA3.1-M [30 µg each]), and F + M +N + P (pcDNA3.1-F, pcDNA3.1-M, pcDNA3.1-N, and pcDNA3.1-P [15 µg each]).

At 24 h posttransfection, cells were washed twice with PBS and 10 mL of fresh growth medium was added. At 72 h posttransfection, supernatants were collected and 1mL of each supernatant was incubated with an F-specific antibody (2 µL). F-specific immune complexes were captured on protein G beads, separated by SDS-PAGE, and viral proteins (F or M) were detected by Western blot using an Odyssey infrared imaging system.

After several rounds of optimization, I determined that VLPs could be reproducibly recovered when 293-F cells were transfected with plasmids encoding the HMPV F and M proteins. 293-F cells transfected with M (40 μg), F (10 μg), and empty vector (10 μg) routinely produced good VLP yields, although M (40 μg) and F (20 μg) produced VLPs with similar yield and protein content. I purified VLPs through a 20% sucrose cushion at 100,000 x g for 90 min at 4°C, and observed white pellets at the bottom of tubes after ultra-centrifugation. The purified VLPs are enveloped particles with surface glycoprotein spikes when examined by electron microscopy (Fig. 3-10A) and contain both the F and M proteins (Fig. 3-10B and C). A detailed characterization of the morphology of VLPs compared to HMPV is described in Chapter IV (Fig. 4-5A and B). Furthermore, I have demonstrated with coimmunoprecipitation experiments that the M and F proteins are incorporated into the same particles and these results are presented in Chapter IV (Fig. 4-5C).

To confirm that VLPs could be used to study HMPV binding, I examined VLP binding to BEAS-2B cells plated in 96-well plates by ELISA. Briefly, serial dilutions of F-VLPs were allowed to bind the cell surface for 1h at 4°C, unbound particles were washed away, and cells were fixed and stained with guinea pig F-specific and guinea pig-specific HRP-conjugated antibodies. ELISA antibody binding was detected with one-step TMB Ultra substrate (Thermo Scientific) followed by neutralization with sulfuric acid. Known concentrations of FΔTM were coated on each ELISA plate to generate a standard curve that was used to quantify the amount of F protein bound to the cell surface. As expected, HMPV F-VLPs bound to cells in a dose-dependent manner that correlated with the level of F protein detected on the cell surface postbinding (Fig. 3-11).

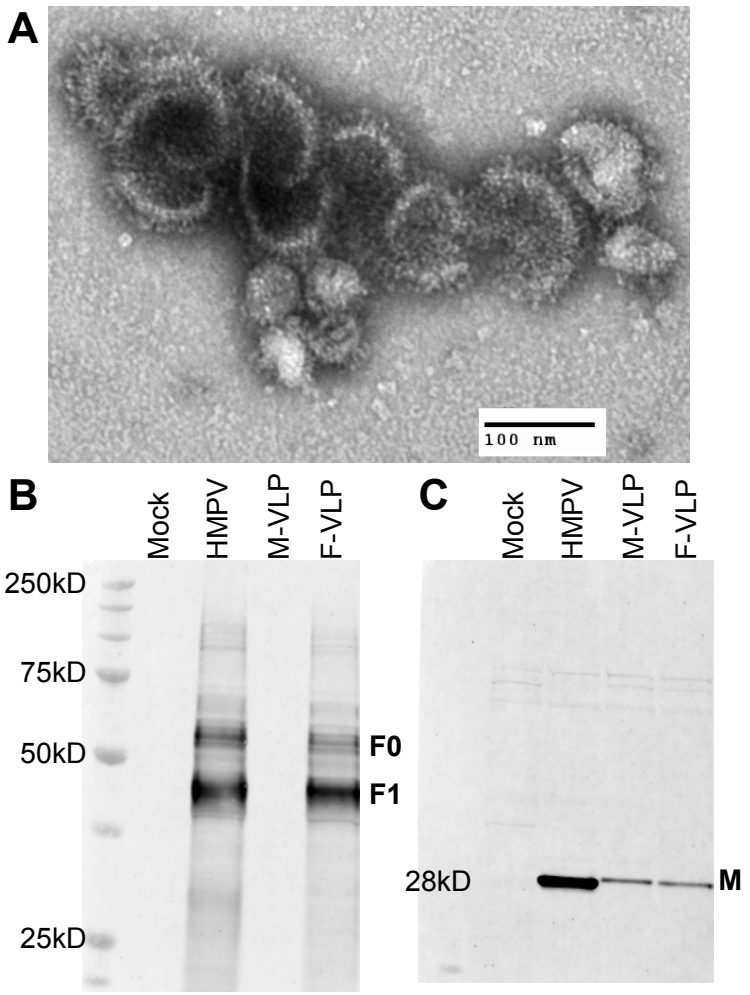

Fig. 3-10. HMPV VLPs resemble virus in morphology and contain F and M proteins.

(A) F-VLPs released from HMPV M and F transfected cells were harvested and purified through a 20% sucrose cushion by ultracentrifugation. An electron micrograph of a negatively stained sample showing a cluster of F-VLPs is shown, magnification = 28,000. Glycoprotein spikes are visible on the VLP surface. (B and C) Particles released from uninfected (Mock), HMPV infected (HMPV), M-transfected (M-VLP) and M+F-transfected (F-VLP) cells were harvested, purified, and analyzed by Western blot to verify their composition. Equivalent amounts (20 μg total protein) of each preparation were separated by denaturing, reducing SDS-PAGE and immunoblotted with (B) anti-F mAb or (C) polyclonal anti-HMPV M antiserum. Molecular mass markers are shown to the left of the protein ladder. Bands corresponding to F0 (uncleaved F), F1 (cleaved F), and M are indicated.

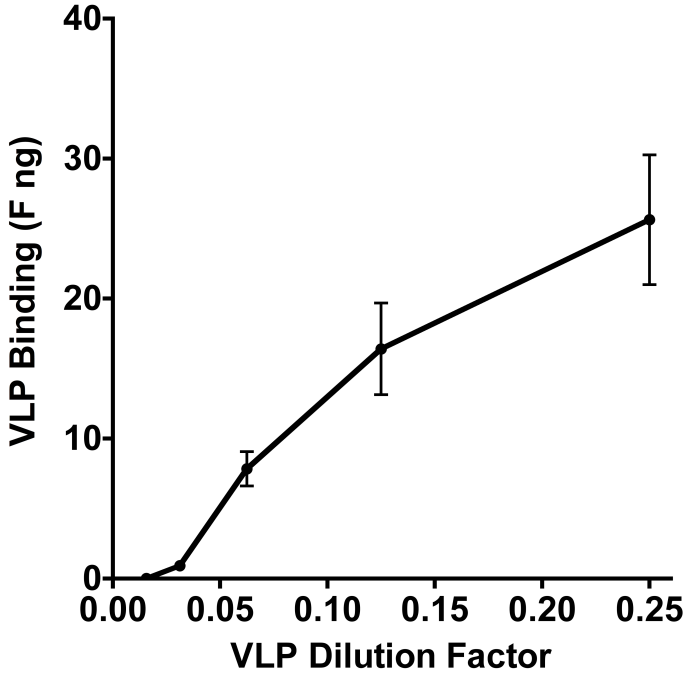

Fig. 3-11. HMPV VLPs bind to BEAS-2B cells in a dose-dependent manner. Serial dilutions of F-VLPs were bound to BEAS-2B cells at 4°C, and HMPV F-specific binding was quantified by ELISA. Results from two independent experiments performed in triplicate are shown as mean ± SEM.

Next, I investigated whether F-VLPs could compete with HMPV during binding. I incubated BEAS-2B cells with serial dilutions of F-VLPs before R18-MPV binding and measured the extent of virus binding. I found that F-VLPs inhibited R18-MPV binding in a dose-dependent manner (Fig. 3-12) but F-VLPs only partially inhibited virus binding. A 30-fold excess of F-VLPs, based upon F protein content, blocked HMPV binding by ~50% (Fig. 3-12, VLP 5 μg column) but higher doses of VLPs did not further inhibit virus binding. These results suggest that F-VLPs and HMPV compete for the same binding sites on the cell surface; however, F-specific binding is saturable. One explanation is that only 50% of R18-labeled particle binding is virus-specific binding. Another possibility is that the G protein mediates 50% of virus binding. Future experiments are needed to distinguish between these two possibilities. Regardless, these preliminary experiments demonstrate that F-VLPs bind to cells and can be used in functional assays to investigate F protein binding activity.

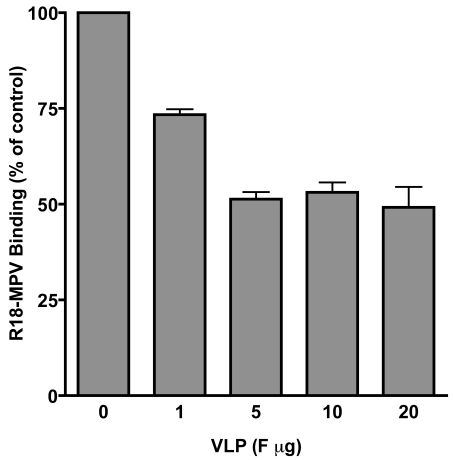

Fig. 3-12. R18-MPV binding is partially inhibited by F-VLPs.
Serial dilutions of F-VLPs were bound to adherent BEAS-2B cells for 30 min on ice before the addition of R18-MPV (F = 0.16 μg), and incubation for an additional 30 min on ice. Unbound particles were washed away with two ice-cold PBS washes. Binding was measured as fluorescence of cell-bound virus after addition of 1% Triton X-100. Results for three independent experiments performed in triplicate are shown as mean ± SEM. R18-MPV and F-VLP F content was determined by Western blot.

HMPV VLPs are a powerful tool to examine F function. Because VLPs are generated by expressing viral structural proteins from transfected plasmids, the viral glycoprotein content of VLPs can be altered to examine the requirements for binding and fusion, i.e. VLPs with F only or F plus G can be compared to assess the contribution of each protein to virus entry (as described in Chapter IV, Fig. 4-5 and Fig. 4-10). Furthermore, the VLPs provide a tractable system to examine how specific mutations in the F protein affect either binding or fusion. For example, in Chapter IV Fig. 4-10H, I examined whether the RGD motif was required for HMPV fusion. Although not directly related to my primary research goals, the HMPV VLPs also provide a system to study virus assembly and egress (or budding). In fact, I collaborated with Fyza Shaikh in the Crowe laboratory to study how mutations in the hRSV F cytoplasmic tail affected VLP budding and was a co-author on her recent manuscript (Shaikh et al., 2012). Finally, my current studies suggest that the VLPs are promising HMPV vaccine candidates because they induce a strong neutralizing antibody response and protect mice from HMPV infection in the lung (manuscript in preparation; data not shown).

Conclusions

In this chapter, I have described the development of new assays and reagents for studies related to HMPV entry. I have used the VLPs, binding assay, and fusion assay to answer critical questions about HMPV entry (described in Chapters IV and V). I think that I have developed important tools to investigate myriad questions about HMPV entry and egress, and believe that future projects in the Williams laboratory will make use of these tools to forward the field's understanding of HMPV biology.

CHAPTER IV

THE HMPV FUSION PROTEIN MEDIATES ENTRY VIA AN INTERACTION WITH RGD-BINDING INTEGRINS

Introduction

Paramyxoviruses use a specialized fusion protein to merge the viral envelope with cell membranes and initiate infection. Most paramyxoviruses require the interaction of two viral proteins to enter cells; an attachment protein binds cell surface receptors, leading to the activation of a fusion (F) protein that fuses the viral envelope and host cell plasma membrane. In contrast, HMPV expressing only the F protein is replication-competent, suggesting a primary role for HMPV F in attachment and fusion. We identified an invariant arginine-glycine-aspartate (RGD) motif that was unique to HMPV F among human paramyxoviruses. This discovery led us to hypothesize that integrins may serve as receptors for HMPV F. In Chapter II, I showed that HMPV infection depends upon RGD-binding integrins and that F ectodomain binding occurred in an RGD-dependent manner. However, whether HMPV F interacted with integrins during virus attachment, whether an F-RGD interaction was sufficient for HMPV binding, or if HMPV F attachment to RGD-binding integrins was linked to fusion activity remained unclear.

I hypothesized that HMPV F binding to RGD-binding integrins was necessary for virus entry and that integrin binding triggered fusion. Using the new HMPV binding and fusion assays, described in Chapter III, I have tested these hypotheses. In this chapter, I show that HMPV binds to RGD-binding integrins and that this interaction is necessary

for virus attachment, virus transcription, and subsequent infection. Multiple RGD-binding integrins are capable of mediating HMPV attachment, and the F protein RGD motif is required for productive infection. While HMPV F-integrin binding is required for efficient virus entry, F binding to RGD-binding integrins is not sufficient to initiate virus-cell membrane fusion. HMPV hemifusion proceeds efficiently both during RGD-binding integrin blockade and in the absence of G protein. We propose that HMPV entry is a stepwise process whereby HMPV F mediates entry through its interactions with RGD-binding integrins and other unidentified cell surface receptors, eliminating the absolute requirement for an additional viral attachment protein.

During the course of these studies, I collaborated with Melanie Ohi and Brent Livesay, a graduate student in Dr. Ohi's laboratory, to obtain electron micrograph images of HMPV and virus-like particles containing the HMPV surface glycoproteins. Both Brent and I collected electron micrographs and measured particles; however, Brent prepared all of the microscopy grids used for the imaging studies. I am grateful for his scientific contributions, and willingness to train me in electron microscopy techniques. I also acknowledge Monika Johnson, from my lab, who performed the quantitative real-time RT-PCR experiments described in Fig. 4-12.

Materials and Methods

Cells. BEAS-2B (ATCC CRL-9609) and LLC-MK2 (ATCC CCL-7) cells were maintained in Opti-MEM I medium (Invitrogen) containing 2% fetal bovine serum (FBS), 2 mM L-glutamine, 50 μg/mL gentamicin, and 2.5 μg/mL amphotericin B. Suspension 293-F cells were maintained as recommended by the manufacturer (293 Freestyle expression system; Invitrogen). BSR T7/5 cells that constitutively express T7 RNA polymerase (Buchholz et al., 1999) were kindly provided by Ursula Buchholz and maintained in Dulbecco modified Eagle medium (DMEM) supplemented with 10% FBS, 2 mM L-glutamine, antimicrobials as described above, and 1 mg/mL geneticin.

Antibodies. Anti-human integrin monoclonal antibodies (mAbs) MAB2021Z (αv; clone AV1), MAB1957 (β3; clone 25E11), MAB1976Z (αVβ3; clone LM609), and MAB1950 (α2; clone P1E6) were purchased from Millipore. Anti-human integrin MAB AIIB2 (β1) and BIIG2 (α5) developed by Caroline H. Damsky were obtained from the Developmental Studies Hybridoma Bank under the auspices of the NICHD and maintained by the University of Iowa, Department of Biology, Iowa City, IA 52242. A heat-inactivated polyclonal HMPV-immune human serum, which neutralizes HMPV infection in an *in vitro* plaque neutralization assay (50% inhibitory concentration [IC_{50}], 1:1,500), was used in fusion experiments. The HMPV F-specific mAb DS7 used for immunoprecipitation experiments has been previously described (Williams et al., 2007). HMPV F-specific mAb 1017 (Ulbrandt et al., 2006) and a rabbit polyclonal antiserum generated against a synthetic peptide representing residues 131 to 145 of the HMPV M protein were used for Western blot analyses.

Viruses. HMPV strain TN/94-49 (virus genotype A2) was used for all virus binding and fusion experiments. HMPV TN/94-49 is a clinical isolate passaged 5 to 7 times and thrice plaque purified in LLC-MK2 cells. Stock virus was propagated using LLC-MK2 cells in serum-free growth medium supplemented with 5 μg/mL trypsin (Invitrogen) as described previously (Williams et al., 2005b). Working virus was propagated in suspension 293-F cells in 293 Freestyle expression medium supplemented with 5 μg/mL trypsin-EDTA (both from Invitrogen). Briefly, 293-F cells were inoculated at 0.1 pfu/cell. At 4 days postinoculation, supernatant was collected and infected cells were freeze-thawed thrice, clarified by centrifugation at 300 x g for 5 min and added to the supernatant fraction. This crude virus preparation was further purified through a 20% sucrose cushion via ultracentrifugation at 100,000 x g for 90 min at 4°C. Octadecyl rhodamine B chloride (R18)-labeled HMPV (R18-MPV) was prepared by incubating 10 mM R18 dissolved in ethanol with sucrose-purified HMPV at 20 nmol R18 per mg total virus protein for 1h at room temperature. The reaction mixture was pelleted through a discontinuous sucrose gradient by ultracentrifugation at 100,000 x g for 90 min at 4°C. Labeled virus (pink by visible light) was collected at the 20/60% sucrose interface, snap-frozen in dry ice-alcohol, and stored at -80°C. All virus preparations were titrated on LLC-MK2 and BEAS-2B cells as previously described (Williams et al., 2005b). Heat-inactivated virus was prepared by heating R18-MPV at 70°C for 15 min.

Recovery of recombinant HMPV with F-RAE mutation. The HMPV reverse genetics system designed and kindly provided by Ron Fouchier was used (Herfst et al., 2004). Nucleotides 4054 to 4059 in the viral genome plasmid FLG NL00-1 were changed from

GGAGAC to GCAGAG by site-directed mutagenesis using Quikchange II (Stratagene) and confirmed by DNA sequencing. This genetic mutation changes the invariant F-RGD motif to F-RAE in the translated fusion protein. We chose the RAE mutation based upon observations from other viruses that utilize RGD binding motifs during virus entry, where often only RGD revertants can be recovered. Thus, we decided to make conservative mutations to two amino acids in the motif, since no comparable amino acids substitute well for the unique Arg structure. Wild-type (F-wt; unmodified FLG NL00-1 genome) and F-RAE viruses were rescued in BSR T7/5 cells using the previously described method (Herfst et al., 2004), except LLC-MK2 cells were used in lieu of Vero cells and viruses were harvested at 13 to 15 days postinfection of LLC-MK2 monolayers. Because the reverse genetics system relies on plasmid-encoded genomes, individual viral clones were recovered in replicate wells from three independent experiments. I rescued four F-RAE virus clones and four F-wt clones as a positive control. The viral genome was extracted from centrifuge-clarified virus preparations with the RNeasy minikit (QIAGEN) according to manufacturer's protocol. A nested PCR amplification strategy was used to amplify the F protein open reading frame, with flanking intragenic genomic sequences. Primers for the nested PCR amplification of F have been previously described (Yang et al., 2009). Reverse transcription-PCR (RT-PCR) bands were gel-purified, subcloned into pGEM (Promega), and sequenced to confirm that the desired genetic mutation was maintained and no other mutations had been introduced during virus propagation.

VLPs. HMPV virus-like particles (VLPs) were generated in suspension 293-F cells by transient expression of the HMPV matrix (M), fusion (F), and glycoprotein (G) proteins. Cloning and sequence optimization for mammalian expression of the full-length F sequence from a pathogenic clinical HMPV isolate TN/92-4 (virus genotype A2) have been previously described (Cseke et al., 2007). The full-length M and G sequences from TN/94-49 (virus genotype A2) were also sequence optimized (GeneArt) and subcloned into pcDNA3.1. Suspension 293-F cells were transfected with pcDNA3.1-M (40 μg), pcDNA3.1-F (10 μg), and either empty vector (pcDNA3.1) (10 μg) for F-VLPs or pcDNA3.1-G (10 μg) for F+G-VLPs using 293fectin transfection reagent (60 μL) as recommended by the manufacturer (Invitrogen). G-VLP producer cells were transfected with pcDNA3.1-M (40 μg), empty vector (pcDNA3.1) (10 μg), and pcDNA3.1-G (10 μg). At 18 hours posttransfection, growth medium was changed and 5μg/mL trypsin was added. At 3 days posttransfection, cells and debris were separated from the supernatant by centrifugation at 300 x g for 5 min. Clarified supernatant was pelleted through 20% sucrose as described above for virus. White VLP pellets were resuspended in MHN solution (0.1 M $MgSO_4$, 50 mM HEPES, 150 mM NaCl), R18 labeled as described for virus, and stored at -80°C.

Western blotting. For the analysis presented in Fig. 4-5C, sucrose-purified HMPV or VLPs were diluted in phosphate-buffered saline (PBS), immunoprecipitated with 2 μg of an F-specific mAb (DS7) (Williams et al., 2007)) for 4 h, and captured on protein G-agarose beads (Sigma). Beads were washed thrice with PBS and heated to 70°C for 10 min in NuPAGE LDS sample buffer (Invitrogen) containing 5% β-mercaptoethanol

(Sigma). Proteins were separated on 10% NuPAGE Bis-Tris gels (Invitrogen), and transferred to polyvinylidene fluoride (PVDF) membranes. Membranes were blocked for 1 h with 5% milk in PBS plus 0.1% Tween (blocking buffer). Polyclonal guinea pig antiserum, which was generated against sucrose-purified HMPV (TN/94-49) and recognizes both HMPV F and G proteins, and rabbit polyclonal anti-M serum were diluted in blocking buffer and incubated with membranes for 12 to 14 h at 4°C. Li-Cor IRDye 800CW anti-guinea pig and IRDye 680CW anti-rabbit secondary antibodies were diluted in blocking buffer and incubated with membranes for 1 h at room temperature. Membranes were washed three times in PBS plus 0.1% Tween and twice in PBS to remove residual detergent and dried. Bands were imaged using an Odyssey infrared imaging system (Li-Cor). For the analysis shown in Fig. 4-10G, producer cell lysates were prepared in lysis buffer containing 20 mM Tris (pH 7.4), 150 mM NaCl, 1 mM EDTA and 1% NP-40 supplemented with a complete protease inhibitor cocktail (Roche). Total protein concentrations for cell lysates and sucrose-purified, R18-labeled VLPs were determined with the Bio-Rad DC protein assay (Bio-Rad). Proteins were separated by SDS-PAGE, transferred to PVDF membranes, and incubated with HMPV F-specific mAb 1017 and Cy5-conjugated anti-Armenian hamster secondary antibody (Jackson ImmunoResearch) as described above.

Flow Cytometry. BEAS-2B cells were harvested and incubated with either isotype control or anti-human integrin antibodies, followed by AlexaFluor 647-conjugated secondary antibodies (Invitrogen). Expression levels of different integrins were detected with a BD LSRII flow cytometer.

Quantifying HMPV infection. At 24 hours postinoculation, BEAS-2B cell monolayers were fixed with buffered formalin (3.3% in growth medium) and immunostained for HMPV infection with a precipitating peroxidase substrate (True Blue; KPL) as previously described (Cseke et al., 2009). Individual wells were imaged on a light box with a macro zoom lens (Navitar, 18 to 108 mm), and infected cells, which appear blue, were enumerated using ImageJ. Cells in entire wells were counted. The image contrast threshold was held constant during counting for all wells in a single plate.

Visualizing HMPV plaques by microscopy. Serial dilutions of F-wt or F-RAE viruses were adsorbed to LLC-MK2 cell monolayers for 1 h at room temperature. Cells were overlaid with Opti-MEM I medium containing 0.75% methylcellulose and 5 μg/mL trypsin and incubated at 37°C with 5% CO_2 for 4 days. Cell monolayers were fixed, immunostained, and plaques were counted. Cell images were captured with a Zeiss Axiovert 200 microscope using a 2.5x or 10x objective.

Electron microscopy. Sucrose-purified HMPV and VLPs were stained with uranyl formate and prepared for transmission electron microscopy (TEM) as described previously (Ohi et al., 2004). Briefly, 2.5 μL of particles was adsorbed to a glow-discharged 200-mesh copper grid covered with carbon-coated collodion film. The grid was washed with water and stained with uranyl formate (0.75%). Samples were imaged on a FEI Morgagni electron microscope operated at an acceleration voltage of 100 kV. Images were recorded at a magnification of 28,000 and collected using a 1,000 by 1,000 charge-coupled device (CCD) camera (AMT). Ten to 30 representative HMPV, F-VLP or

F+G-VLPs were chosen for morphology analysis. Measurements of particle diameters and glycoprotein spike length were made using AMT Image Capture Engine software.

Fluorescence microscopy. Viral fusion was monitored by fluorescence microscopy as R18-MPV fused with live cells. BEAS-2B cells, grown to ~90% confluence on a thin layer of Matrigel (BD Biosciences) in 6-well plates, were incubated with 25 μg/mL 4',6-diamidino-2-phenylindole (DAPI) in culture medium for 1 h at 37°C. Excess DAPI was washed away, and cells were incubated with R18-MPV (0.2 pfu/cell) for 1 h on ice. Unbound virus was washed away, and Opti-MEM I medium (without phenol red) supplemented with 2% FBS was added to cells. The zero time point was imaged with cells at 4°C. Virus fusion was initiated by incubating cells at 37°C. Live cell images were captured with a Zeiss Axiovert 200 microscope using a 40x objective with 359/461-nm (DAPI) and 556/573-nm (R18) filters at the indicated time points.

R18-MPV binding assay. To study HMPV binding, I developed a fluorescence-based assay to quantify binding independently of fusion and infection, allowing me to discriminate the first critical step in the entry process. I loaded HMPV particles with self-quenching concentrations of octadecyl rhodamine B chloride (R18-MPV) (Hoekstra et al., 1984). To measure binding, R18-MPV was bound to cells and subsequently solubilized with detergent, resulting in fluorescence proportional to the amount of bound virus. Specifically, R18-MPV (0.02 pfu/cell) was incubated with BEAS-2B cells grown to 90 to 95% confluence on a thin layer of Matrigel (BD Biosciences) in 48-well plates for 1 h on ice. Cells were washed with ice-cold PBS to remove unbound virus. PBS plus

1% Triton X-100 was added to each well, and fluorescence (excitation, 544nm; emission, 590nm) was measured using a SpectraMax M5 (Molecular Devices) plate reader. For function-blocking antibody experiments, integrin-specific antibodies were diluted in Opti-MEM I medium plus 5% FBS and incubated with BEAS-2B cell monolayers for 1 h at 37°C, followed by 30 min on ice, before addition of ice-cold virus inoculum. Binding was expressed as mean percent inhibition relative to an untreated control. For infectivity experiments, instead of detergent, growth medium was added and cells were incubated at 37°C with 5% CO_2. At 24 hours postinoculation, cell monolayers were fixed with buffered formalin and immunostained for HMPV infection as previously described (Cseke et al., 2009). Infected cells were enumerated as described above, and infectivity was expressed as mean percent inhibition relative to an untreated control. R18-VLP experiments were conducted as described for R18-MPV.

R18-MPV fusion assay. To measure fusion, I incubated cells with R18-MPV at 4°C, washed away unbound virus, added fresh cell culture medium, and incubated cells at 37°C, monitoring R18 fluorescence in real time. During virus-cell fusion, R18 dilutes from the virus membrane into unlabeled cell membranes, resulting in a measureable increase in fluorescence that reflects the extent of virus fusion. This assay allowed me to monitor HMPV fusion while virus and cell membranes were in the process of merging. Background fluorescence during experiments was typically 20-fold lower than the initial R18 fluorescence reading (see Fig. 4-9B). For experiments described here, R18-MPV (0.1 pfu/cell) was bound to BEAS-2B cells grown to 90 to 95% confluence on a thin layer of Matrigel (BD Biosciences) in 48-well plates for 1 h on ice. Unbound virus was removed by washing with ice-cold PBS before Opti-MEM I medium (without phenol red)

supplemented with 2% FBS was added to cells. Ice-cold plates were transferred to a preheated (37°C) SpectraMax M5 plate reader. Fluorescence (excitation, 544nm; emission, 590nm; top-read mode) was measured in real time for 2 h with readings collected every 2 min or for 4 h with readings in 5-min intervals. At the end of the time course, Triton X-100 (final concentration of 1%) was added to each well, and final fluorescence readings were acquired. R18-VLP experiments were conducted as described for R18-MPV. Function-blocking integrin antibody experiments were performed as described above. The ability of bound R18-MPV or R18-VLPs to subsequently undergo fusion was defined as R18 dequenching and calculated according to the following equation: % R18 dequenching = 100 x $(F - F_0)/(F_d - F_0)$, where F is fluorescence, F_0 is fluorescence at t = 0 min, and F_d is fluorescence after the addition of Triton X-100 (at the end of the experiment).

Real-time RT-PCR. Function-blocking integrin-specific antibodies (anti-α2 [10 μg/mL] or a combination of anti-αV [40 μg/mL], anti-α5 [6 μg/mL], and anti-β1 [7.5 μg/ml]) were diluted in Opti-MEM I medium and incubated with 90% confluent BEAS-2B cells grown on a thin layer of Matrigel in 48-well plates for 1 h at 37°C and then for 30 min on ice. Cells incubated with Opti-MEM I medium only (no mAb) were used as the negative control. HMPV (0.25 pfu/cell) was added to cells and allowed to bind for 1 h on ice with occasional rocking. Cells were washed twice with ice-cold PBS to remove unbound virus. Half of the wells were used to determine the input viral genome (lysed immediately [t = 0]), and half of the wells were incubated in Opti-MEM I supplemented with 2% FBS for 8 h at 37°C to allow virus entry and transcription. At t = 0 or 8 h, cells were washed with

PBS to remove medium, and lysates were prepared in 350 µL of MagNA Pure LC total nucleic acid lysis/binding buffer (Roche Applied Sciences) and stored at 4°C. RNA was extracted using the MagNA Pure LC total nucleic acid isolation kit (Roche Applied Sciences) on a MagNA Pure LC using the total NA external lysis protocol and stored at -80°C until further use. Real-time RT-PCR was performed in 25-µL reaction mixtures containing 5 µL of extracted RNA on an ABI StepOnePlus real-time PCR system (Life Technologies/Applied Biosystems) using the AgPath-ID one-step RT-PCR kit (Applied Biosystems/Ambion). Primers and probe targeting the HMPV N gene have been previously published (Ali et al., 2011) and were used to detect HMPV genome and transcripts. Cycling conditions were 50°C for 30 min, followed by an activation step at 95°C for 10 min and then 45 cycles of 15 s at 95°C and 30 s at 60°C. All sample cycle threshold (C_T) values were less than 26 and were considered positive; the HMPV N C_T values for mock-infected cells were undetectable at >45. To determine the amount of HMPV N transcript for each treatment condition, values were normalized to the glyceraldehyde-3-phosphate dehydrogenase (GAPDH) housekeeping gene and compared to input genome levels using the $2^{-\Delta\Delta CT}$ method, where $\Delta\Delta C_T$ = (HMPV N C_{T8} – GAPDH C_{T8}) – (HMPV N C_{T0} – GAPDH C_{T0}) (AppliedBiosystems, 2001; Livak and Schmittgen, 2001; Pfaffl, 2001). The effect of integrin inhibitors was determined by comparing the fold change in HMPV N over time relative to the treatment control (no mAb).

Statistical Analysis. For binding and infectivity experiments, data are expressed as mean percent inhibition, relative to an untreated control, for at least three independent experiments performed in triplicate. Student's *t* test was used to determine whether the level of inhibition observed in the presence of integrin-blocking antibodies was significantly greater than the untreated control (no mAb). For the combination blockade experiments, a *t* test was used to determine whether the level of inhibition observed for one mAb differed from the level of inhibition observed when two mAbs were used to target different integrins during HMPV binding or infection. Virus and VLP fusion extent were compared using a one-way analysis of variance (ANOVA) and a Tukey's multiple-comparison test. For all analyses, a P value ≤ 0.05 was considered statistically significant.

Results

HMPV binding and subsequent infection depend upon RGD-binding integrins. In Chapter II, we showed that RGD-binding integrins promote HMPV infection (Cseke et al., 2009) but did not determine whether integrin engagement was required for HMPV entry. Investigating HMPV entry presented methodological challenges because both attachment and fusion are necessary for virus entry; therefore, a complete understanding of virus entry required assays that quantify binding and measure fusion. As virus receptors, RGD-binding integrins could be required for HMPV F binding, fusion, or both steps in virus entry. First, I developed a fluorescence-based assay to quantify binding independently from fusion and infection, allowing us to discern virus attachment. Details of this assay were presented in Chapter III. HMPV binding resulted in a dose-dependent increase in fluorescence that directly correlated with infectivity (Chapter III, Fig. 3-2), confirming that the assay measured productive virus binding to cells.

Next, I sought to determine whether HMPV binds RGD-binding integrins during virus attachment to human bronchial epithelial (BEAS-2B) cells. BEAS-2B cells express several RGD-binding integrin subunits, i.e., αV, α5, β1, β3, and β5, and the collagen-binding integrin subunit α2 (Fig. 4-1). Therefore, all the heterodimeric RGD-binding integrins on BEAS-2B cells contain αV, α5, and/or β1 integrin subunits. I blocked each individual integrin subunit with function-blocking antibodies and examined the effect on HMPV attachment and infectivity. I found that HMPV binding and infection were inhibited in a dose-dependent manner as a result of RGD-binding integrin blockade (Fig. 4-2). HMPV bound in an α5, β1, and αV integrin-dependent manner (Fig. 4-2C-E), but β3 mAb had no effect (Fig. 4-2B).

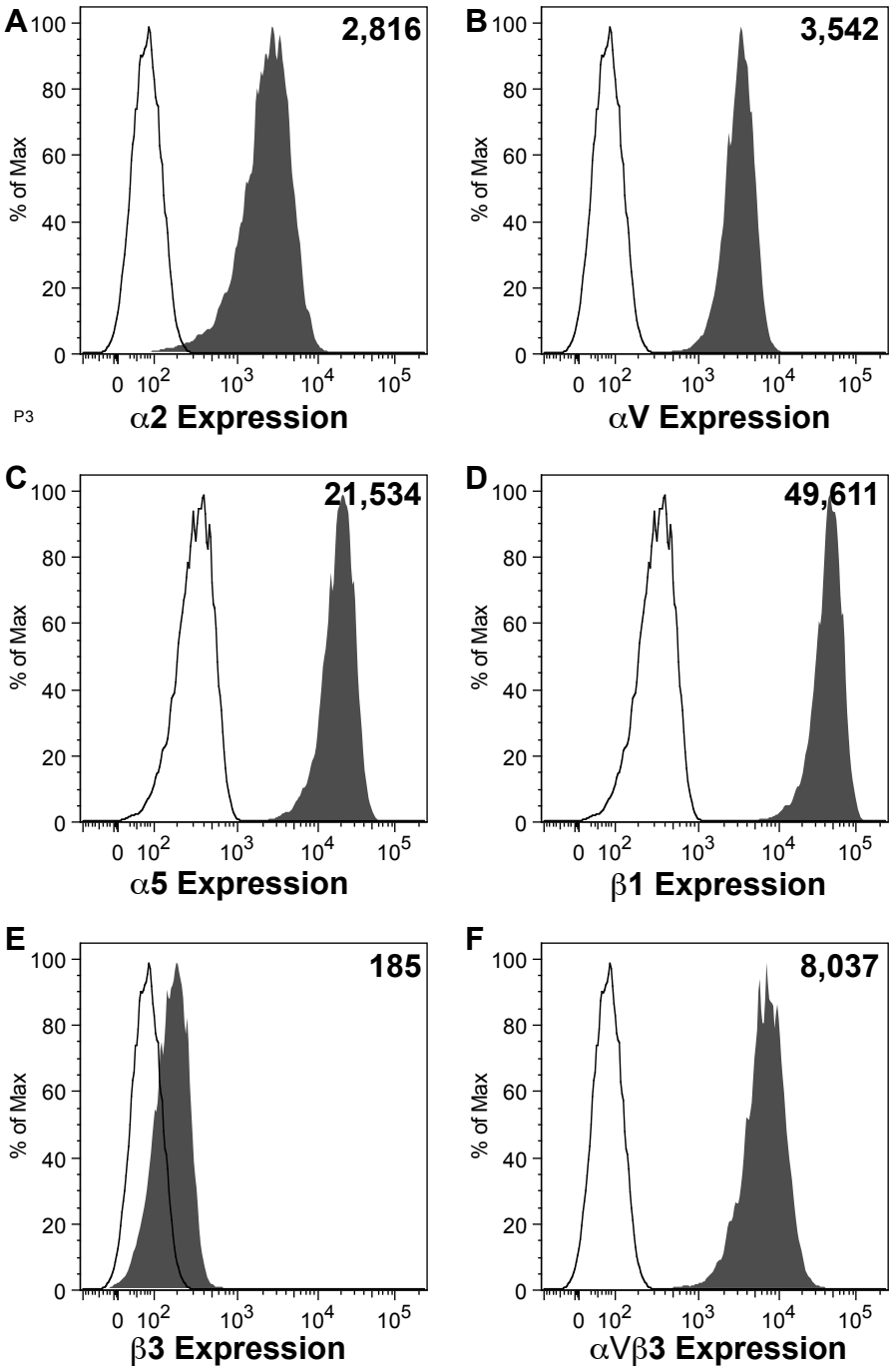

Fig. 4-1. Integrin expression on human bronchial epithelial (BEAS-2B) cells. BEAS-2B cells were stained for surface expression of specific integrins and analyzed by flow cytometry. Expression of α2 (A), αV (B), α5 (C), β1 (D), and β3 (E) integrin subunits or the αVβ3 heterodimer (F) is shown in shaded histograms, relative to an isotype control antibody (open histograms). The number in the upper right corner of each panel represents mean fluorescence intensity of integrin expression.

Based upon the low expression level of β3 that I observed in the flow cytometry experiments despite high expression levels of the αVβ3 heterodimer (compare Fig. 4-1E and F), I was concerned that the β3 mAb might not efficiently bind αVβ3 integrin on the surface of BEAS-2B cells. Therefore, I tested whether αVβ3 function-blocking mAb (40 μg/mL) inhibited HMPV binding or infectivity and found that blocking αVβ3 had no effect (infectivity data shown in Chapter II, Fig. 2-3). HMPV binding and infection did not depend upon the collagen-binding integrin α2, as expected (Fig. 4-2A). These results indicate that HMPV can bind to different RGD-binding integrins, i.e., α5β1 and either αVβ1, αVβ5, αVβ6, or αVβ8 on BEAS-2B cells.

To further explore whether HMPV engaged multiple RGD-binding integrins during entry, I measured HMPV binding while all RGD-binding integrins were blocked using combinations of mAbs. Blocking all RGD-binding integrins resulted in ~40% reduced virus binding, comparable to the inhibition observed when individual integrins were blocked (Fig. 4-2F, αV + β1 and αV + α5). This suggests to me that HMPV is capable of engaging different RGD-binding integrins at the cell surface but that integrin-mediated attachment is saturable. Residual virus binding is mediated by other cell surface molecules that participate in initial HMPV attachment, such as heparan sulfate, which has recently been identified as critical for HMPV F attachment (Chang et al., 2012b). Further, the HMPV G protein has been shown to bind cellular glycosaminoglycans (Thammawat et al., 2008) and likely contributes to HMPV binding, in an integrin-independent manner.

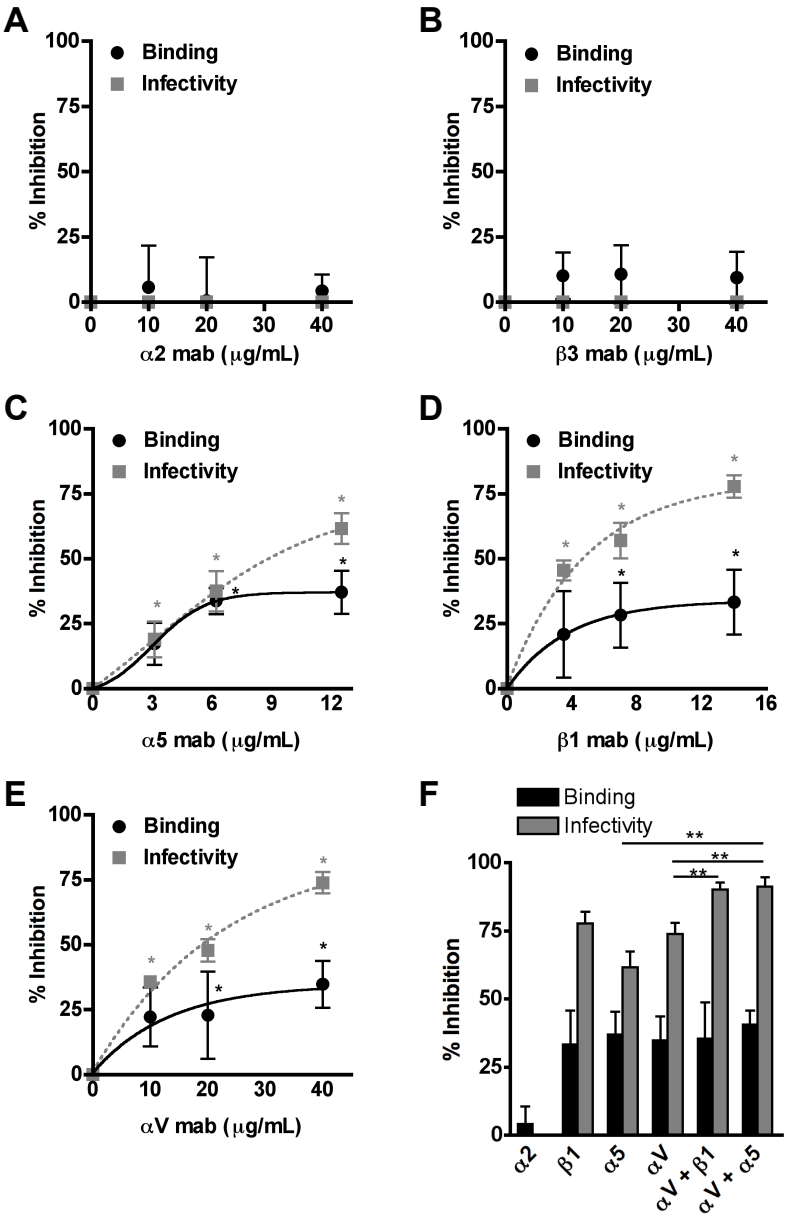

Fig. 4-2. HMPV binding and subsequent infection depend upon RGD-binding integrins.

(A to E) HMPV binding (black circles) or infection at 24 h (gray squares) was determined in the absence or presence of α2 (A), β3 (B), α5 (C), β1 (D), or αV (E) integrin function-blocking antibodies. Results from at least three independent experiments performed in triplicate are expressed as mean percent inhibition relative to untreated control; error bars indicate SEM. *, $P \leq 0.05$ from Student's *t* test, comparing antibody treatment to no treatment. (F) The highest concentrations of αV, β1, or α5 function-blocking antibodies were used alone or in combination to target multiple integrins, and HMPV binding (black bars) or infectivity (gray bars) was determined. Asterisks indicate an additive effect of combination blockade on HMPV infectivity (gray bars); Student's *t* test comparing two treatments, $P \leq 0.05$.

Blocking all RGD-binding integrins resulted in a 90% reduction of HMPV infection, significantly more than when individual integrin subunits were blocked (Fig. 4-2F, αV + β1 and αV + α5). Thus, I observed an additive inhibitory effect on infectivity when all RGD-binding integrins were blocked during entry. The additive effect on HMPV infectivity was also observed when lower, nonsaturating concentrations of α5 and αV mAbs were used to block integrin receptors during HMPV entry (Fig. 4-3). These results suggest that HMPV is capable of engaging multiple RGD-binding integrins rather than a single, specific integrin during the entry process. Further, infection was inhibited to a greater degree than binding for all RGD-binding integrins (Fig. 4-2C-F), suggesting that RGD-binding integrins serve a postbinding role during HMPV infection. I confirmed that the integrin mAbs did not exert an indirect effect on endocytosis by measuring the uptake of fluorescent dextran, which was not inhibited in the presence of integrin mAbs (Fig. 4-4). As expected, dextran uptake was significantly impaired by dynasore treatment, which potently inhibits endocytosis (Fig. 4-4). Further, I performed integrin antibody binding at 4°C with similar results, showing that mAb binding at 37°C did not induce an indirect effect on HMPV entry. Thus, while ~50% of HMPV particles are capable of binding in an integrin-independent manner, these attachment events do not lead to productive entry in the presence of RGD-binding integrin-specific antibodies. These data indicate that HMPV engages RGD-binding integrins during virus attachment and that integrin-mediated binding is necessary for infection.

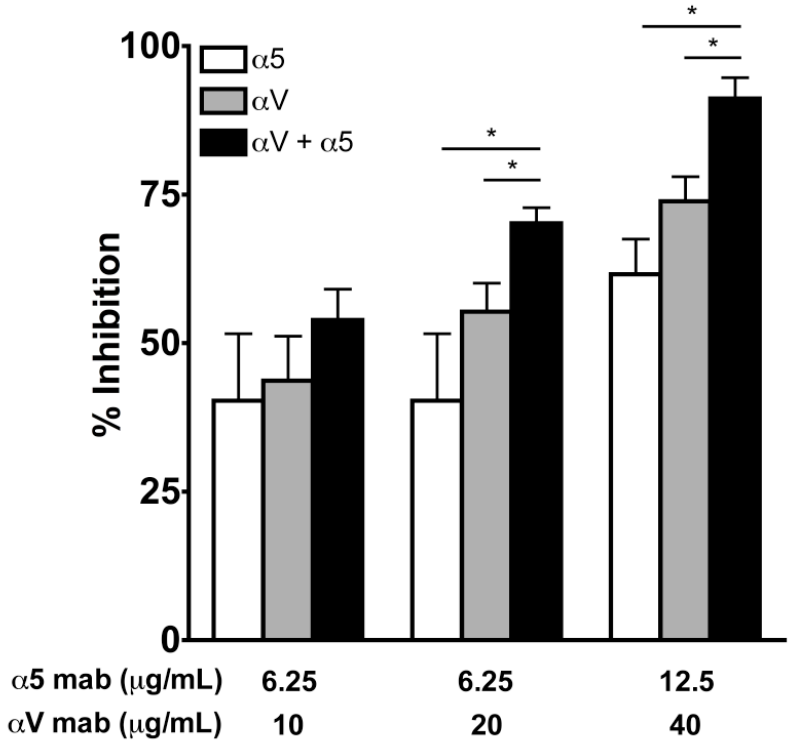

Fig. 4-3. HMPV infection depends upon α5β1 and αV integrins.
HMPV infection at 24 h was determined in the absence or presence of αV, α5, or a combination of the two integrin function-blocking antibodies. Infected cells were enumerated as described in Materials and Methods. Results from at least three independent experiments performed in triplicate are expressed as mean percent inhibition relative to untreated control (no mAb); error bars indicate SEM. *, additive effect of combination blockade on HMPV infectivity; Student's *t* test comparing two treatments, $P \leq 0.05$.

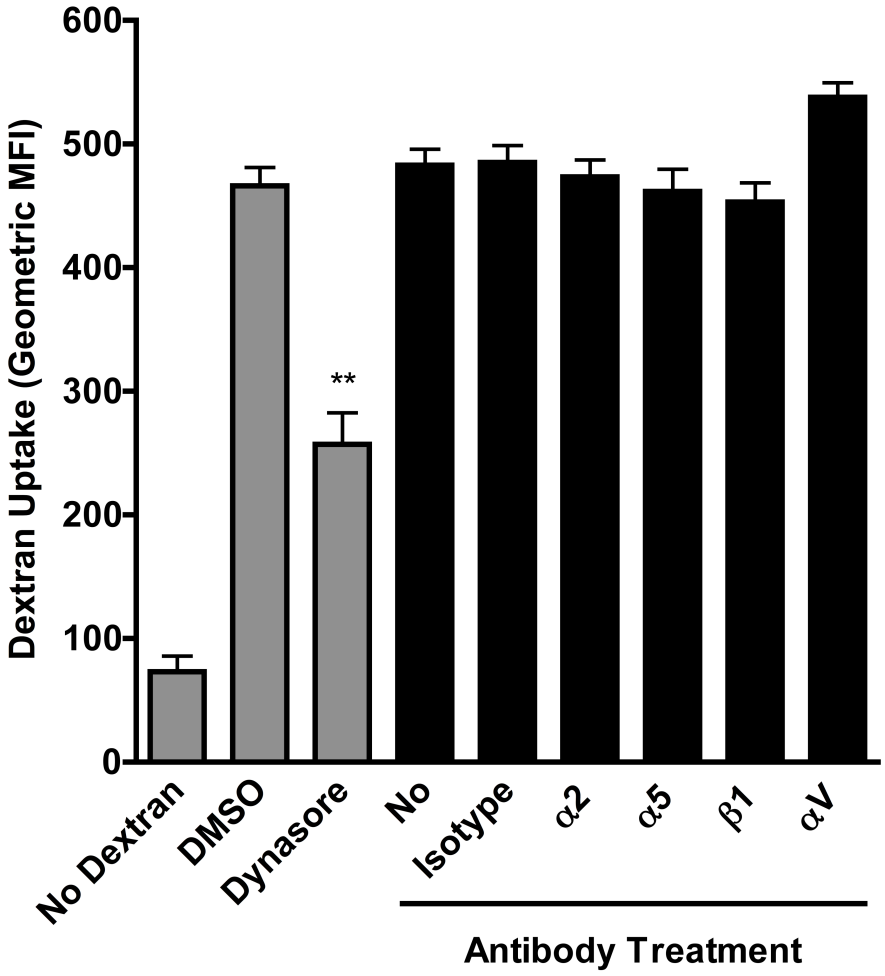

Fig. 4-4. Integrin function-blocking antibodies do not significantly alter the endocytic capacity of BEAS-2B cells.
BEAS-2B cells were incubated with DMSO, dynasore hydrate (50 μM), an isotype control antibody (25 μg/mL), or integrin-specific antibodies (α2 [10 μg/mL], α5 [12.5 μg/mL], β1 [14 μg/mL], or αV [40 μg/mL]) diluted in Opti-MEM I medium for 1 h at 4°C. Unbound antibody was removed and virus growth medium containing 100 μg/mL Texas Red 10,000 MW, neutral dextran was incubated with cells for 20 min at 4°C followed by 1 h at 37°C. Cells were lifted from plates, washed in PBS plus 1% FBS, fixed with 0.5% paraformaldehyde, and analyzed by flow cytometry for dextran uptake (y-axis). Results are from four independent experiments; error bars indicate SEM. **, $P \leq 0.05$ from Student's *t* test, comparing DMSO vehicle and Dynasore treatment.

The αV mAb treatment resulted in an increase in dextran uptake in a small percentage of cells, although 90% of cells were identical to isotype mAb and untreated (no mAb) cells and the effect was not statistically significant.

HMPV F binds to RGD-binding integrins in the absence of G. To test the hypothesis that HMPV F directly engages RGD-binding integrins during attachment, I established a system to investigate F-mediated binding in the absence or presence of the viral attachment (G) protein. I generated virus-like particles (VLPs) with only HMPV F (F-VLP) or both the F and G proteins (F+G-VLP) (see Materials and Methods). F-VLPs and F+G-VLPs were similar to virus in morphology, and F glycoprotein spikes measuring 13.3 nm were visible on the surface of virus and VLPs (Fig. 4-5A-B). The majority of the F spikes appear to resemble the "ball-and-stem" conformation observed for prefusion soluble paramyxovirus F protein (Connolly and Lamb, 2006). Rarely, we observed F spikes that appeared elongated with a wider base and compacted head domain, which may be F trimers that have adopted the postfusion conformation, as the shape is consistent with previous TEM images of paramyxovirus postfusion soluble F protein (Connolly and Lamb, 2006). Spikes with a stem and a branched head domain were occasionally visible in the virus and F+G-VLP electron micrographs (Fig. 4-5A and C). These "tree-shaped" spikes may be the HMPV G protein, but further characterization would be required to confirm this speculation. I confirmed the incorporation of HMPV M, F, and G by Western blot analysis, following immunoprecipitation of virus and VLPs with a mAb recognizing the F protein. HMPV M and G coimmunoprecipitated with the F protein (Fig. 4-5C), indicating that these viral proteins were contained in VLPs with F protein. Two forms of the fusion protein were detected: the uncleaved precursor (F0) and a large subunit from the cleaved form (F1). Although I observed differences in F cleavage (conversion of F0 to F1) in the virus preparation, the F-VLP and F+G-VLP preparations contained similar levels of HMPV F in both forms.

HMPV G bands migrate as a hazy smear at 70 to 90 kDa due to heavy glycosylation of the G protein (Biacchesi et al., 2004; Liu et al., 2007; Ryder et al., 2010). Levels of G were similar for virus and F+G-VLPs.

HMPV, F-VLP and F+G-VLP binding were significantly impaired by αV, α5, and β1 integrin blockade, while blocking α2 integrin had no effect (Fig. 4-5D). Both HMPV and VLP binding were inhibited by ~50% in the presence of RGD-binding integrin-specific antibodies. Importantly, there were no differences in binding or susceptibility to mAb blockade between F-VLPs and F+G-VLPs. Thus, HMPV F binding occurs in an RGD-binding integrin-dependent manner, independently of any contribution that HMPV G-receptor binding may add to virus binding. These results indicate that F engages RGD-binding integrins during attachment and the viral G protein does not contribute to integrin engagement during virus attachment.

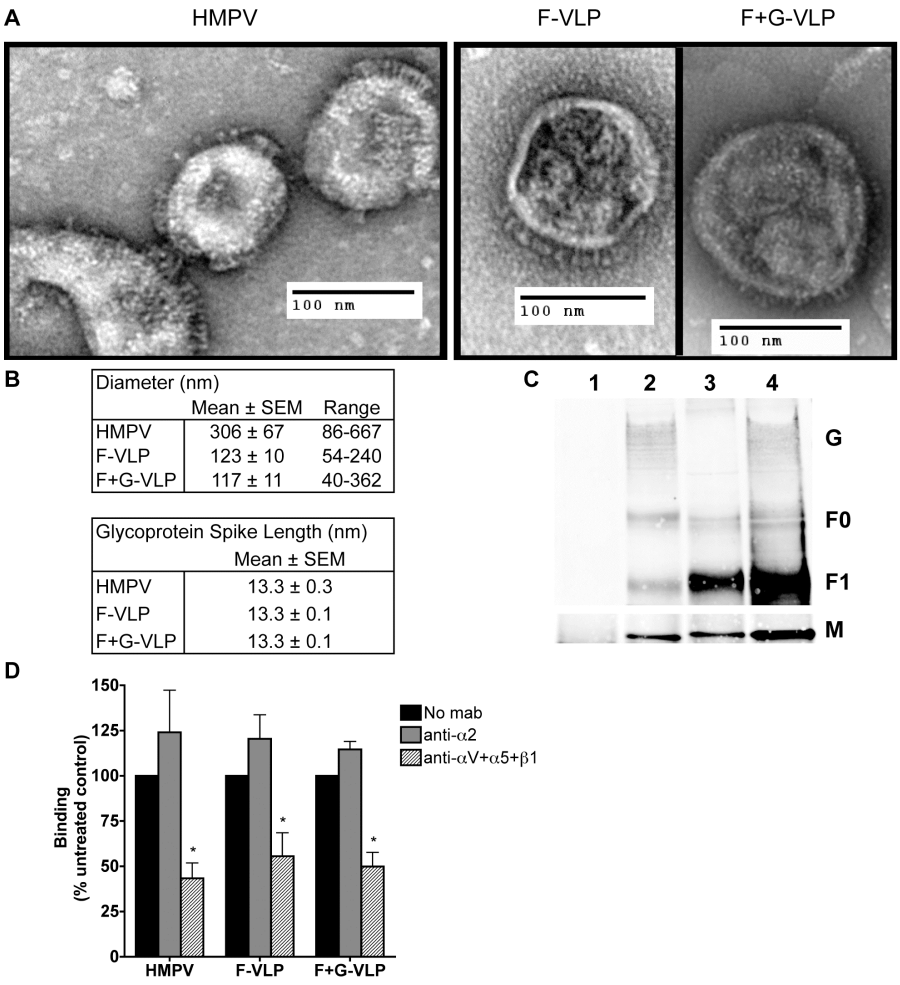

Fig. 4-5. HMPV F binds to RGD-binding integrins in the absence of G.
(A) Electron micrographs of HMPV and F-only and F+G virus-like particles (VLPs). Sucrose-purified particles were stained with uranyl formate and imaged on an FEI Morgagni electron microscope (magnification, ×28,000). Protein spikes are visible projecting from the surfaces of both virus and VLPs. (B) Ten to 30 particles were chosen for morphology analysis; diameters and glycoprotein spike lengths were measured using AMT Image Capture Engine software. (C) Viral matrix (M), fusion (F), and attachment (G) protein incorporation into VLPs was confirmed by Western blotting. Virus and VLPs were immunoprecipitated with an anti-F monoclonal antibody (2μg) and analyzed by Western blotting. Viral proteins were detected with HMPV M-specific or HMPV polyclonal A2 virus-specific (F and G) antibodies and fluorescent secondary antibodies using the Li-Cor Odyssey infrared imaging system. Lanes: 1, mock; 2, HMPV; 3, F-VLP; 4, F+G-VLP. Uncleaved protein (F0) and the large subunit from the cleaved form (F1) of the fusion protein were detected. M bands were detected in a different channel than F and G bands on the same blot and thus appear on a different image. (D) R18-MPV or R18-VLP binding was measured in the absence or presence of integrin function-blocking antibodies (α2 or a combination of αV, α5, and β1 to block all available RGD-binding integrins). Results from three independent experiments are expressed as mean percent inhibition relative to an untreated control (no mAb). Error bars indicate SEM. *, $P \leq 0.05$.

The HMPV F RGD motif is required for HMPV infection. To further define the importance of HMPV F binding to RGD-binding integrins, I investigated whether the conserved RGD motif was necessary for HMPV infection. I used reverse genetics to replace the F protein RGD motif with an RAE mutation in the viral genome. F-RAE virus growth was delayed and attenuated, resulting in >2-$\log_{10}$-lower peak titers in the supernatant (Fig. 4-6A). Total F-RAE virus yield obtained from pooling supernatant and cell-associated virus fractions, harvested 13 to 15 days postinoculation when F-wt virus infected cells exhibited maximal cytopathic effect, had >3-$\log_{10}$-lower titers compared to F-wt viruses, indicating that lower supernatant titers were not due to a defect in virus budding. F-RAE plaques were tiny and could not be enumerated without microscope magnification, while F-wt plaques could be counted by eye (Fig. 4-6B). F-RAE plaques also lacked characteristic syncytia visible in F-wt plaques (Fig. 4-6C), suggesting that budding F-RAE virus cannot infect neighboring cells and that cell-cell F-mediated fusion was also impaired when the conserved RGD motif was changed to RAE. To confirm that the RAE mutation did not alter F expression, I expressed HMPV F-RAE from a plasmid and determined that F-RAE was expressed on the surface of transfected cells at wild-type levels (Fig. 4-7) and was cleaved from the immature (F0) form to the functional (F1/F2) form by the addition of trypsin with the same efficiency as F-wt (Fig. 4-8). Therefore, the defect in F-RAE virus replication is unlikely to be due to a defect in fusion protein expression or cleavage. These results suggest that F-RGD-mediated binding is required for HMPV infection, and support a mechanism where F interacts directly with RGD-binding integrins during attachment.

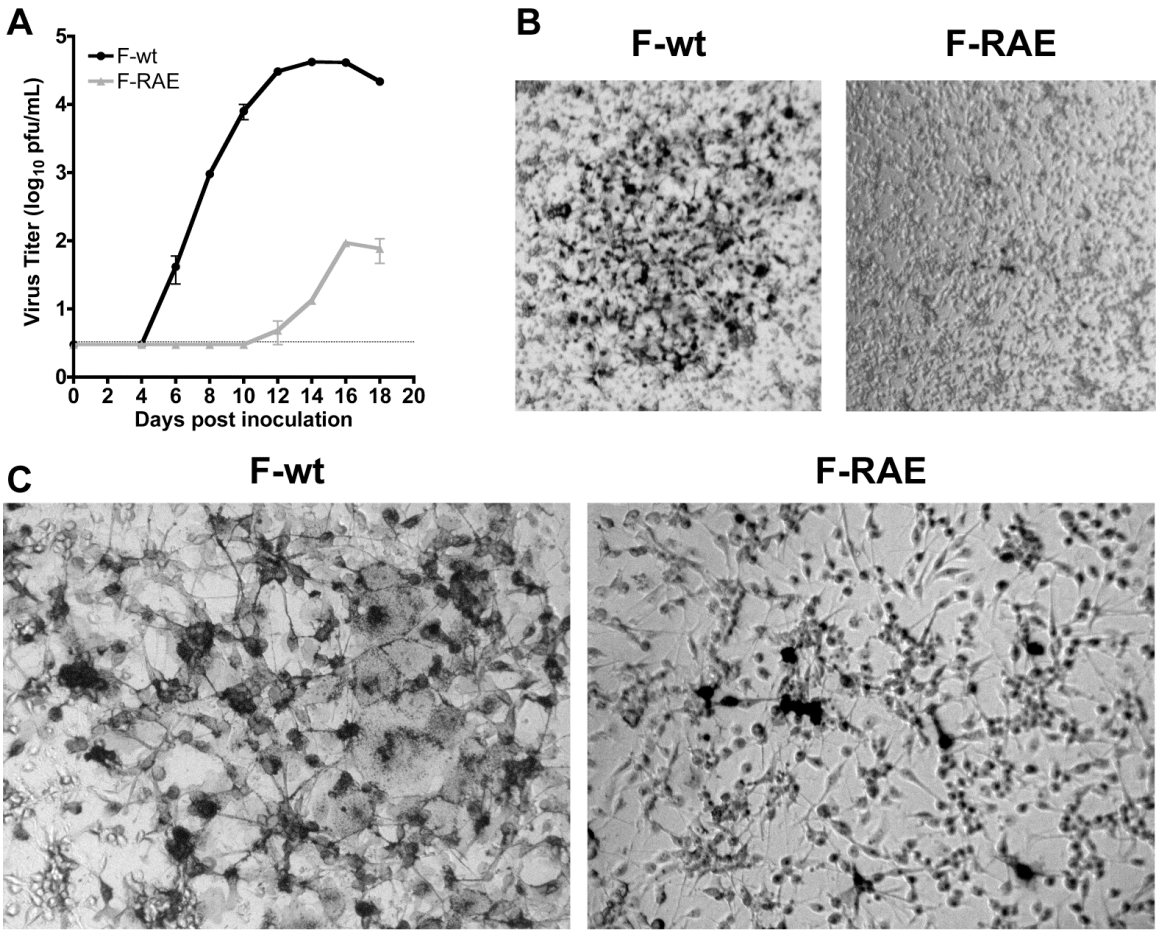

Fig. 4-6. The HMPV F RGD motif is required for HMPV infection.
(A) Titers from reverse-engineered viruses recovered with either the native RGD motif (F-wt) or F-RAE are shown as mean titer for two independently recovered viruses; error bars indicate SEM. The limit of detection is shown as a dotted line. (B and C) Light microscopy images depicting typical plaque size and morphology for HMPV F-wt and F-RAE. LLC-MK2 cells were infected with either HMPV F-wt or F-RAE and incubated for 4 days under a semisolid medium, permitting only cell-to-cell virus spread. HMPV-infected cells are stained black. Magnifications, 2.5x (B) and 10x (C).

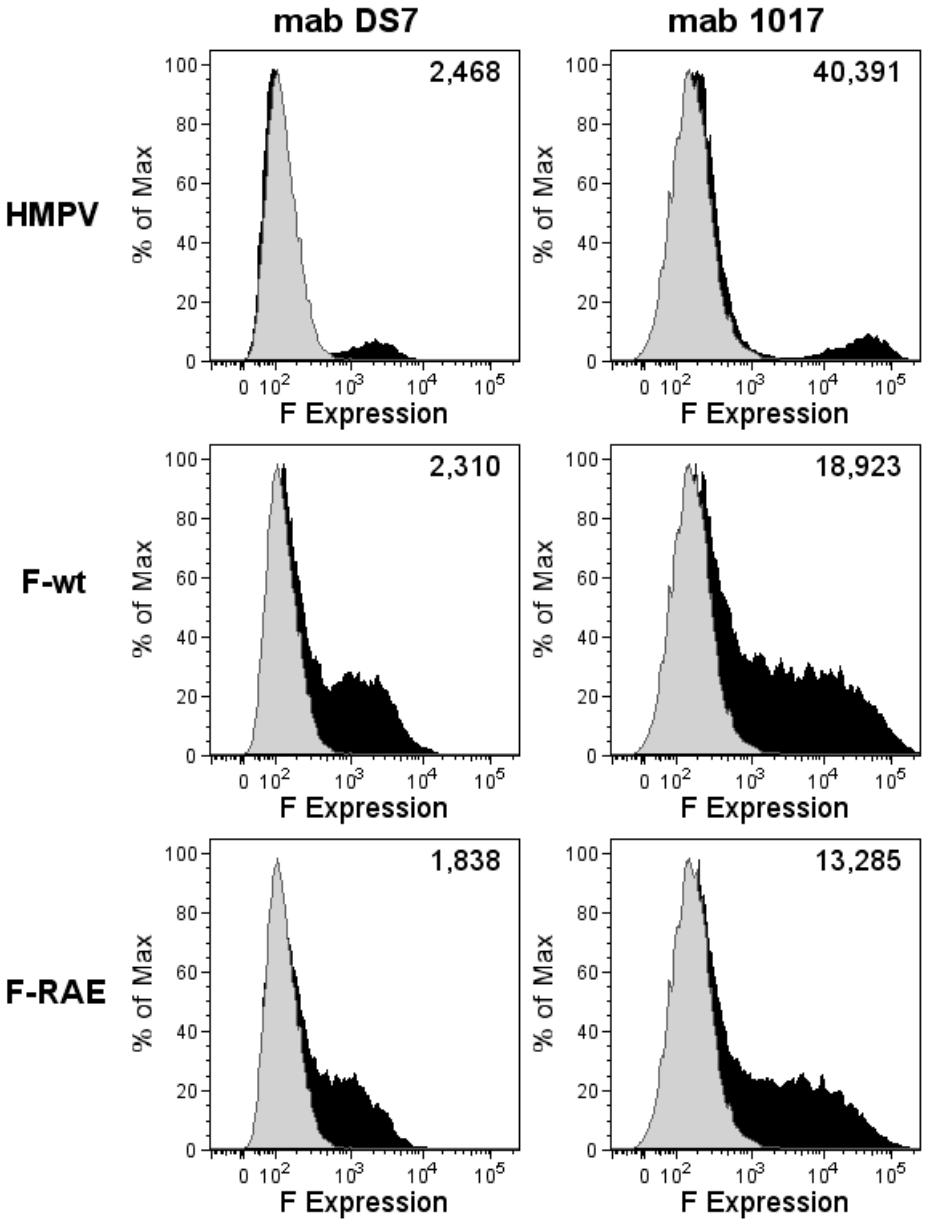

Fig. 4-7. HMPV F-RAE is expressed on the surface of transfected cells at wild-type levels.
BEAS-2B cells were infected with HMPV or transfected with empty vector (pcDNA3.1), pcDNA3.1-F-wt, or pcDNA3.1-F-RAE expression plasmids. At 48 hours postinfection or posttransfection, cells were stained for surface expression of F protein with HMPV F-specific mAbs, mAb DS7 or mAb 1017, and analyzed by flow cytometry. F expression is shown in black histograms, relative to background staining on cells transfected with empty vector (gray histograms). The number in the upper right corner of each panel represents mean fluorescence intensity of F expression.

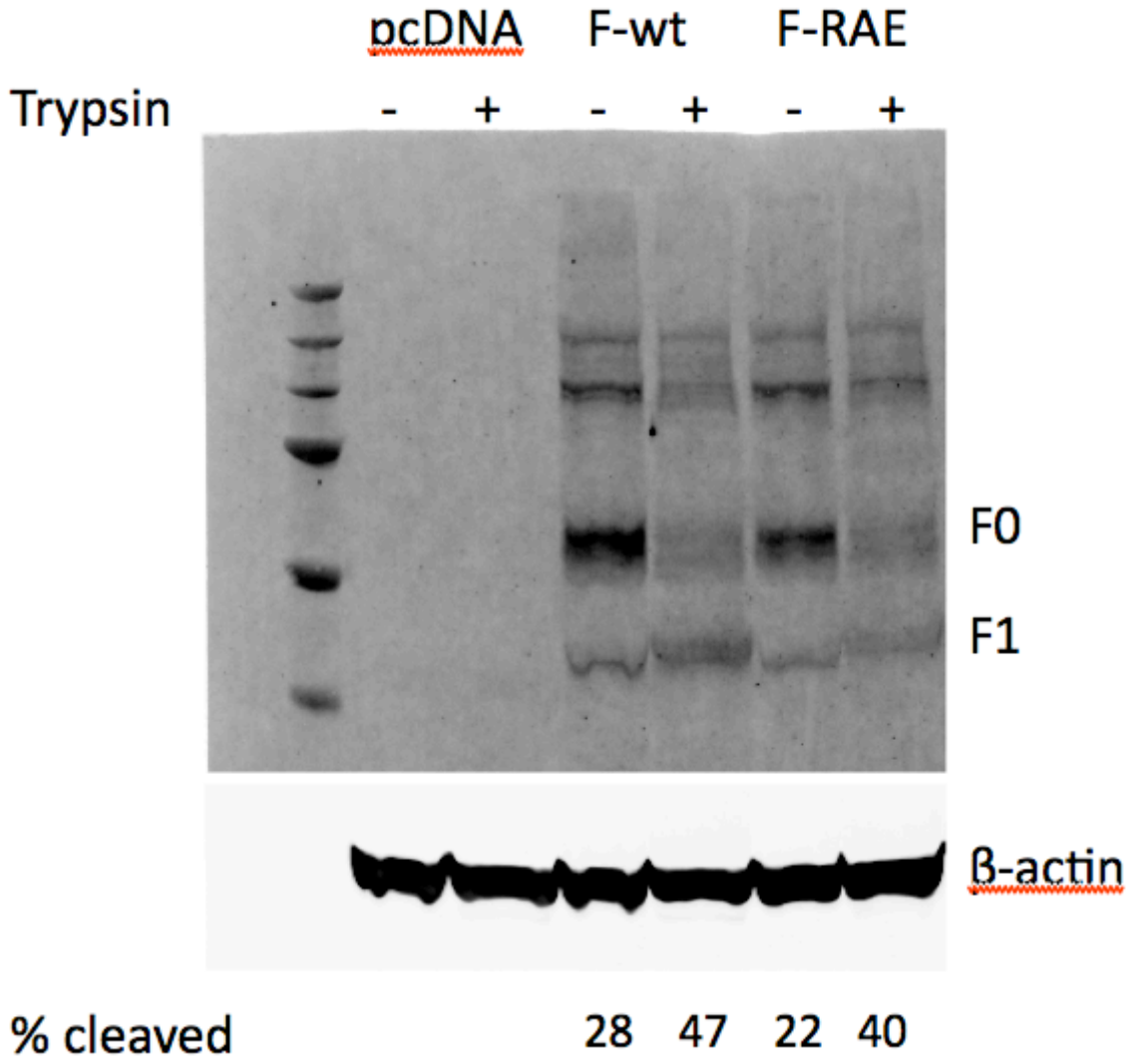

Fig. 4-8. HMPV F-RAE is processed from the F0 to the F1 form with similar efficiency as wild-type F protein.
BEAS-2B cells were transfected with empty vector (pcDNA), pcDNA3.1-F-wt, or pcDNA3.1-F-RAE expression plasmids. At 72 hours post-transfection, cells were lifted from the plate with 10 mM EDTA or 0.25% trypsin-EDTA, washed in serum medium, pelleted, and used to prepare cell lysates. Lysates were analyzed by Western blotting. HMPV F protein was detected (as described in Material and Methods for the analysis shown in Fig. 4-10G) using the Li-Cor Odyssey infrared imaging system. Uncleaved protein (F0) and the large subunit from the cleaved form (F1) of the fusion protein were detected. HMPV F0 and F1 bands were quantified and used to calculate the fraction of cleaved F [% cleaved = 100 x F1 / (F0 + F1)]. β-actin bands were detected in a different channel than F on the same blot and thus appear on a different image.

HMPV fusion is not triggered by HMPV G or RGD-binding integrins. The finding that HMPV infection was inhibited more potently than attachment by RGD-binding integrin blockade suggested that not only binding but also subsequent fusion depends upon RGD-binding integrin engagement. To investigate whether HMPV F fusion activity was linked to RGD-integrin binding, I sought to determine HMPV virus-cell fusion kinetics.

I developed an R18-dequenching assay to monitor virus-cell membrane fusion in real time (details described in Chapter III). During virus-mediated fusion, R18 dilutes from a quenched state in the viral membrane into unlabeled cell membranes, resulting in fluorescence (R18 dequenching) that reflects the extent of virus fusion. R18-MPV attached to the cell surface resulted in minimal R18 fluorescence (Fig. 4-9A, time = 0 min). However, during virus-cell fusion, I observed a steady increase in R18 fluorescence over time (Fig. 4-9A). HMPV fusion appeared to progress from punctuate foci to fluorescent cell membranes. R18-MPV fusion resulted in a linear increase in R18 fluorescence over 2 h, and reached a plateau after 160 min (Fig. 4-9B, red circles). As expected, fusion was temperature dependent, because cells maintained at 4°C did not increase in fluorescence intensity over time (Fig. 4-9B, blue squares).

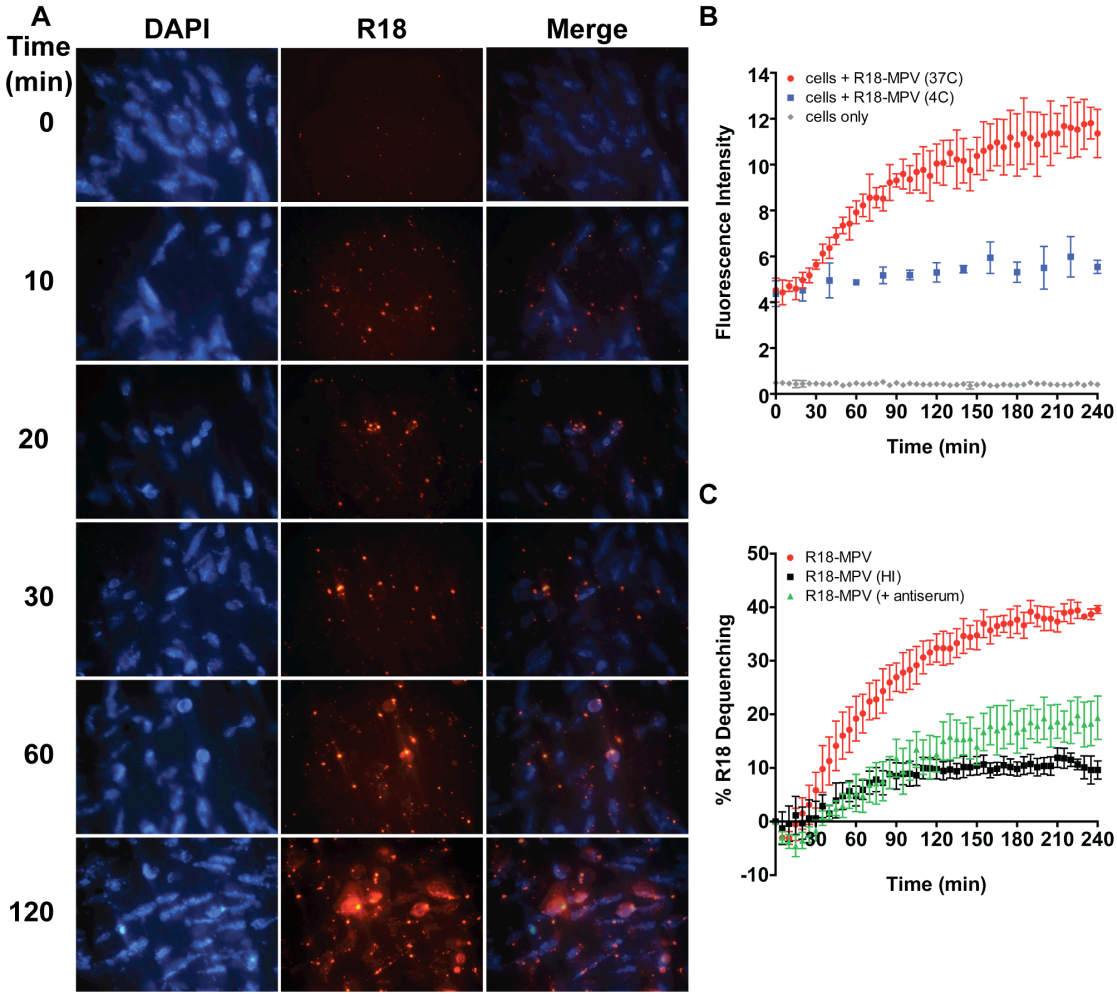

Fig. 4-9. HMPV fusion occurs slowly over the course of several hours.
(A) R18-MPV fusion with live, adherent human bronchial epithelial (BEAS-2B) cells. R18 fluorescence increases over time as R18 dye self-quenched in the virus membrane dilutes into cellular membranes during virus-mediated membrane fusion. The zero time point was imaged before incubating cells at 37°C to initiate virus fusion. Live cell images were captured with a Zeiss Axiovert 200 microscope using a 40× objective with 359/461-nm (DAPI) and 556/573-nm (R18) filters at the indicated time points. (B) R18-MPV fusion was measured with a plate reader. Curves represent fluorescence of cells (gray diamonds), cells plus R18-MPV at 4°C (blue squares), or cells plus R18-MPV at 37°C (red circles). Results for triplicate wells (mean ± standard deviation [SD]) from a representative experiment are shown. (C) R18-MPV fusion was measured in the absence (red circles) or presence (green triangles) of neutralizing HMPV antiserum (dilution, 1:40) or for heat-inactivated virus (black squares). Percent R18 dequenching was calculated as described in Materials and Methods. Curves represent mean percent R18 dequenching for three independent experiments, monitored for triplicate wells. Error bars indicate SEM.

HMPV fusion appeared to be a slow process, but I sought to confirm that the increased R18 signal was due to virus fusion and that known inhibitors of HMPV fusion could inhibit R18 dequenching in our assay. To monitor HMPV fusion kinetics but normalize for any differences in particle binding, I converted the R18 fluorescence intensity to percent R18 dequenching over time (as described in Materials and Methods) for the positive inhibition controls (Fig. 4-9C) and all conditions tested and reported in Fig. 4-10. Paramyxovirus fusion proteins can be artificially triggered to refold into an inactive postfusion structure by heat (Connolly and Lamb, 2006). Heat-inactivated R18-MPV could bind but not fuse with cells (Fig. 4-9C, black squares), confirming that the R18 fusion signal was due to active virus fusion rather than passive transfer of R18 dye. R18-MPV fusion was significantly inhibited in the presence of neutralizing HMPV antiserum (Fig. 4-9C, green triangles). The polyclonal antiserum reduced R18-MPV binding by ~50% but completely neutralized HMPV infection. Thus, HMPV F-specific antibodies in the serum blocked binding but also prevented bound virus from fusing with cells. Importantly, this inhibition of virus-cell fusion resulted in significantly less R18 dequenching in the fusion assay. Thus, our findings indicate that HMPV fusion is a slow process that occurs over several hours.

Next, I investigated whether the HMPV attachment (G) protein was required for virus-cell fusion. Schowalter et al. previously reported that HMPV G was not required for HMPV F-mediated cell-cell fusion, although the authors suggested that the G protein might enhance fusion in certain cell types (Schowalter et al., 2006). HMPVΔG is attenuated *in vivo,* although it is currently not clear whether lower viral titers are due to a defect in virus binding and/or entry (Biacchesi et al., 2005; Biacchesi et al., 2004).

Further, no previous studies have assessed whether virus-cell fusion requires the presence of the HMPV G protein. To determine whether HMPV G was required for fusion, I analyzed VLP fusion kinetics. Results for R18-F-VLP fusion controls are shown in Fig. 4-10A. As expected from my virus-cell fusion experiments, heat-inactivation abolished R18 dequenching. G-VLP dequenching (Fig. 4-10A, diamonds) provided a measure of background R18 transfer in the VLP fusion assay, as these particles are expected to bind but not fuse because they do not have HMPV F. Neutralizing antiserum significantly reduced HMPV F-mediated VLP fusion, nearly to the background levels observed for G-only VLPs. These fusion controls indicate that there is some nonspecific R18 dye transfer in the VLP fusion assay but that HMPV F-mediated fusion kinetics can be quantified because F-VLP dequenching was significantly over background. Next, F-only and F+G VLP fusion kinetics were monitored to define whether the HMPV G protein contributed to HMPV fusion. I found that F-only VLP and F+G-VLP fusion proceeded with the same kinetics (Fig. 4-10B) and to the same extent (Fig. 4-10C). Thus, G does not contribute to F-mediated VLP fusion in the *in vitro* fusion assay. I noted that VLP fusion was not as efficient as virus fusion (Fig. 4-10B and C); however, despite differences in fusion extent, the early kinetics of virus and VLP fusion were identical. Fusion began after a short delay, the initial fusion rate became lower after 2 h, and fusion reached a plateau at around 4 h. These similarities suggest that VLP fusion represents an appropriate model for early virus fusion kinetics. Thus, these results indicate that the HMPV F protein is necessary and sufficient for virus-cell fusion and can regulate fusion in the absence of G. Our findings suggest that HMPV F-receptor interactions are sufficient to trigger fusion, and G interactions with F are not essential for HMPV virus-cell fusion *in vitro*.

I hypothesized that HMPV F binding to RGD-binding integrins may serve to trigger fusion. To explore this possibility, I assessed HMPV and VLP fusion kinetics in the presence of integrin function-blocking antibodies. As expected, blockade of RGD-binding integrins significantly decreased the amount of virus and VLP binding (inhibiting binding by ~50%), while blocking the collagen-binding integrin subunit α2 had no effect. However, I found that HMPV fusion was not significantly impaired by RGD-binding integrin blockade (Fig. 4-10D, E, and F). Blocking RGD-binding integrins during virus or VLP binding altered neither fusion kinetics nor fusion extent after 4 h. In other words, even though ~50% less virus or VLPs bound to the surface of cells during RGD-binding integrin blockade, the particles that did bind were still capable of mediating fusion.

In order to examine the importance of the integrin-binding motif on F-mediated particle-cell fusion, I generated F-RAE VLPs. F-RAE VLPs budded with slightly less efficiency than F-wt VLPs, although the fusion protein was efficiently cleaved into the fusogenic form (indicated by F0-to-F1 conversion) (Fig. 4-10G). I found that F-RAE VLPs fused with kinetics identical to those of wild-type F-VLPs (Fig. 4-10H), which would be expected if integrin binding was not the primary trigger for the initiation of HMPV fusion. I tested F-RAE vs. F-RGD VLP fusion at different concentrations of bound particles (a range of 30-fold) to confirm that the number of particles bound did not effect fusion kinetics, and I found that R18-dequenching kinetics were unaltered, despite declining fluorescence intensity signal for lower multiplicities of infection (Fig. 4-11). These results strongly suggest that although efficient HMPV binding and productive infection require RGD-binding integrin engagement, integrin binding alone does not trigger fusion.

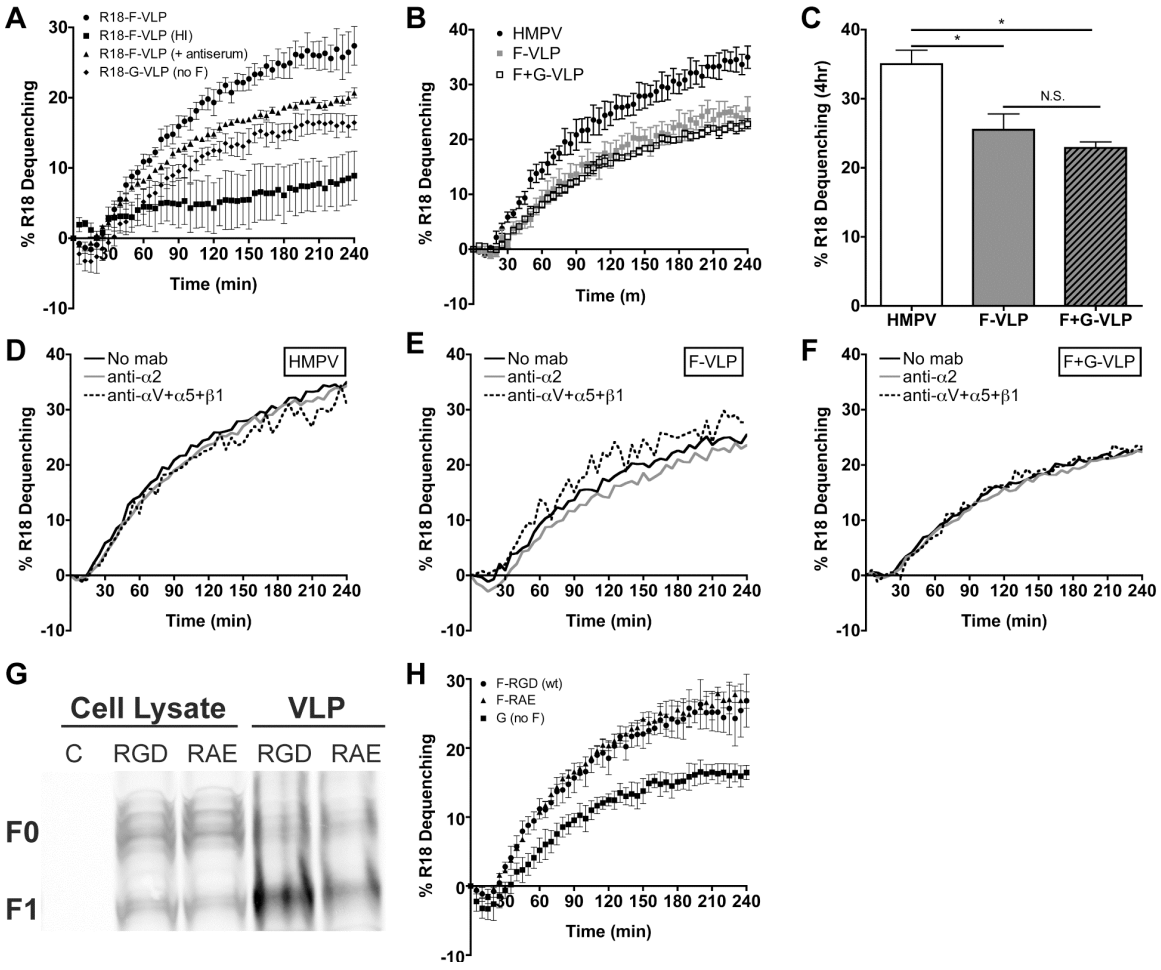
A
R18-F-VLP
R18-F-VLP (HI)
R18-F-VLP (+ antiserum)
R18-G-VLP (no F)
% R18 Dequenching
Time (min)
B
HMPV
F-VLP
F+G-VLP
% R18 Dequenching
Time (m)
C
% R18 Dequenching (4hr)
N.S.
HMPV
F-VLP
F+G-VLP
D
No mab
anti-α2
anti-αV+α5+β1
HMPV
% R18 Dequenching
Time (min)
E
No mab
anti-α2
anti-αV+α5+β1
F-VLP
% R18 Dequenching
Time (min)
F
No mab
anti-α2
anti-αV+α5+β1
F+G-VLP
% R18 Dequenching
Time (min)
G
Cell Lysate
VLP
C
RGD
RAE
RGD
RAE
F0
F1
H
F-RGD (wt)
F-RAE
G (no F)
% R18 Dequenching
Time (min)

Fig. 4-10. HMPV fusion is not triggered by HMPV G or RGD-binding integrins. (A) R18 F-VLP fusion was measured in the absence (circles) or presence (triangles) of neutralizing HMPV antiserum or for heat-inactivated particles (squares). R18-G-VLP (diamonds) dequenching was monitored as a background control. Percent R18 dequenching was calculated as described in Materials and Methods, and curves represent means for three independent experiments monitored for triplicate wells. Error bars indicate SEM. (B and C) HMPV G does not alter HMPV F-mediated fusion kinetics or the extent of fusion at 4 h. R18-labeled HMPV (black circles), F-VLPs (gray squares), or F+G-VLPs (open squares) were bound to the surface of BEAS-2B cells, and R18 fluorescence was monitored for 4 h. Triton X-100 was added after 4 h to determine the extent of virus or VLP fusion. Curves in panel B represent mean percent R18 dequenching for three independent experiments, monitored for duplicate wells. Bars in panel C represent the extent of fusion observed after 4 h for three independent experiments; error bars indicate SEM. *, $P \leq 0.05$; N.S., $P > 0.05$. (D to F) HMPV F binding to RGD-binding integrins does not alter HMPV fusion kinetics. R18-labeled HMPV (D), F-VLP (E), or F+G-VLP (F) fusion was assessed in the absence of antibodies (black lines) or in the presence of integrin function-blocking antibodies against α2 integrins (gray lines) or all RGD-binding integrins (αV plus α5 plus β1) (dotted lines). Curves represent mean percent R18 dequenching for three independent experiments monitored for duplicate wells. Error bars are not shown for figure clarity. Dequenching rates were not significantly altered in the presence of integrin antibodies; however, significantly less HMPV and VLPs bound during RGD-binding integrin blockade (data not shown). (G) F-RGD (wt) VLPs (10 μg), F-RAE VLPs (10 μg), and producer cell lysates (50 μg) were analyzed by Western blotting. Uncleaved (F0) and cleaved (F1) HMPV F were detected with an F-specific mAb and fluorescent secondary antibody using the Li-Cor Odyssey infrared imaging system. C, untransfected 293-F cell lysate. (H) The RGD integrin-binding motif is not required for efficient F-mediated hemifusion. R18 VLP fusion was measured for F-RGD (circles), F-RAE (triangles), or G-only (squares) particles as described for panel A.

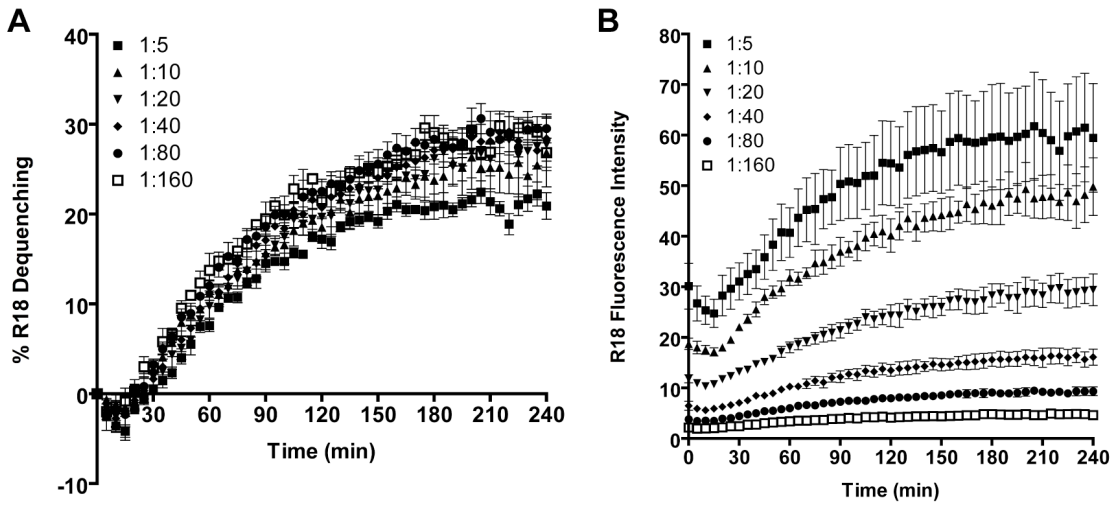

Fig. 4-11. R18-MPV fusion kinetics are not significantly altered by reduced virus binding.

Serial dilutions of R18-MPV were bound to BEAS-2B cells, unbound virus was washed away, and R18-MPV fusion was monitored for 4 h. Results (mean ± SEM) for three independent experiments are shown as percent R18 dequenching (A) or fluorescence intensity (B). The dilution of R18-MPV is indicated in the legend.

Productive HMPV transcription depends upon RGD-binding integrin mediated virus entry. R18 dequenching measures virus hemifusion, mixing of the outer lipid leaflets of virus and cellular membranes as fusion begins. After hemifusion, HMPV fusion and virus entry require merging of the inner leaflets of the virus and cell membranes, formation of a fusion pore, fusion pore expansion, and, finally, delivery of the viral genome into the cytoplasm for viral transcription. Thus, productive virus transcription can be used as a measure of the entire virus entry process. Because RGD-binding integrins were not required for HMPV hemifusion, I next investigated whether integrins were required for full fusion and virus genome entry, as measured by virus transcription at 8 h postinfection. I sought to determine whether RGD-binding integrins mediated virus entry postbinding and designed the experiment to elucidate whether HMPV bound in the presence of RGD-binding integrin function-blocking antibodies was capable of entering cells and producing virus transcripts. We used real-time RT-PCR to quantify the level of HMPV nucleoprotein (N) transcribed during the first 8 h of infection (see Materials and Methods) and found that blocking the interaction between HMPV F and all RGD-binding integrins (αV plus α5 plus β1) resulted in 50% fewer viral transcripts than for an untreated control (Fig. 4-12, hashed bar versus black bar). As expected, blocking the collagen-binding α2 integrin subunit had no effect on HMPV transcription (Fig. 4-12, gray bar). These results suggest that RGD-binding integrins mediate postbinding events required for productive virus entry and necessary for efficient virus transcription early in HMPV infection.

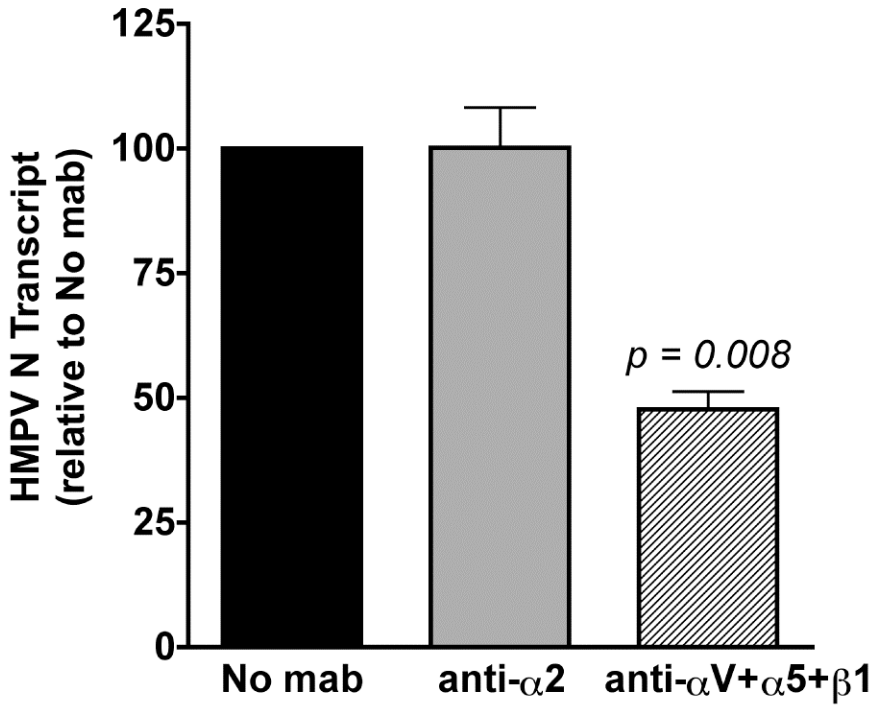

Fig. 4-12. Productive HMPV transcription depends upon RGD-binding integrin-mediated virus entry.
HMPV (MOI = 0.25 PFU/cell) was bound to the surface of BEAS-2B cells in the absence or presence of α2 integrin or RGD-binding integrin (αV plus α5 plus β1) function-blocking antibodies. Levels of HMPV N transcript were determined at 8 h postinfection by real-time RT-PCR, relative to the GAPDH cellular gene. The $2^{-\Delta\Delta CT}$ method was used to correct for input genome and compare transcript levels in treated and untreated samples. Data are presented as the average level of HMPV N transcript detected relative to an untreated (no mAb) control; error bars indicate SEM for six biological replicates from two independent experiments.

Discussion

HMPV gains entry into cells in a manner that can be mediated solely by one surface glycoprotein, the fusion (F) protein. How HMPV F mediates both attachment and fusion has not been clearly defined. In this chapter, I have presented evidence that F mediates HMPV entry through an interaction with RGD-binding integrins. HMPV F binds to RGD-binding integrins during virus attachment, and this binding event is necessary for virus entry and subsequent productive infection. In lieu of an interaction between the viral attachment (G) protein and cellular receptors, F is capable of initiating virus entry by binding directly to cellular receptors, including RGD-binding integrins. Interestingly, while an F-integrin interaction is necessary for virus entry, integrin binding does not appear to trigger F-mediated hemifusion. RGD-binding integrins are important for postbinding events, which occur after virus hemifusion but before HMPV transcription. Thus, we propose a model of HMPV entry as a stepwise process where i) F binds to cell surface receptors, including RGD-binding integrins, ii) unidentified events trigger virus hemifusion, and iii) RGD-binding integrins facilitate postbinding events that promote virus entry and lead to efficient virus transcription and productive infection.

In Chapter II, I demonstrated that HMPV infection depends upon RGD-binding integrins (Cseke et al., 2009). In this chapter, I show that multiple RGD-binding integrins are required for HMPV attachment and entry. HMPV F-mediated attachment depends, in part, upon RGD-binding integrin engagement on the surface of human respiratory epithelial cells. RGD-binding integrin-specific binding accounted for about 50% of total R18-MPV binding in my experiments, indicating that other cell surface receptors also bind HMPV. When all RGD-binding integrins were blocked, I observed a ~50% decrease

in HMPV attachment that resulted in a 90% reduction in HMPV infectivity. This discrepancy led me to explore whether RGD-binding integrins were required for virus entry after initial virus binding, and I found that RGD-binding integrins promote virus entry after HMPV hemifusion begins. HMPV transcription was reduced by 50% when HMPV F-integrin binding was blocked. This suggests that although HMPV binds to cell surface receptors other than integrins, most of these particles are not capable of delivering the genome into target cells for virus transcription. Although it appears that HMPV attaches to more than one receptor on the cell surface, HMPV F must engage RGD-binding integrins during attachment for efficient virus entry and productive infection.

Chang et al. recently reported that HMPV binding and infection are mediated by interactions between the F protein and heparan sulfate and suggested that heparan sulfate is the first binding partner for HMPV F (Chang et al., 2012b). In experiments using β1 integrin-deficient murine fibroblasts, β1 integrin was critical for HMPV infection, but the authors concluded that β1 integrin is involved after initial binding and is not a direct cellular receptor for HMPV because virus still bound β1 integrin-deficient cells (Chang et al., 2012b). In light of my findings that HMPV F binds multiple integrins during attachment, HMPV F would be expected to bind to other RGD-binding integrins such as αVβ5, αVβ6, and/or αVβ8. HMPV F binding to αV integrins could explain some of the residual F-mediated virus-cell binding and low levels of infection that Chang et al. (Chang et al., 2012b) observed in β1 integrin-deficient cells at higher multiplicity of infection. Moreover, when β1-null fibroblasts were complemented with human β1 integrin, HMPV F-only virus bound more readily and infection was significantly enhanced (Chang et al., 2012b). These findings are consistent with my results implicating

multiple RGD-binding integrins (including α5β1) in regulating HMPV entry following initial virus attachment. This suggests that heparan sulfate may be an important adhesion factor for HMPV F but that integrin engagement is critical for infection. My results do not exclude the possibility that F also interacts with other adhesion factors during cell attachment. Indeed, my results strongly suggest that HMPV F binds to multiple cellular receptors, and further investigation is required to clarify which F-receptor interactions are necessary to trigger F refolding and initiate virus hemifusion. Taken together, the data suggest that HMPV F interacts with multiple binding partners during attachment, perhaps first attaching to heparan sulfate before engaging specific proteinaceous receptors such as RGD-binding integrins, which mediate postbinding events that lead to productive HMPV infection.

The HMPV F protein alone is necessary and sufficient for virus attachment, and VLPs with only F protein require RGD-binding integrins for binding. Moreover, mutating the RGD to RAE resulted in a 3-$\log_{10}$ defect in HMPV replication, showing that the invariant RGD motif in the F protein is required for HMPV infectivity. This strongly suggests that integrin binding is mediated largely by the RGD motif and that HMPV F-integrin engagement is essential for receptor-binding activity. The F RAE mutation did not completely abolish HMPV infection, although F-RAE viruses did not replicate efficiently and exhibited clear defects in cell-to-cell spread. It is possible that simply mutating the tripeptide motif is not sufficient to completely abolish an F-integrin interaction during virus binding; there are likely other residues in both proteins that contribute to the interaction. The reproducible recovery of low levels of an F-RAE virus and the detection of F-RAE protein on the surface of infected cells suggest that the F-

RAE protein is expressed and folded into a fusion-competent form that mediates low levels of virus entry. I confirmed that the F-RAE mutation did not alter cell surface F expression or cleavage levels when the protein was expressed from a plasmid in transfected cells. Unfortunately, due to the extremely low virus titer, it was not feasible to measure F-RAE virus binding and fusion. However, I was able to compare F-RGD and F-RAE VLP fusion kinetics, and I found that the integrin-binding motif was not required for efficient HMPV hemifusion. Collectively, these results provide evidence that supports a mechanism where F engages RGD-binding integrin receptors during virus entry. My VLP experiments suggest that HMPV F-mediated attachment and virus-cell fusion are regulated independently of HMPV G. Because HMPVΔG is not defective for replication *in vitro* (Biacchesi et al., 2004) and HMPV F-RAE is quite debilitated, my findings are consistent with a mechanism whereby HMPV F interacts with cell surface receptors in a manner that triggers fusion and facilitates virus entry in a G-independent manner. It is important to note that HMPVΔG is attenuated in hamsters and nonhuman primates (Biacchesi et al., 2005; Biacchesi et al., 2004), and G is clearly important for virus fitness *in vivo*. As discussed in Chapter I, pneumovirus G proteins contribute to virus attachment and are likely important for strengthening particle adhesion and concentrating virions on the cell surface. However, because G is dispensable for viral entry, it is not absolutely required for the membrane fusion activity of F during the virus entry process.

By definition, virus receptors mediate attachment and facilitate entry. In principle, cellular receptors for HMPV F could facilitate entry by inducing conformational changes in F, recruiting co-receptors to sites of virus attachment, recruiting cellular factors that facilitate fusion pore expansion, or promoting internalization of virus particles. Although

HMPV F attachment was inhibited, virus entry leading to efficient viral replication was further impaired in the presence of RGD-binding integrin antibodies. These results explain why the inhibition of attachment is much less potent than the inhibition of infectivity (Fig. 4-2). If HMPV binding and postbinding events during entry depend upon RGD-binding integrins, then infectivity should be affected to a greater degree than attachment during integrin blockade. My experiments suggest that integrin engagement does not trigger HMPV hemifusion but that RGD-binding integrins do promote HMPV entry. The mechanism by which RGD-binding integrins regulate HMPV entry requires further investigation.

CHAPTER V

THE HMPV FUSION PROTEIN MEDIATES VIRUS-CELL FUSION AT AN INTRACELLULAR MEMBRANE

Introduction

Paramyxovirus fusion is thought to occur at the plasma membrane. This dogma is largely based upon the observation that paramyxoviruses fuse in a pH-independent manner and commonly induce cell-cell fusion or syncytia formation when grown in cell culture. In general, enveloped viruses are divided into two types, those for which membrane fusion is triggered by low pH and those that fuse at neutral pH, presumably at the plasma membrane. For the well-studied influenza virus and vesicular stomatitis virus (VSV), a drop in pH triggers conformational changes in the viral fusion protein (Bullough et al., 1994; Hernandez et al., 1996; Roche et al., 2008; Rucker et al., 2012; Wilson et al., 1981). For these viruses, endosomal entry and acidification are required for productive infection. In contrast, infection by most retroviruses and paramyxoviruses is resistant to cell treatment with ammonium chloride, a weak base that buffers against acidification. This has been interpreted to mean that these viruses induce membrane fusion at neutral pH and do not require endocytosis. However, a recent study suggests that while capable of mediating fusion at the cell surface, HIV-1 can also productively enter cells via endocytosis and dynamin-dependent fusion with endosomes in a pH-independent manner (Miyauchi et al., 2009). Thus, pH-independent virus fusion can occur either at the cell surface or after internalization. These findings indicate that virus

sensitivity to acidification inhibitors does not necessarily provide any spatial information for where virus-cell membrane fusion occurs.

Much of our knowledge about HMPV entry is by analogy to other paramyxoviruses, and has not been tested directly. Further, several studies have investigated the ability of HMPV F to induce cell-cell fusion, but none have investigated particle-cell fusion. The few studies in the field of HMPV fusion have led to a debate about whether HMPV cell-cell fusion can occur at neutral pH. A few HMPV isolates have been found to require low pH treatment to induce cell-cell fusion (Herfst et al., 2008; Mas et al., 2011; Schowalter et al., 2009; Schowalter et al., 2006), while other HMPV isolates induce cell-cell fusion at neutral pH (Herfst et al., 2008; Mas et al., 2011). These observations about syncytia formation are difficult to interpret with respect to virus entry, because inhibitors of endosomal acidification do not impair HMPV infection of virus strains with a low pH-dependent cell-cell fusion phenotype (Mas et al., 2011). Because most HMPV isolates induce cell-cell fusion at neutral pH and are resistant to endosomal acidification inhibitors, it is plausible that HMPV could enter cells directly at the cell surface or via endocytosis; however, the site of HMPV fusion is still unclear.

While investigating HMPV fusion kinetics, I routinely observed a 20 to 30 minute delay before HMPV began fusing with adherent cells. I found this delay very interesting because the few studies of paramyxovirus virus-cell fusion had all reported a rapid initiation of virus fusion with cells (Connolly and Lamb, 2006; Krishnan et al., 2009; Pedroso de Lima et al., 1992). Furthermore, Dr. Rebecca Dutch's laboratory had previously reported evidence to suggest that HMPV entry may require endocytosis

(Schowalter et al., 2009). Thus, I began to investigate whether the delay I observed in HMPV fusion kinetics was related to virus internalization and sought to identify the cellular site of virus-cell fusion.

In this chapter, I show that HMPV F-mediated virus-cell fusion occurs at an intracellular membrane. HMPV F binding is not sufficient to trigger fusion, as indicated by a discernable delay in the kinetics of HMPV hemifusion. Using confocal microscopy experiments I demonstrate that HMPV particles are internalized during the first 20 minutes of entry, which correlates with the lag phase observed in the fusion experiments. Furthermore, HMPV particles escape antibody neutralization at the cell surface between 10 and 30 minutes postbinding. I also determined that chemical inhibitors of endocytosis impair HMPV fusion and infection. Finally, using a novel cell imaging approach, I show that HMPV fusion occurs with intracellular vesicles. These results suggest that HMPV does not fuse at the plasma membrane where paramyxovirus fusion is thought to occur. Further, it appears that HMPV regulates entry differently than other paramyxoviruses by separating fusion triggering from receptor binding at the cell surface.

I collaborated with Dr. Bernardo Mainou in Dr. Terry Dermody's laboratory during the course of these studies. He taught me confocal microscopy techniques and collected numerous images for me during my preliminary experiments. I am extremely grateful for his time, scientific contributions, and expert guidance during the design of my confocal microscopy experiments. Bernardo helped design the experiment, took the micrographs, and analyzed the data presented in Fig. 5-6.

Materials and Methods

Cells. BEAS-2B (ATCC CRL-9609) cells were maintained in Opti-MEM I medium (Invitrogen) containing 2% fetal bovine serum (FBS), 2 mM L-glutamine, 50 μg/mL gentamicin, and 2.5 μg/mL amphotericin B. Suspension 293-F cells were maintained as recommended by the manufacturer (293 Freestyle expression system; Invitrogen).

Antibodies. A heat-inactivated polyclonal HMPV-immune human serum, which neutralizes HMPV infection in an *in vitro* plaque neutralization assay (50% inhibitory concentration [IC_{50}], 1:1,500), was used in fusion experiments. The HMPV F-specific mAb, DS7, used for confocal microscopy experiments has been previously described (Williams et al., 2007).

Viruses. HMPV strain TN/94-49 (virus genotype A2) was used for all virus binding and fusion experiments. HMPV TN/94-49 is a clinical isolate passaged 5 to 7 times and thrice plaque purified in LLC-MK2 cells. Stock virus was propagated using LLC-MK2 cells in serum-free growth medium supplemented with 5 μg/mL trypsin (Invitrogen) as described previously (Williams et al., 2005b). Working virus was propagated in suspension 293-F cells in 293 Freestyle expression medium supplemented with 5 μg/mL trypsin-EDTA (both from Invitrogen). Briefly, 293-F cells were inoculated at 0.1 pfu/cell. At 4 days postinoculation, supernatant was collected and infected cells were freeze-thawed thrice, clarified by centrifugation at 300 x g for 5 min and added to the supernatant fraction. This crude virus preparation was further purified through a 20% sucrose cushion via ultracentrifugation at 100,000 x g for 90 min at 4°C. Octadecyl rhodamine B chloride

(R18)-labeled HMPV (R18-MPV) was prepared by incubating 10 mM R18 dissolved in ethanol with sucrose-purified HMPV at 20 nmol R18 per mg total virus protein for 1 h at room temperature. The reaction mixture was pelleted through a discontinuous sucrose gradient by ultracentrifugation at 100,000 x g for 90 min at 4°C. Labeled virus (pink by visible light) was collected at the 20/60% sucrose interface, snap-frozen in dry ice-alcohol, and stored at -80°C. DiD-labeled HMPV (DiD-MPV) was prepared by incubating 10 mM DiD dissolved in ethanol with sucrose-purified HMPV at 5 μM for 1 h at room temperature. The reaction mixture was purified and labeled virus (blue by visible light) was frozen and stored as described for R18-MPV. DiD-Red-MPV was prepared by metabolically labeling HMPV-infected 293-F cells. At 12 hours post virus inoculation, cells were incubated with 10 μM CellTracker Orange CMRA (Invitrogen) and 5 μM DiD for 45 min at 37°C. Cells were washed extensively to remove any unincorporated dyes, resuspended in virus growth medium, and incubated at 37°C with 5% CO_2 with shaking. At fours days postinculation, cell supernatant was sucrose-purified as described above, and labeled virus (purple by visible light) was frozen and stored at -80°C. All virus preparations were titrated on LLC-MK2 cells as previously described (Williams et al., 2005b).

Quantifying HMPV infection. At 24 hours postinoculation, BEAS-2B cell monolayers were fixed with buffered formalin (3.3% in growth medium) and immunostained for HMPV infection with a precipitating peroxidase substrate (True Blue; KPL) as previously described (Cseke et al., 2009). Individual wells were imaged on a light box with a macro zoom lens (Navitar, 18 to 108 mm), and infected cells, which appear blue,

were enumerated using ImageJ. Cells in entire wells were counted. The image contrast threshold was held constant during counting for all wells in a single plate.

Confocal microscopy. For the analysis presented in Fig. 5-2, BEAS-2B cells, grown to ~90% confluence on glass cover slips coated with a thin layer of Matrigel (BD Biosciences) in 24-well plates, were incubated with HMPV (~2 pfu/cell) for 1 h at 4°C with occasional rocking. Unbound virus was washed away, and cell culture medium was added to cells. The zero time point was fixed immediately. Virus entry was initiated by incubating cells at 37°C. At indicated time points, cells were fixed with 5% buffered formalin for 20 min at room temperature and washed three times with phosphate-buffered saline (PBS). Cells were permeabilized with 1% Triton X-100 in PBS for 5 min at room temperature. Following fixation, cells were blocked in PBS plus 0.5% BSA, 0.1% glycine, and 0.05% Tween-20 (PBS-BGT) for 30 min at room temperature, followed by the addition of anti-HMPV F mAb DS7 at 2.5 μg/mL for 1 h at room temperature. Cells were washed thrice in PBS-BGT and anti-human IgG Alexa Fluor 568 antibody (Invitrogen) was added at a dilution of 1:1,000 in PBS-BGT solution for 1 h at room temperature to detect anti-F primary antibody. Cells were washed thrice with PBS-BGT, incubated with Alexa Fluor 488-phalloidin (Invitrogen) at a dilution of 1:40 and TO-PRO-3 (Invitrogen) at a dilution of 1:1,000 in PBS-BGT for 20 min at room temperature. Cells were washed three times in PBS-BGT, twice in PBS, and fixed on glass slides using AquaPolyMount (Polysciences). Images were obtained on a Zeiss inverted LSM510 confocal microscope using a 63x oil objective lens.

R18-MPV binding assay. R18-MPV (1 pfu/cell) was incubated with BEAS-2B cells grown to confluence in black (opaque) transparent-bottom 96-well plates for 1 h on ice. Cells were washed with ice-cold PBS to remove unbound virus. PBS plus 1% Triton X-100 was added to each well, and fluorescence (excitation, 544nm; emission, 590nm; top-read mode) was measured using a SpectraMax M5 (Molecular Devices) plate reader. For endocytosis inhibitor experiments, dynasore hydrate and chlorpromazine hydrochloride (both from Sigma) were dissolved in dimethyl sulfoxide (DMSO) at 10 mM, and diluted freshly into Opti-MEM I immediately before use. For pre-treatment experiments, cells were incubated with media containing DMSO or inhibitor for 1 h at 37°C followed by 30 min at 4°C and removed during R18-MPV binding. For postbinding treatment experiments, R18-MPV was bound to cells as described above, unbound virus was washed away, and media containing DMSO or inhibitor was added and incubated with cells for 30 min on ice before R18-MPV binding was measured.

R18-MPV fusion assay. R18-MPV (1 pfu/cell) was incubated with BEAS-2B cells grown to confluence in black (opaque) transparent-bottom 96-well plates for 1 h on ice. Cells were washed with ice-cold PBS to remove unbound virus before Opti-MEM I medium (without phenol red) supplemented with 2% FBS was added to cells. Ice-cold plates were transferred to a preheated (37°C) SpectraMax M5 plate reader. Fluorescence (excitation, 544nm; emission, 590nm; top-read mode) was measured in real time for 4 h with readings collected every 5 min. At the end of the time course, Triton X-100 (final concentration of 1%) was added to each well, and final fluorescence readings were acquired. Endocytosis inhibitor treatments were performed as described above. The ability of bound R18-MPV to subsequently undergo fusion was defined as R18

dequenching and calculated according to the following equation: % R18 dequenching = 100 x (F - F_0)/(F_d – F_0), where F is fluorescence, F_0 is fluorescence at t = 0 min, and F_d is fluorescence after the addition of Triton X-100 (at the end of the experiment).

DiD-MPV fusion assay. For the analysis presented in Fig. 5-7, BEAS-2B cells, grown to ~90% confluence on glass cover slips coated with Matrigel (BD Biosciences) in 24-well plates, were loaded with CellTracker Green CMFDA (Invitrogen) at 0.5 μM for 30 min immediately before the experiment. CellTracker green-labeled cells were incubated with DiD-MPV (0.25 pfu/cell) for 1 h at 4°C with occasional rocking. Unbound virus was washed away, and cell culture medium was added to cells. For inhibitor treatment, HMPV-specific neutralizing antiserum at a dilution of 1:20 or chlorpromazine (100 μM) was added to the cell medium. Cells were incubated at room temperature for 15 min, to allow time for inhibitors to affect HMPV fusion, and virus fusion was initiated by incubating cells at 37°C. After one hour, cells were washed with PBS, fixed with 5% buffered formalin for 20 min at room temperature and washed three times with PBS. Cover slips were fixed on glass slides using AquaPolyMount. Images were obtained on a Zeiss inverted LSM510 confocal microscope using a 20x objective lens. Fifteen random images containing 30 to 40 cells per field for each condition were collected and analyzed by Bernardo Mainou, who had been blinded to the treatment condition. Cells were examined for the presence of DiD fluorescence and cells with any DiD fluorescence were considered to be DiD-positive.

DiD-Red-MPV fusion assay. To identify the cellular site of HMPV fusion, I modified a method used by Miyauchi et al. (Miyauchi et al., 2009). The principle of the assay relies on visualizing fusion of viruses colabeled with the lipophilic dye DiD and a small, diffusible content marker dye. Fusion at the cell surface should lead to the disappearance of DiD and the content dye due to dilution of the membrane dye into the plasma membrane and the content dye into the cytoplasm. However, virus fusion with a small intracellular vesicle should lead to an increase in the DiD fluorescence intensity and a loss of the content dye marker after virus-cell membrane fusion is complete (see Fig. 5-8). Thus, the cellular site of fusion can be identified based on the visualization of virus-associated fluorescent labels. For the analysis presented in Fig. 5-9, BEAS-2B cells, grown to ~90% confluence on glass cover slips coated with Matrigel (BD Biosciences) in 24-well plates, were loaded with CellTracker Green CMFDA (Invitrogen) at 0.5 μM for 30 min immediately before the experiment. CellTracker green-labeled cells were incubated with DiD-Red-MPV (0.1 pfu/cell) for 1 h at 4°C with occasional rocking. Unbound virus was washed away, and cell culture medium pre-warmed to 37°C was added to cells. For inhibitor treatment, HMPV-specific neutralizing antiserum at a dilution of 1:20 was added to the cell medium. Cells were incubated at 37°C and at indicated time points cells were washed with PBS and fixed with 5% buffered formalin. Cells were washed three times with PBS, and cover slips were fixed on glass slides using AquaPolyMount. Images were obtained on a Zeiss inverted LSM510 confocal microscope using a 63x oil objective lens. The confocal imaging parameters were kept constant for each time point in an experiment for comparative analysis of fluorescence intensity. Z-stacks for random fields containing about 30 cells for each time point were

collected. For all images, the entire z-stack was analyzed and the number of red, blue or red plus blue particles was enumerated. For the analysis presented in Fig. 5-9C, DiD intensity was quantified using MetaMorph software with the intensity threshold held constant for all images.

Statistical Analysis. Virus binding and fusion extent were compared using a one-way analysis of variance (ANOVA) and Dunnett's test comparing all treatment conditions to untreated. For all analyses, a P value ≤ 0.05 was considered statistically significant.

Results

HMPV hemifusion begins after a discernable delay. In Chapter III, I described an R18-dequenching assay that I used to monitor virus-cell fusion in real time. I investigated R18-MPV fusion with human bronchial epithelial (BEAS-2B) cells using eight different R18-MPV preparations in the experiments reported in Chapters III and IV. All of these experiments suggested that HMPV fusion was a slow process that occurs over several hours. A representative fusion curve is shown in Fig. 5-1. HMPV fusion results in a dynamic increase in R18 signal over time (Fig. 5-1A), which reflects R18 dye diluting from virus membranes into cell membranes during virus-cell fusion or R18 dequenching as shown in Fig. 5-1C. Interestingly, I did not observe a significant increase in R18 signal over the initial fluorescence intensity until after about 25 to 30 minutes after virus fusion was initiated by shifting cells from 4°C to 37°C (Fig. 5-1B, indicated by red asterisk). The discernable delay is also observed in the R18-dequenching kinetics, as R18-MPV dequenching curves begin with diminished dequenching (or further quenching) before

significant dequenching begins to occur around 25 to 30 minutes into the fusion experiment (Fig. 5-1C). These observations of HMPV fusion kinetics indicate that HMPV fusion triggering is a lengthy process. I hypothesized that HMPV binding to receptors on the cell surface would trigger fusion, and anticipated that the R18 signal would begin increasing immediately after cells were shifted to 37°C. However, I consistently observed a discernable delay before the onset of fusion, indicating that HMPV binding alone is not sufficient to trigger fusion.

HMPV is internalized before virus-cell membrane fusion occurs. The discernable delay in HMPV hemifusion kinetics led me to speculate that HMPV might be internalized into an intracellular compartment before membrane fusion occurs. To test this idea, I investigated the cellular location of HMPV particles early during infection. After HMPV binding at 4°C, I incubated cells at 37°C for different times before fixing cells, staining for HMPV particles with an F-specific mAb, and visualizing cells by confocal florescence microscopy. Representative images from these experiments are shown in Fig. 5-2. I found that HMPV particles were predominantly located on cell surface projections after binding (Fig. 5-2B), and appeared to move directly against the cell surface after a 5 min incubation at 37°C (Fig. 5-2C). By 20 to 30 minutes, the majority of HMPV particles had been internalized into cells (Fig. 5-2D and E). These results suggest that HMPV particles are trafficking from the cell surface into intracellular vesicles during the first 20 to 30 minutes of infection. The time required for virus internalization correlated well with the delay in HMPV fusion kinetics (Fig. 5-1).

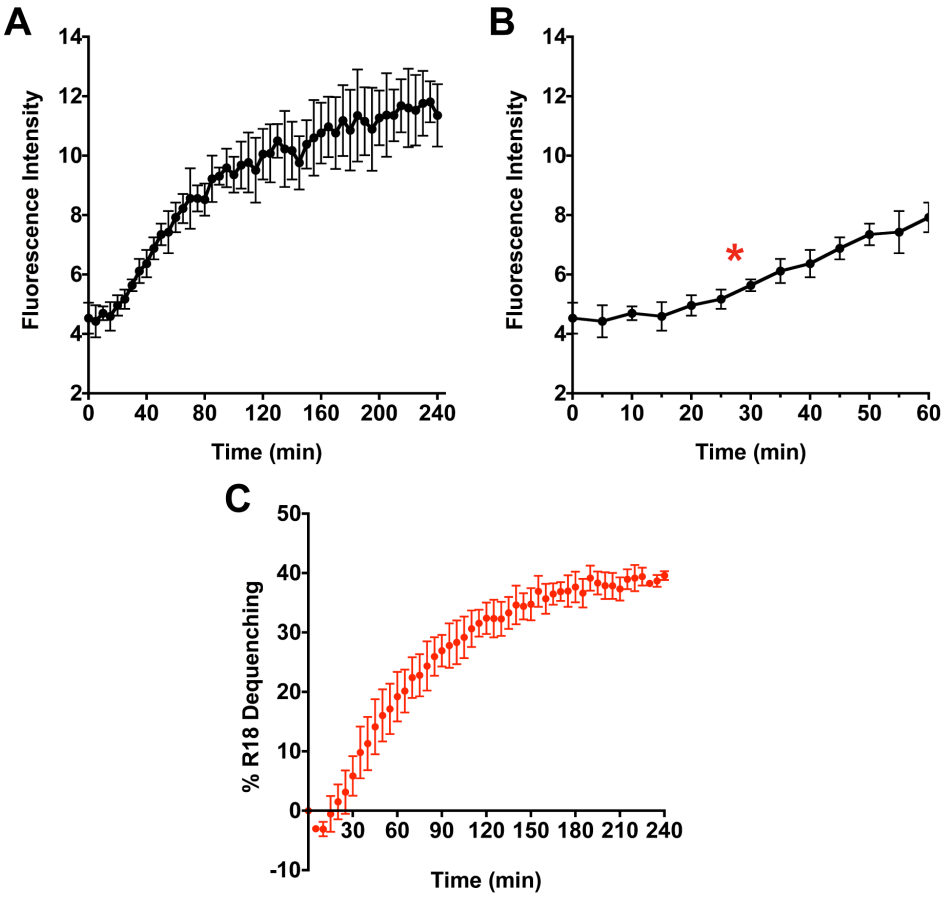

Fig. 5-1. HMPV hemifusion begins after a discernable delay.
R18-MPV was bound to BEAS-2B cells, unbound virus was washed away, and R18-MPV fusion was monitored for 4 h. Results (mean ± SEM) for three independent experiments are shown as fluorescence intensity (A and B) or percent R18 dequenching (C). (B) The x-axis was adjusted to show 0 to 60 min of the graph shown in (A); red asterisk indicates time at which R18 fluorescence intensity was significantly over initial intensity based upon reading at t = 0 min.

Based upon these observations, I hypothesized that HMPV was internalized before HMPV hemifusion initiates.

I hypothesized that if HMPV particles were being trafficked inside cells before fusion, than HMPV F should be able to escape F-specific antibodies at the cell surface. To test this idea, I investigated HMPV susceptibility to neutralizing antibody at the cell surface by adding HMPV neutralizing antiserum to cells at different times after virus attachment. I found that over time, HMPV escapes neutralization at the cell surface (Fig. 5-3). HMPV escapes neutralization between 10 and 30 minutes postbinding, which correlates with the time required for virus particle internalization (Fig. 5-2). The majority (60%) of HMPV particles escape neutralization before fusion initiates, because HMPV F is most susceptible to neutralizing antibodies during the time associated with the lag phase between binding and fusion. These results indicate that HMPV F is internalized before fusion begins.

As a complementary approach, I explored the effect of chemical inhibitors of endocytosis on HMPV fusion and infection. Chlorpromazine inhibits clathrin-mediated endocytosis by preventing the formation of nascent endosomes at the cell surface (Wang et al., 1993), and dynasore is a small molecule inhibitor of dynamin (Macia et al., 2006), the enzyme that mediates endosome scission at the plasma membrane. I pre-treated BEAS-2B cells with different concentrations of each inhibitor and assessed whether the inhibitor affected R18-MPV binding or fusion. Chlorpromazine and dynasore inhibited HMPV fusion in a dose-dependent manner; however, both drugs also significantly inhibited HMPV binding (Fig 5-4). The effect on fusion was greater than binding and inhibition of HMPV binding was not dose-dependent (Fig. 5-4). However, it was unclear

whether the endocytosis inhibitors were inhibiting HMPV particle uptake during the entry process or partially preventing receptor engagement by reducing HMPV receptor expression at the cell surface. To eliminate the effect that chlorpromazine and dynasore had on HMPV binding, I incubated cells with R18-MPV before adding the inhibitors and confirmed equivalent levels of HMPV binding (Fig. 5-5A). This allowed me to examine the effect of each inhibitor on HMPV fusion alone. HMPV fusion was significantly inhibited in cells treated with chlorpromazine (Fig. 5-5B and D). Fusion onset was delayed (Fig. 5-5D), fusion rate was impaired (Fig. 5-5D), and fusion extent at 4 h was substantially reduced (Fig. 5-5B) by chlorpromazine treatment. Further treatment with chlorpromazine (50 μM) reduced HMPV infectivity by 89% (Fig. 5-5E). These results suggest that blocking clathrin-mediated endocytosis significantly impairs HMPV infectivity because fusion cannot occur.

HMPV fusion was also inhibited in a dose-dependent manner by dynasore treatment (Fig. 5-5B and C). Dynasore treatment blocked fusion extent (Fig. 5-5B) but did not appear to affect the lag phase between binding and fusion onset (Fig. 5-5C). Further, dynasore treatment (50 μM) inhibited HMPV infection by 73% (Fig. 5-5E). These results suggest that endosome formation without scission from the plasma membrane may be sufficient to support HMPV fusion initiation. However, if endosome scission does not occur, then HMPV fusion and thus infectivity are significantly impaired. These results demonstrate that endosome formation is required before HMPV initiates fusion, and support a mechanism whereby HMPV fusion occurs after internalization.

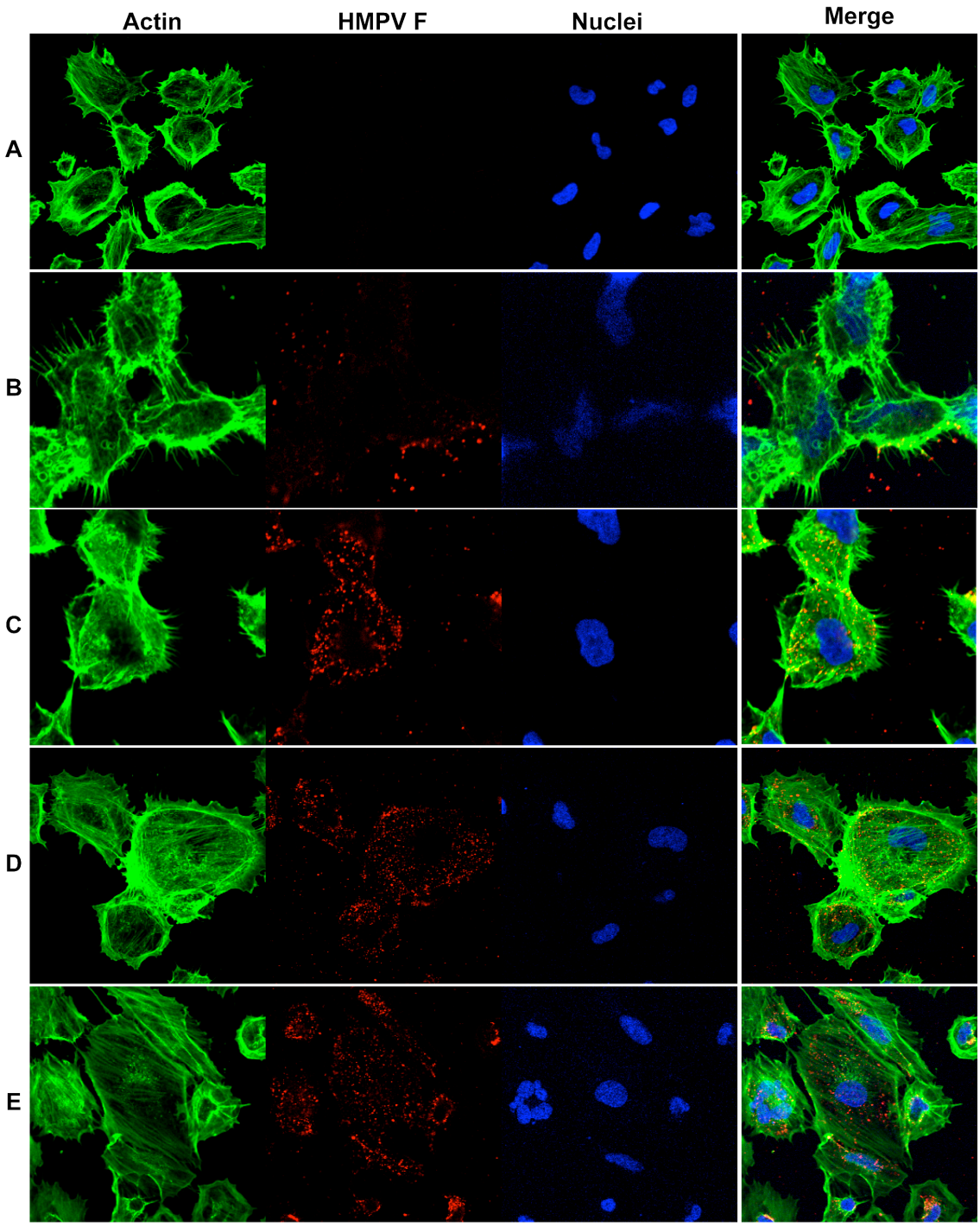

Fig. 5-2. HMPV particles are internalized within 20 minutes of binding.
HMPV (~2 pfu/cell) was bound to BEAS-2B cells, unbound virus washed away, and cells were shifted from 4°C to 37°C to initiate virus entry. After 5 min (C), 20 min (D) or 30 min (E), cells were fixed and stained as described in Materials and Methods. HMPV particles were detected by staining for the F protein (shown in red). Mock-treated cells (A) were stained as a negative control. Cells with bound HMPV, incubated at 4°C only are shown in (B).

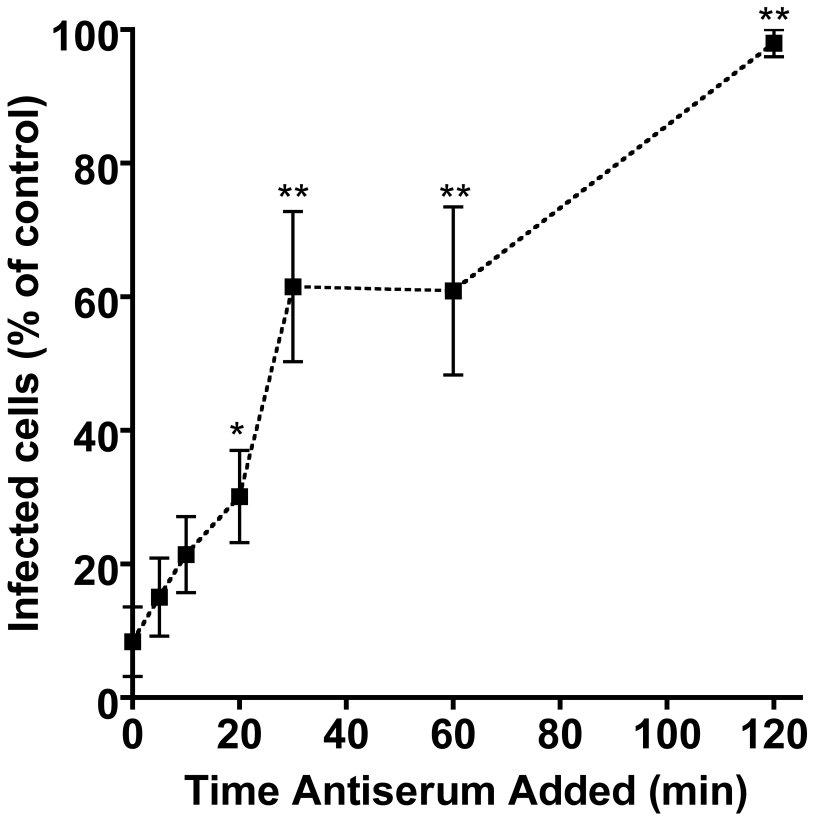

Fig. 5-3. HMPV escapes antibody neutralization at the cell surface.
HMPV (0.3 pfu/cell) was bound to BEAS-2B cells on ice to prevent fusion. Fusion media was added and cells were transferred to 37°C to initiate fusion, then media supplemented with neutralizing HMPV antiserum was added at subsequent times. HMPV-infected cells were identified at 24 h by indirect immunostaining. Results from five independent experiments performed in triplicate are shown as mean percent infection relative to an untreated control; error bars = SEM. *, $p < 0.05$, ** $p < 0.001$ (Student's *t* test comparing time of addition to addition at t = 0 min).

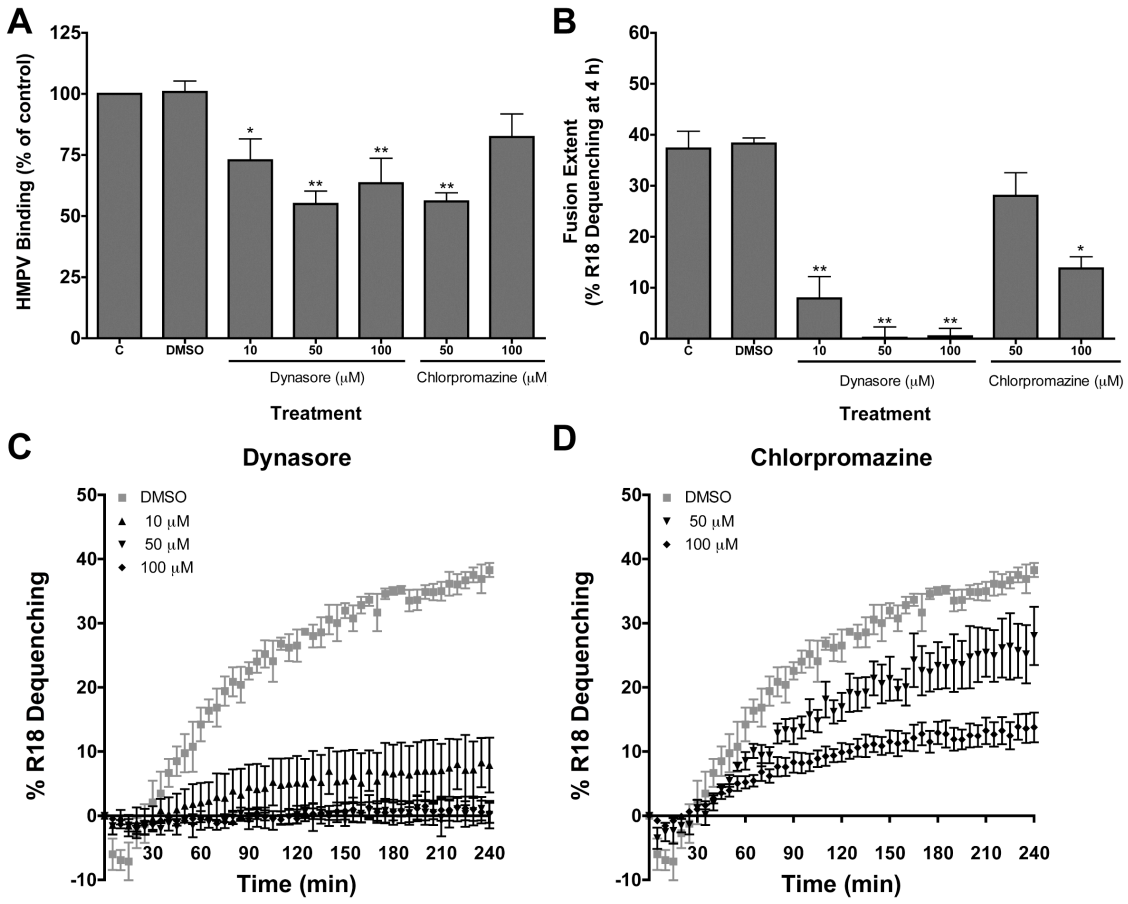

Fig. 5-4. Dynasore and chlorpromazine pretreatment significantly reduce HMPV binding and fusion.

BEAS-2B cells were treated with medium (*C*), DMSO, or the indicated concentrations of dynasore or chlorpromazine for 1 h at 37°C, followed by 30 min at 4°C. Cells were washed and R18-MPV (1 pfu/cell) was bound to BEAS-2B cells for 1h on ice. Unbound virus was removed and either virus binding or fusion was measured. For fusion experiments, inhibitors were added to fusion medium. (A) R18-MPV binding in the presence of inhibitors. (B) R18-MPV fusion extent after 4 h. Inhibitors were present before virus binding and during the 4 h fusion experiment. (C) R18-MPV fusion kinetics in the presence of dynasore. (D) R18-MPV fusion kinetics in the presence of chlorpromazine. Results for (A-D) represent means from three independent experiments performed in triplicate. Error bars = SEM. *, $p < 0.05$ or **, $p < 0.01$, ANOVA with Dunnett's test using medium (*C*) treatment as the reference.

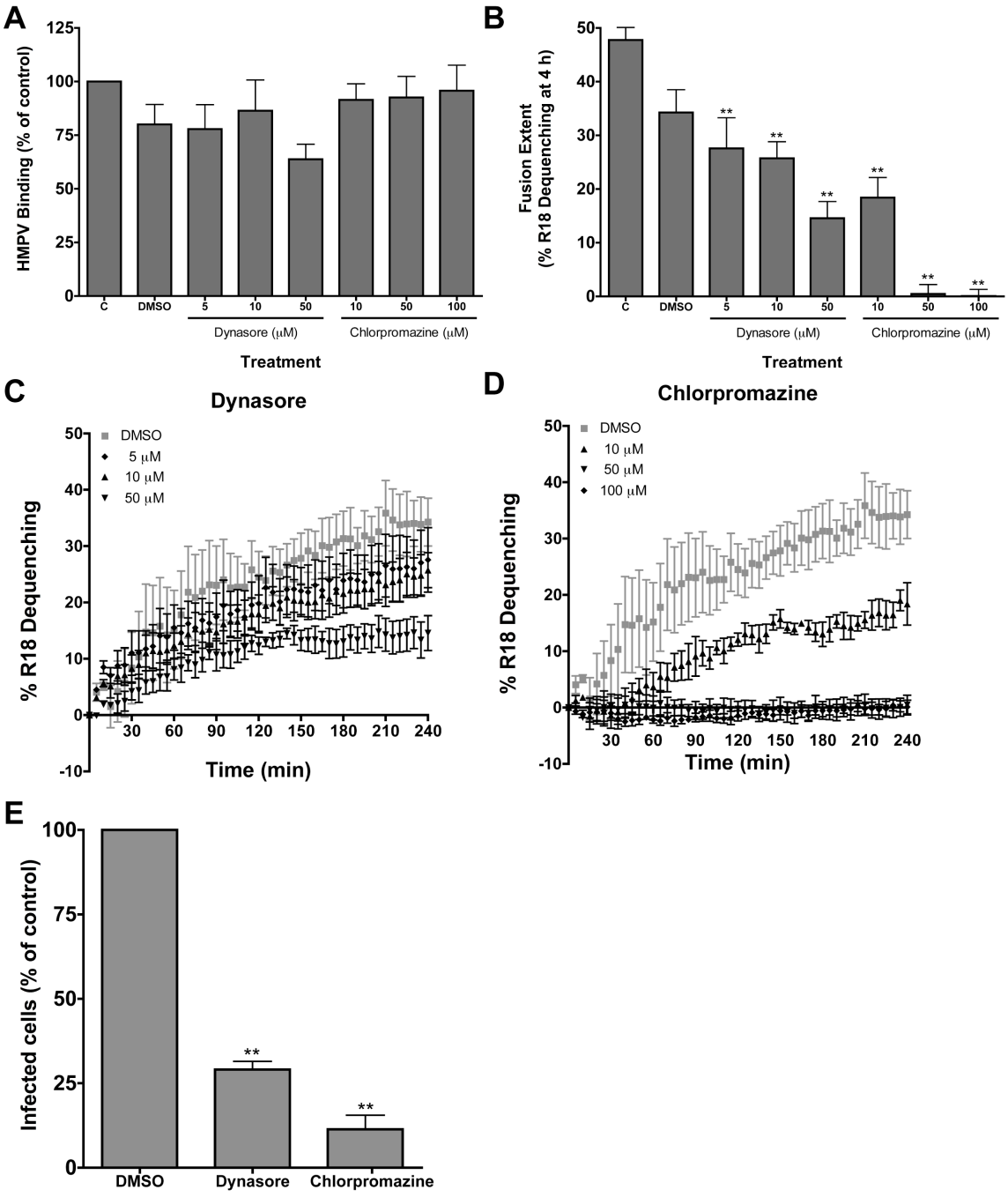
A
HMPV Binding (% of control)
125
100
75
50
25
0
C
DMSO
5
10
50
10
50
100
Dynasore (μM)
Chlorpromazine (μM)
Treatment
B
Fusion Extent
(% R18 Dequenching at 4 h)
50
40
30
20
10
0
**
C
DMSO
5
10
50
10
50
100
Dynasore (μM)
Chlorpromazine (μM)
Treatment
C
Dynasore
% R18 Dequenching
DMSO
5 μM
10 μM
50 μM
50
40
30
20
10
0
-10
30
60
90
120
150
180
210
240
Time (min)
D
Chlorpromazine
% R18 Dequenching
DMSO
10 μM
50 μM
100 μM
50
40
30
20
10
0
-10
30
60
90
120
150
180
210
240
Time (min)
E
Infected cells (% of control)
100
75
50
25
0
**
**
DMSO
Dynasore
Chlorpromazine

Fig. 5-5. Dynasore and chlorpromazine treatment after virus binding significantly inhibit HMPV fusion and infection.
R18-MPV (1 pfu/cell) was bound to BEAS-2B cells for 1h on ice and unbound virus was washed away. Fusion medium alone (*C*) or medium supplemented with DMSO or the indicated concentrations of dynasore or chlorpromazine was added to cells that were incubated for 30 min on ice before binding or fusion was measured. (A) R18-MPV binding is shown. (B) R18-MPV fusion extent after 4 h. Inhibitors were present during the 4 h fusion experiment. (C) R18-MPV fusion kinetics in the presence of dynasore. (D) R18-MPV fusion kinetics in the presence of chlorpromazine. (E) R18-MPV (0.2 pfu/cell) was bound to BEAS-2B cells in suspension. Inhibitors were incubated with cells after virus binding for 2 h at 37°C. After two hours, DMSO and inhibitors (50 μM dynasore or chlorpromazine) were removed, cells were washed, neutralizing antiserum was added to the culture medium, and cells were plated in 48-well plates. Cells were incubated for 24 h at 37°C with 5% CO_2, and infected cells were identified by indirect immunostaining. DMSO treated cells were infected at the same rate at medium-treated cells and cells without neutralizing antiserum addition (not shown). Results for (A-E) represent means from three independent experiments performed in triplicate. Error bars = SEM. *, $p < 0.05$ or **, $p < 0.01$, ANOVA with Dunnett's test using medium (*C*) treatment as the reference (A and B) or Student's *t* test comparing inhibitor to DMSO (E).

HMPV fusion occurs with intracellular vesicles. Collectively, my data suggested that HMPV fusion occurred at an intracellular membrane after virus particles were internalized. In order to visualize the site of HMPV-cell fusion, I needed an assay that could distinguish between fusion at the plasma membrane and fusion at an intracellular vesicle membrane. In my initial experiments, I investigated whether I could visualize R18 dye transfer from R18-labeled HMPV to cell membranes by fluorescence confocal microscopy. Unfortunately, the R18 dye transferred during R18-MPV fusion with BEAS-2B cells resulted in a very bright, diffuse fluorescence signal and it was impossible to distinguish whether the dye had been transferred to the plasma membrane or to intracellular membranes. Although the R18 signal appeared to be perinuclear rather than on the cell surface, I did not think the experiments were conclusive and began developing another HMPV fusion assay for my microscopy experiments. The principle of the microscopy fusion assay is similar to the R18-MPV fusion assay, in that virus particles are loaded with a self-quenching concentration of the lipophilic dye DiD. However, I loaded HMPV particles with a 10-fold lower concentration of DiD so that the DiD contained within particles was only partially quenched. The level of DiD in the particles was sufficient to observe DiD-dequenching if virus fused with a limited membrane, such as an endosomal vesicle. However, virus-cell fusion at the plasma membrane should result in DiD dilution into a large surface area and a loss of DiD signal on the cell upon virus fusion. A schematic of the DiD-MPV fusion assay is shown in Fig. 5-6.

To validate the assay, I collaborated with Bernardo Mainou to test whether DiD-MPV fusion with BEAS-2B cells was inhibited by neutralizing antiserum and chlorpromazine treatment. We found that HMPV fusion resulted in DiD-positive cells

that could be visualized (Fig. 5-7B) and enumerated by fluorescence confocal microscopy (Fig. 5-7E). Treatment with neutralizing antiserum or chlorpromazine to inhibit virus endocytosis significantly impaired the number of DiD-positive cells (Fig. 5-7 C-E). These results confirmed that the DiD-MPV fusion assay could be used to visualize virus-cell fusion by microscopy.

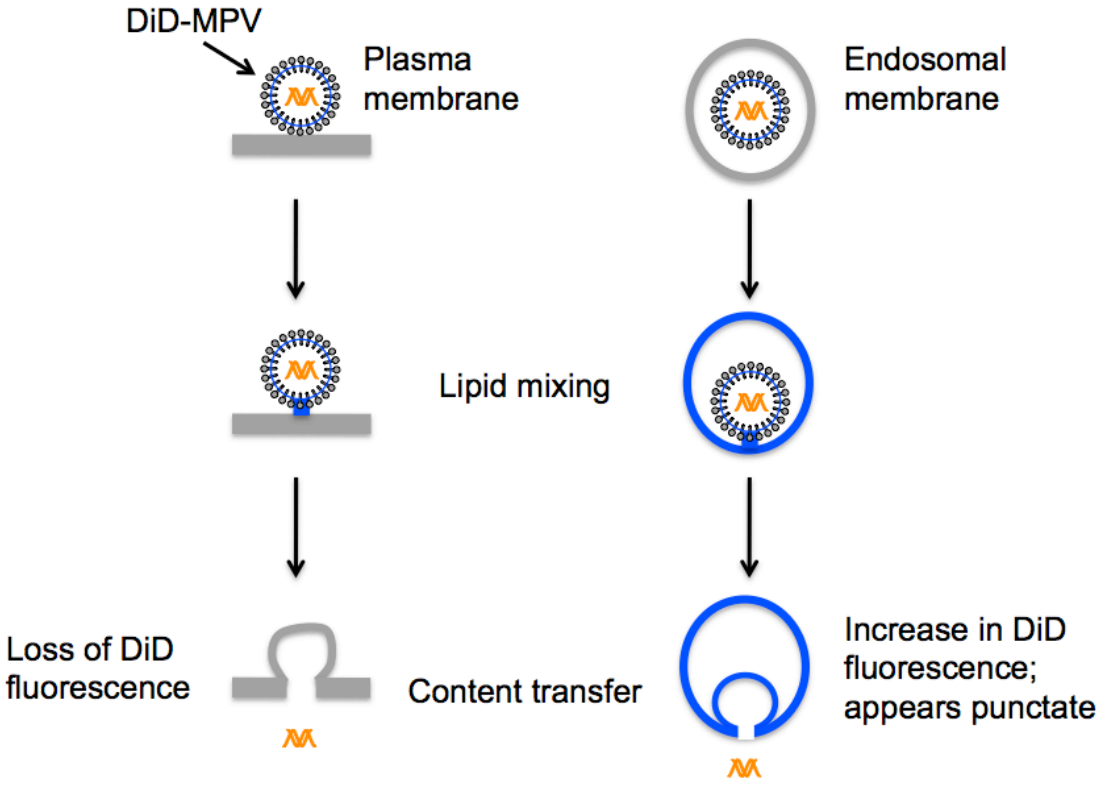

Fig. 5-6. Schematic of DiD-MPV fusion assay.

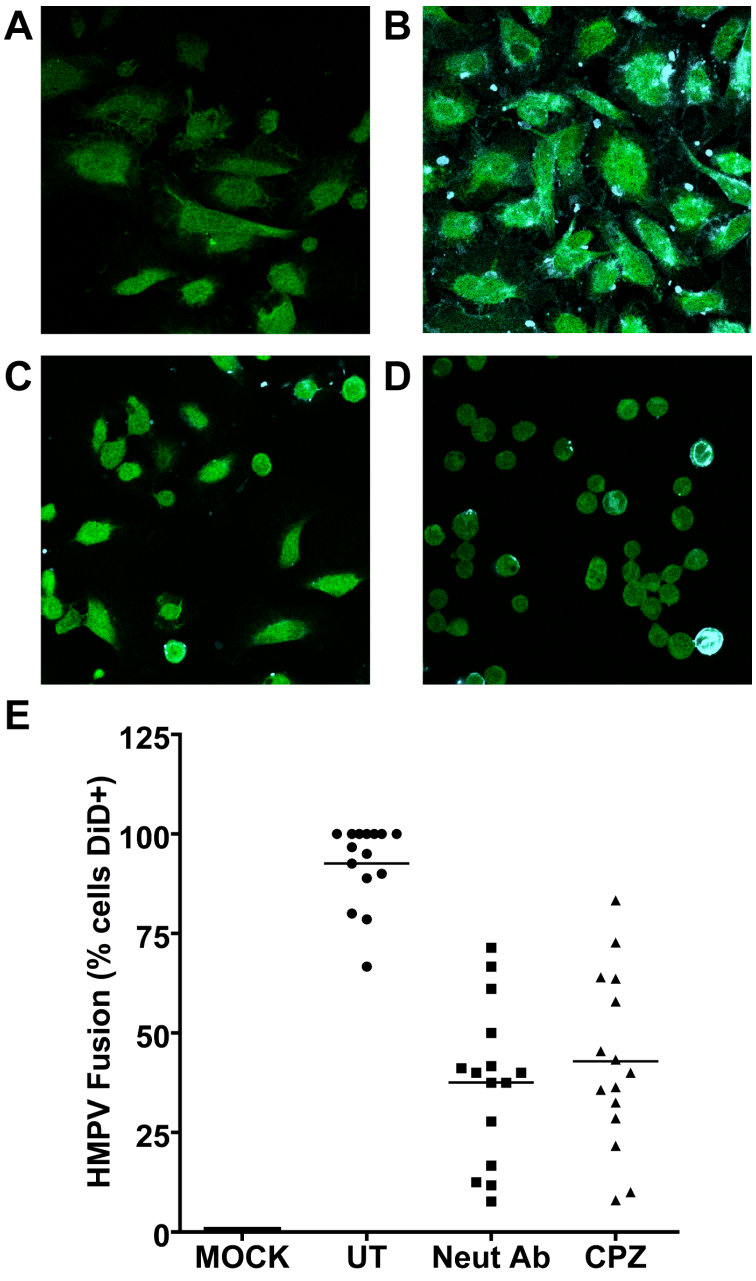

Fig. 5-7. DiD-MPV fusion is inhibited by neutralizing antiserum and chlorpromazine treatment.
DiD-MPV (0.25 pfu/cell) was bound to BEAS-2B cells labeled with an intracellular CellTracker green fluorescent dye. Cell medium alone or containing either neutralizing HMPV antiserum (Neut Ab, 1:20) or chlorpromazine (CPZ, 100 μM) was added to cells for 15 min before virus fusion at 37°C for 1 h. Fixed cell images were captured with a Zeiss inverted LSM510 confocal microscope using a 20x objective lens. Representative images for mock (A), DiD-MPV with medium (B), DiD-MPV with antiserum (C), and DiD-MPV with chlorpromazine (D) are shown. Cells were analyzed for any DiD fluorescence (light blue). Fifteen random fields containing 30 to 40 cells were analyzed for the percentage of cells with any DiD fluorescence and results are shown in (E).

The DiD-MPV fusion assay provided me with a method to visualize HMPV fusion by microscopy; however, like R18-MPV fusion, DiD dequenching (the appearance of a bright blue fluorescence signal) occurs during virus hemifusion. In an effort to visualize the entire HMPV fusion process, I optimized the assay to distinguish between bound virus, virus at the hemifusion stage of membrane merging, and virus particles that had completely fused and delivered the virion contents into the cell's cytoplasm. I did this by co-labeling virus particles with a red content dye and the membrane dye DiD (DiD-Red-MPV). A schematic of the DiD-Red-MPV fusion assay is shown in Fig. 5-8 and the principle of the assay is described in Materials and Methods.

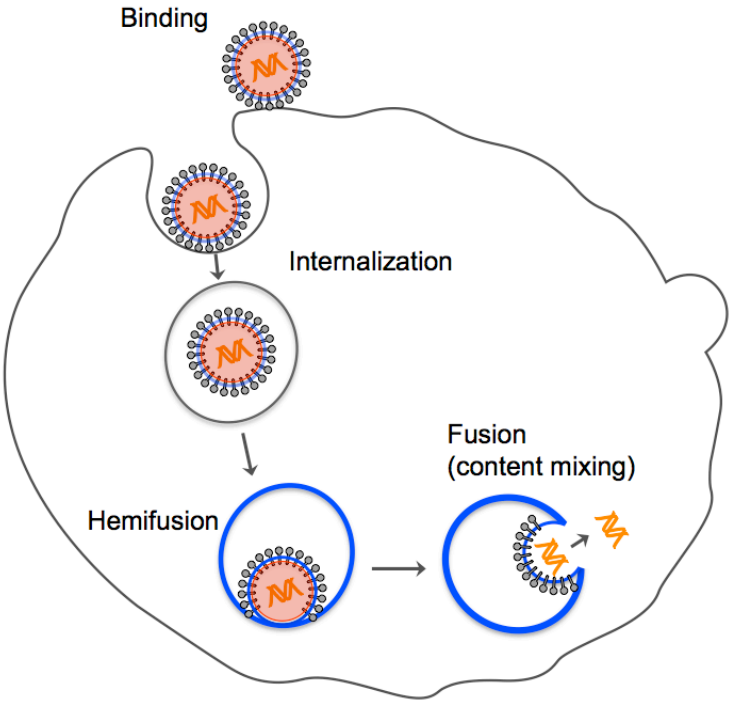

Fig. 5-8. Schematic of DiD-Red-MPV fusion assay.
DiD-Red-MPV fusion with cells can be visualized by fluorescence confocal microscopy. Bound virus particles appear red on the cell surface and during internalization. Virus hemifusion is marked by the appearance of particles that appear red and blue (pink or purple in merged fluorescence images). Full virus fusion, merging of membranes to form a pore through with the content of virus particles is delivered to the cytoplasm, results in bright blue intracellular vesicles that have no red fluorescence.

I monitored fusion of DiD-Red-MPV with CellTracker green-labeled BEAS-2B cells over time by fluorescence confocal microscopy (Fig. 5-9). Representative images from time points collected over 4 h are shown in Fig. 5-9A. The increase in DiD-positive (blue) puncti over time indicates that HMPV hemifusion results in DiD membrane dye transfer to intracellular vesicles (Fig. 5-9B), as hemifusion at the plasma membrane would be expected to result in a loss of DiD fluorescence. It is also possible that DiD transfer could occur at the plasma membrane resulting in the appearance of blue fluorescence at the plasma membrane but this was not observed. Instead I observed an increase in DiD-positive puncti within the cell's cytoplasm (Fig. 5-9B) that increased in DiD fluorescence intensity over time (Fig. 5-9C). These results strongly suggest that HMPV fusion occurs with vesicles inside the cell. The number of unfused (red) virus particles decreased (Fig. 5-9D, red squares), while the number of hemifused particles (Fig. 5-9D, purple triangles) and fused particles (Fig. 5-9D, blue circles) increased significantly over time. These results suggest that HMPV particles are internalized before membrane fusion because co-labeled particles (purple triangles) disappeared while bright DiD vesicles (blue circles) increased with time. The red-to-blue fluorescence shift was significantly inhibited by HMPV-specific neutralizing antibodies, indicating that the increase in DiD (blue) fluorescence was due to active virus fusion (Fig. 5-9E). These data indicate that HMPV hemifusion occurs during the first hour postbinding, and is completed within 60 to 90 minutes. From one to 4 hours postbinding, HMPV fusion was completed, delivering virus particle contents to the cytoplasm of cells and resulting in blue vesicles that no longer contain the red dye contained within virus particles. These

data confirm that HMPV fusion is a slow process that occurs over several hours, but indicate that HMPV fuses with intracellular membranes rather than at the cell surface.

Discussion

Paramyxovirus binding to cell surface receptors is thought to induce conformational changes in the F protein that drive virus fusion at the plasma membrane. However, our data suggest that HMPV binding alone is not sufficient to trigger fusion, as we consistently observed a 20 minute delay before the onset of R18-MPV fusion at 37°C. Studies examining the fusion kinetics of other R18-labeled viruses provide evidence that a fusion lag correlated with entry mechanisms that separate binding from fusion by an internalization event. For example, parainfluenza virus 5 (PIV5) and Sendai virus fusion begins nearly immediately when ice-cold cells are warmed to 37°C (Connolly and Lamb, 2006; Krishnan et al., 2009; Pedroso de Lima et al., 1992). PIV5 and Sendai virus are paramyxoviruses that fuse at the plasma membrane. In contrast, vesicular stomatitis virus (VSV) requires endocytosis before fusion, and R18-VSV fusion occurs after a discernable delay (Puri et al., 1992). Thus, the lag phase we observe in HMPV fusion curves resembles what is observed for viruses that enter cells before fusing with endosomal membranes. Furthermore, if F binding triggered fusion, then we would expect the kinetics of HMPV fusion to be more rapid because PIV5 and Sendai fusion curves begin to plateau after 15 to 20 minutes (Connolly and Lamb, 2006; Krishnan et al., 2009; Pedroso de Lima et al., 1992) and Sendai virus fusion at the plasma membrane completes within 10 minutes at 37°C (Morgan and Howe, 1968).

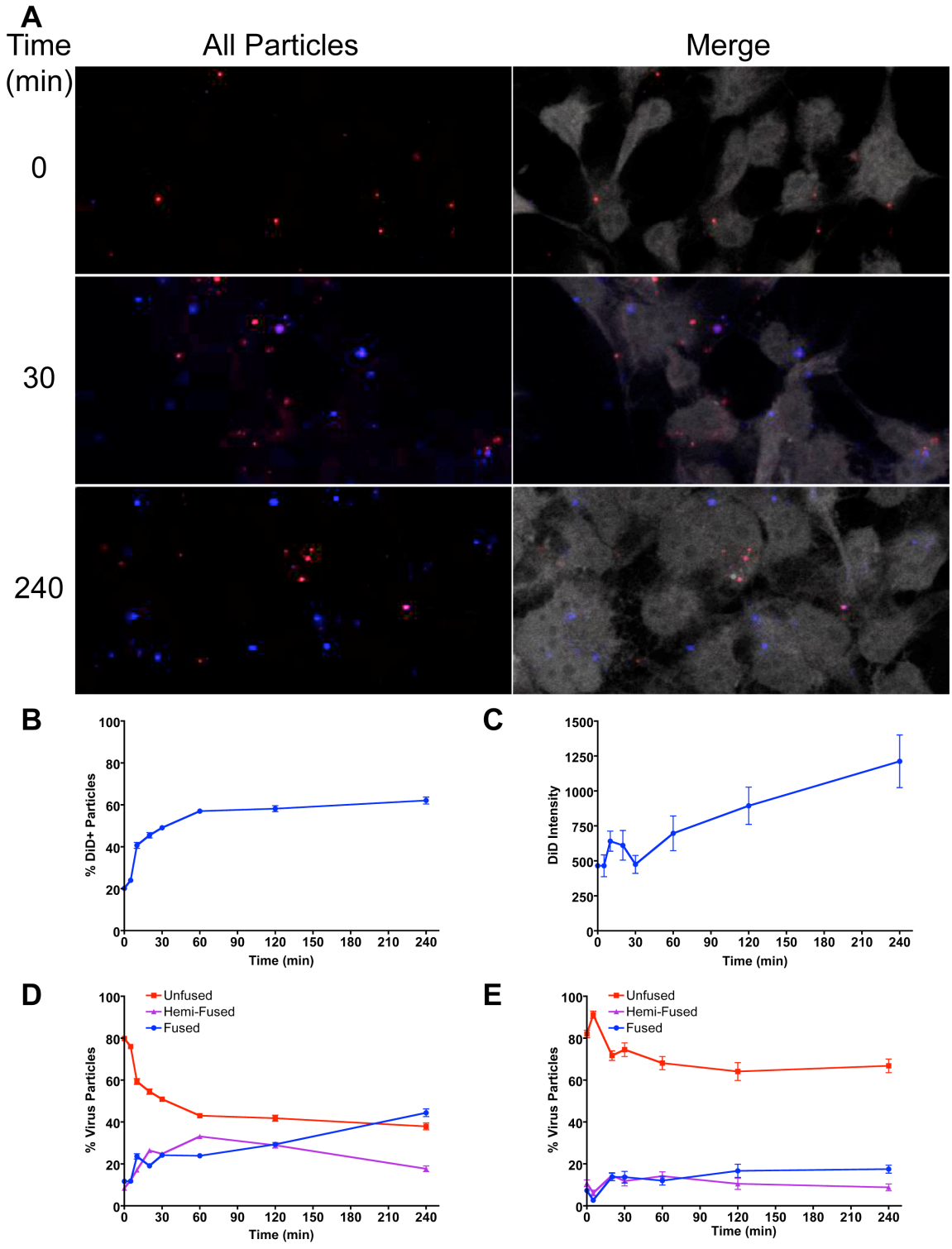
A
Time (min)
All Particles
Merge
0
30
240
B
% DiD+ Particles
Time (min)
C
DiD Intensity
Time (min)
D
% Virus Particles
Unfused
Hemi-Fused
Fused
Time (min)
E
% Virus Particles
Unfused
Hemi-Fused
Fused
Time (min)

Fig. 5-9. HMPV fuses with intracellular vesicles.
DiD-Red-MPV fusion with BEAS-2B cells. Red HMPV particles are internalized and blue fluorescence appears at intracellular vesicles during virus-mediated hemifusion. Red plus blue particles become brighter blue and there is a loss of red fluorescence as virus content is released into the cytoplasm. (A) BEAS-2B cells were loaded with CellTracker green fluorescent dye to visualize the cytoplasm during imaging. Green fluorescence has been pseudocolored as white in the merged images to enhance red and blue particle contrast. The zero time point was imaged before incubating cells at 37°C to initiate virus fusion. Fixed cell images were captured with a Zeiss inverted LSM510 confocal microscope using a 63x oil objective lens. A single z-plane near the center of the cell thickness is shown for representative images at each indicated time point. Time (min) of 37°C incubation is shown to the left of each image. (B-E) Individual cells from each time point were analyzed for red, blue, or red plus blue particles. The percentage of total particles with DiD (blue) fluorescence indicating HMPV hemifusion (B) and the intensity of DiD fluorescence (C) was quantified. DiD-Red-MPV fusion in the absence (D) and presence of neutralizing HMPV antiserum (E) was quantified. The percentage of unfused (red), hemifused (red plus blue), or fused (blue) particles per cell was calculated. Results represent at least 180 cells per time point for untreated and at least 60 cells per time point for neutralizing antiserum-treated cells from four independent experiments. Error bars = SEM.

The delay in HMPV fusion led me to investigate early postbinding events. I found that HMPV particles are internalized by 20 minutes postbinding and they become resistant to antibody neutralization at the cell surface during the first 30 minutes postbinding. This suggests that either the majority of fusion occurs within the first 30 minutes postbinding or that virus particles escape neutralization because they are internalized. My results favor the latter explanation, because the majority of R18-MPV fusion occurs between 30 and 120 minutes postbinding, after HMPV particles have been internalized. Moreover, I demonstrate that inhibitors of the endocytic pathway impair HMPV fusion in a dose-dependent manner and significantly inhibit infectivity. Thus, my results favor a mechanism whereby HMPV is internalized before membrane fusion occurs. Schowalter et al. suggested a role for endocytosis in HMPV entry by demonstrating that dynasore and chlorpromazine inhibited HMPV infection measured after 20 hours, but these experiments did not take into account the decrease in binding due to drug treatment (Schowalter et al., 2009). My results are consistent with this previous report, but reveal that the block to infection occurs postbinding and before membrane fusion.

To conclusively demonstrate that HMPV fusion occurs at an intracellular membrane, I developed a microscopy-based fusion assay and found that HMPV particles are internalized and transfer a fluorescent membrane dye to intracellular vesicles during hemifusion before releasing a virus content dye into the cytoplasm. Collectively, the data presented in this chapter show that HMPV is internalized before virus fusion. Thus, the site of HMPV fusion does not appear to be at the cell surface as predicted by analogy to other paramyxoviruses. Whether HMPV is internalized by clathrin-mediated endocytosis, caveolin-mediated endocytosis, clathrin- and caveolin-independent endocytosis, and/or

macropinocytosis is still unclear. My results showing that chlorpromazine inhibits HMPV fusion and infection suggest that HMPV entry is mediated by clathrin-mediated endocytosis, although more specific inhibitors of this pathway should be tested as chlorpromazine can affect cellular signaling pathways other than clathrin-dependent endocytosis. HMPV entry appears to be dynamin-dependent, but dynamin is required for several cellular endocytosis pathways. Thus, the cellular pathway for HMPV internalization requires further investigation.

CHAPTER VI

SUMMARY AND FUTURE DIRECTIONS

Thesis Summary

The research I present in this thesis examines the mechanism by which the HMPV F protein initiates virus entry. I demonstrate that HMPV F is necessary and sufficient for both virus binding and fusion with cells *in vitro*. I show that HMPV F attaches to RGD-binding integrins on the surface of human bronchial epithelial cells, thereby identifying cellular receptors used by the F protein during entry. My results indicate that an F-RGD-mediated interaction with integrins is required for efficient binding, virus transcription, and productive infection. However, I show that F binding to integrins is not sufficient to trigger HMPV hemifusion. Instead, my results indicate that HMPV binding and fusion are separate events, whereby fusion initiates after a discernable delay during which virus particles are internalized and fusion pore formation occurs within intracellular vesicle membranes.

We identified an invariant arginine-glycine-aspartate (RGD) motif within the F protein and hypothesized that RGD-binding integrins served as receptors for HMPV. Our initial experiments sought to determine whether integrins were required for HMPV infection, and in Chapter II we show that RGD-binding integrins promote HMPV infection. This conclusion was based upon evidence from a series of loss-of-function and gain-of-function experiments. EDTA, which chelates divalent cations required for integrin function, inhibits HMPV but not hRSV infection. Synthetic RGD peptides block

HMPV infection, while RGE peptides do not. Function-blocking monoclonal antibodies (mAbs) directed against RGD-binding integrins inhibit HMPV infection, with mAbs against αV and β1 exhibiting the most potent effect. Similarly, reduction of αV and β1 integrin expression by siRNA reduces HMPV infection. Furthermore, transfection of nonpermissive cells with human αV or β1 integrin cDNAs confers HMPV infectivity. Finally, recombinant F protein binds specifically to permissive cells, and mutation of the F protein RGD motif abolishes binding. These data suggest that RGD-binding integrins are receptors for the HMPV F protein during infection.

The experiments presented in Chapter II did not define the precise step in HMPV infection mediated by RGD-binding integrins. Most of our initial experiments examined cell surface viral protein expression in infected cells at 24 hours postbinding. To determine if HMPV F binds directly to integrins during entry, I developed new assays to specifically examine HMPV binding and fusion (presented in Chapter III). To study HMPV binding, I developed a fluorescence-based assay to quantify binding independently of fusion and infection, allowing me to discriminate the first critical step in the entry process. To study HMPV fusion, I developed a fluorescence-based kinetic assay to monitor the merging of virus and cell membranes during virus entry. I also developed a system to generate HMPV virus-like particles (VLPs) that allowed me to generate particles with F alone or F plus G proteins. The VLPs provided a model system to study virus-cell fusion and examine the contribution of individual virus surface glycoproteins to virus binding and fusion.

Using the new methodology described in Chapter III, I examined whether HMPV F directly interacted with integrins. The data I present in Chapter IV provide evidence

that HMPV F utilizes RGD-binding integrins as cellular receptors to mediate entry. Using both virus and VLPs, I present evidence that HMPV F binds multiple RGD-binding integrins, specifically α5β1 and other αV-integrin heterodimers that may differ depending upon target cells. I demonstrate that HMPV F binds RGD-binding integrins during attachment, and this interaction is necessary for virus attachment, virus transcription, and subsequent productive infection. Furthermore, mutating the conserved RGD motif significantly attenuates HMPV growth *in vitro* and alters the extent of virus-infected cell-cell fusion, suggesting a key role for the integrin-binding motif during F-mediated entry and fusion. Although an F-integrin interaction is required for efficient binding, I show that integrins are also important for postbinding events during virus entry as RGD-binding integrin blockade significantly impairs HMPV transcription. These data suggest that RGD-binding integrin engagement is essential for HMPV attachment leading to productive infection and for post-binding events that occur during HMPV entry.

My next experiments tested the hypothesis that F binding to integrins triggered the initiation of HMPV fusion. My experimental results did not support this hypothesis. In Chapter IV, I show that blocking the HMPV F interaction with RGD-binding integrins did not alter virus-cell hemifusion kinetics, and VLPs bearing an F-RAE mutation fuse with the same hemifusion kinetics as wild type F particles. This evidence suggests that F binding to integrins is not sufficient to trigger F-mediated hemifusion. However, my results did support a postbinding role for RGD-binding integrins during HMPV entry, as integrin blockade reduces HMPV transcription at 8 hours by 50%, in addition to a 40 to 50% block during virus attachment. Further, when I introduced an F-RAE mutation into HMPV, the F-RAE virus is severely attenuated and exhibits a small plaque phenotype

that lacks the characteristic syncytia (indicative of F-mediated cell-cell fusion) of wild type virus. Thus, while it appears that an F-integrin interaction is not required for efficient HMPV hemifusion, it remains possible that this interaction promotes fusion pore opening during virus-cell fusion.

The experiments presented in Chapter IV confirm that RGD-binding integrins mediate approximately 50% of HMPV F-mediated binding. Thus, HMPV F binds to other receptors on the cell surface during virus attachment. My results indicate that HMPV F binding to integrins is not sufficient to trigger fusion, so I next sought to determine whether binding to other receptors was sufficient to initiate HMPV fusion at the cell surface. While investigating the kinetics of HMPV fusion, I made an observation that was quite unexpected and exciting. My experiments show that HMPV hemifusion does not begin immediately after virus binding. Instead HMPV hemifusion begins after a 20-minute delay, indicating that there is a considerable lag phase between virus binding and the initiation of fusion. I sought to determine whether this lag phase indicated that HMPV binding and fusion were spatially separated during virus entry. In Chapter V, I show that HMPV F-mediated virus-cell fusion occurs at an intracellular membrane indicating that F binding and fusion are separated by virus particle internalization. Using confocal microscopy experiments I demonstrate that HMPV particles are internalized during the first 20 minutes of entry, which correlates with the lag phase observed between binding and HMPV hemifusion. Furthermore, I show that HMPV particles escape antibody neutralization at the cell surface between 10 and 30 minutes postbinding. I also show that chlorpromazine and dynasore, inhibitors of endocytosis, impair HMPV fusion and infection. Finally, using a novel cell imaging approach, I demonstrate that

HMPV is internalized and fusion occurs with intracellular vesicles. These data suggest that HMPV does not fuse at the plasma membrane where paramyxovirus fusion is thought to occur. Further, it appears that HMPV regulates entry differently than other paramyxoviruses by separating fusion triggering from receptor binding at the cell surface.

HMPV is a leading cause of lower respiratory illness in adults and children. Although the virus was discovered in 2001, remarkable progress has been made in elucidating the biology of HMPV. Unlike paramyxoviruses with a strict requirement for two separate viral proteins to mediate fusion and virus entry, the HMPV F protein serves both to bind cellular receptors and to mediate fusion. The mechanism by which HMPV F both attaches to the cell surface and mediates fusion is not well understood. My research findings have contributed to our knowledge of HMPV biology by identifying RGD-binding integrins as functional cellular receptors for HMPV entry. Moreover, my data have revealed that HMPV fusion occurs after virus internalization. A mechanism of entry where receptor binding is separated from membrane fusion has not been previously described for any other paramyxoviruses. Thus, while HMPV F shares many features of other paramyxovirus fusion proteins, there are distinct aspects of the attachment, entry, and fusion mechanisms of this recently discovered virus that my research studies have uncovered.

Future Directions

How do RGD-binding integrins regulate HMPV entry?

The mechanism by which RGD-binding integrins regulate HMPV entry requires further investigation. My data suggest that HMPV binding and postbinding events during entry depend upon RGD-binding integrins. Further, my experiments suggest that integrin engagement promotes HMPV entry at a step in the process after hemifusion initiates but before viral transcription begins. These findings suggest to me that F engagement of RGD-binding integrins may facilitate either particle internalization or fusion pore enlargement. HMPV internalization could be tested with fluorescently labeled HMPV, e.g. DiD-Red-MPV, by confocal microscopy. I would examine DiD-Red-MPV entry in the absence or presence of integrin function-blocking antibodies: α2 (as a negative control) and αV plus α5 plus β1 (to block all available RGD-binding integrins). With this assay, the timing and extent of particle internalization can be quantified using confocal microscopy images collected over a 4-hour time course. If integrins were required for HMPV internalization, then I would expect to observe fewer HMPV particles inside cells when RGD-binding integrin-mediated binding was blocked. The data should be normalized to the number of particles observed at t = 0 minutes, as I would expect a ~50% reduction in particle binding. Complementary experiments to examine the extent of HMPV particle internalization in the presence of integrin function-blocking antibodies assessed by confocal fluorescence microscopy using the F-specific mAb to identify particles (as shown in the analysis presented in Fig. 5-2) should also be performed. Furthermore, live cell imaging of fluorescently labeled HMPV entry into cells could be used to observe whether integrin function-blocking antibodies affect either virus uptake

or the timing of virus internalization. Alternatively, an ELISA-based assay could be used to monitor the presence of HMPV F protein at the cell surface during virus entry. Briefly, cells with HMPV bound at 4°C would be incubated at 37°C for different times, fixed, and immunostained for surface HMPV F. Virus internalization should result in a loss of HMPV F staining at the cell surface. The timing and extent of HMPV F internalization could be quantified in the absence or presence of integrin function-blocking antibodies. A potential problem with this experimental approach is cross-reactivity of integrin blocking antibodies with the HMPV F detection antibodies, thus assay development to limit or eliminate cross-reactivity may be necessary. Parainfluenza virus 5 (PIV5), which fuses at the cell surface, and vesicular stomatitis virus (VSV), which fuses after virus internalization, should be monitored in parallel as negative and positive controls, respectively.

Fusion pore enlargement during HMPV entry could be examined with the DiD-Red-MPV microscopy-based fusion assay. I would examine DiD-Red-MPV fusion in the absence or presence of integrin function-blocking antibodies: α2 (as a negative control) and αV plus α5 plus β1 (to block all available RGD-binding integrins). With this assay, HMPV internalization, hemifusion, and fusion pore formation can all be quantified using confocal microscopy images collected over a 4-hour time course. If integrins were required for fusion pore enlargement, then in the presence of RGD integrin function-blocking antibodies I would expect to observe HMPV particles that were internalized at the appropriate frequency and particles that transition from red to red/blue fluorescence (indicative of hemifusion), but significantly fewer intracellular vesicles that convert to blue only fluorescence (indicative of viral content release). These predicted results would

indicate that RGD-binding integrin engagement at the cell surface was required for later stages in the HMPV fusion process. Other microscopy experiments could also be used to examine genome delivery to the cytoplasm. For these experiments, I would perform an HMPV entry time course with fixed cells (as shown in the analysis presented in Fig. 5-2). I would use antibodies to stain for HMPV F and use a fluorescently labeled RNA probe to identify HMPV genomic RNA in the cytoplasm. This strategy has been successfully used to probe for hRSV genomic RNA in hRSV-infected cells (Santangelo et al., 2009). The appearance of HMPV genomic RNA in the cytoplasm would indicate that HMPV fusion pores had enlarged to sufficiently deliver viral genomes into cells following virus entry. If integrin engagement were required for fusion pore enlargement, then I would expect to observe less genomic RNA (less signal from the fluorescent RNA probe) in cells during treatment with RGD integrin-specific antibodies. Alternatively, I would use antibody staining to identify the HMPV N protein. The N protein is a core virion structural protein that coats the HMPV genome packaged inside virions. The appearance of N protein in the cytoplasm would also indicate that HMPV fusion pore enlargement had occurred and the genome had been delivered to the cell. Staining for HMPV N may likely result in a higher signal-to-noise ratio in the fluorescence microscopy imaging because the protein is more abundant than single copies of HMPV genomic RNA contained within infectious virions. However, if possible, probing for viral genomic RNA would directly address whether the fusion pore had enlarged enough to delivery the infectious viral genome into a cell.

Numerous signaling molecules and cytoskeletal proteins complex with integrins at patches on the plasma membrane called focal adhesions. Integrin engagement by

physiological ligands is known to activate an outside-in signaling pathway that is necessary for integrin-mediated cytoskeletal rearrangements, cell motility and proliferation. A hallmark of outside-in signaling is the autophosphorylation of Tyr_{397} of focal adhesion kinase (FAK) in response to ligand engagement to integrins (Hynes, 2002). FAK autophosphorylation is required for integrin-mediated cytoskeletal reorganization, i.e. actin assembly, and linked to integrin endocytosis (Cox et al., 2006). My preliminary data suggest that HMPV induces FAK autophosphorylation of Tyr_{397} (data not shown), suggesting that integrin-mediated signaling may be required for productive HMPV entry. Whether integrin-mediated signaling is required for i) HMPV internalization, ii) driving lipid curvature or actin assembly/disassembly in a manner that supports HMPV fusion, and/or iii) altering the host cell environment for favorable virus replication will require further investigation.

What other cellular receptors facilitate HMPV attachment?

HMPV F interacts with at least two different cell surface receptors during attachment. Chang et al. recently showed that HMPV F attaches to heparan sulfate on the cell surface (Chang et al., 2012b) and I have shown that HMPV F interacts with RGD-binding integrins during virus binding (Cox et al., 2012). Chang et al. also suggested that efficient HMPV infection depends upon the expression of a proteinaceous receptor that is trypsin- and proteinase K-sensitive (integrins are reportedly resistant to both types of protease treatment) (Chang et al., 2012b). Thus, efficient HMPV attachment may depend upon more than one cell surface receptor: heparan sulfate, RGD-binding integrins, and other protease-sensitive surface proteins. However, further studies are needed to identify

the other putative proteinaceous receptors that may be required for HMPV infection. I proposed three different approaches to identify other protein receptors that may be required for efficient HMPV F binding during virus attachment. Two biochemistry approaches could be used to identify protein receptors. One approach is based upon co-immunoprecipitation of the F protein followed by mass spectrometry analysis to identify any cellular proteins that bound to F. For these experiments, HMPV or recombinant F protein would be bound to the surface of cells on ice to prevent virus entry. After binding, cells would be lysed and immunoprecipitated with an F-specific mAb or an irrelevant isotype control mAb. Immune complexes would be captured on protein-G-agarose beads, eluted from beads with a denaturing buffer, incubated with proteases such as trypsin or chymotrypsin to produce peptide fragments, and analyzed by mass spectrometry. Differential bioinformatic analysis, including BLAST searches, of the resulting peptides would be used to determine the cellular proteins that specifically coprecipitated with the HMPV F protein. The second approach is a technique called a virus protein overlay binding assay (VOPBA). For this experimental approach, membrane proteins are extracted from cells with detergent, separated by SDS-PAGE, and used to probe for virus binding. A schematic of the experimental approach is shown in Fig. 6-1. Sucrose-purified HMPV should be used in the VOPBA binding experiment, and replicate membranes should be incubated with a sucrose-purified preparation from mock-infected cells as a specificity control for HMPV F protein detection. If a one-dimensional separation by SDS-PAGE does not provide enough resolution of proteins to identify discrete banding after HMPV binding, a two-dimensional separation by pH and mass can be employed (as described in (Tio et al., 2005)).

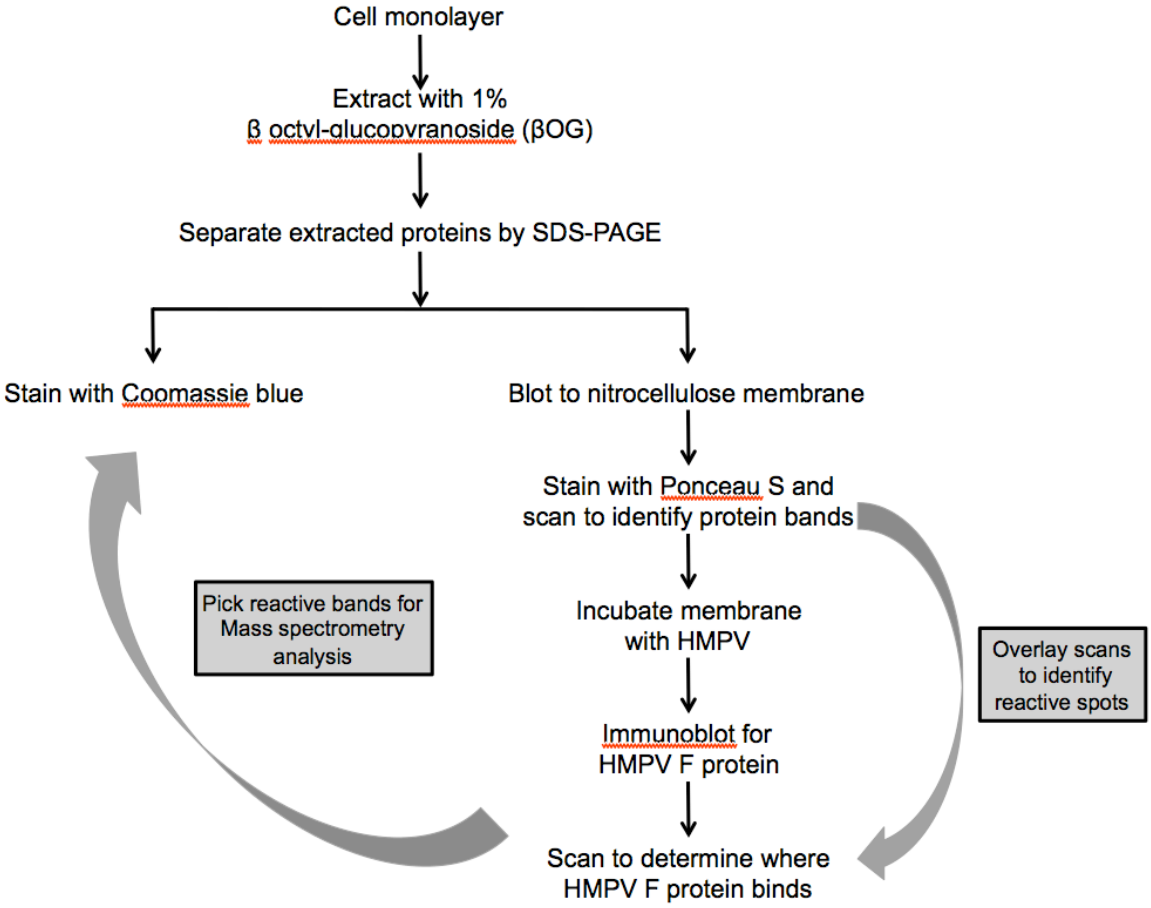

Fig. 6-1. Flowchart of VOPBA experimental design.
This flowchart describes the steps in the process to identify cellular proteins that bind to the HMPV F protein.

The third approach to identify a protein receptor for the HMPV F protein is a genetic approach. CHO cells, which are poorly permissive for HMPV infection, would be transfected with a human lung cDNA library (SuperScript, Life Technologies). After 48 h incubation, HMPV F protein would be bound to the cell surface and protein binding detected by indirect immunostaining with a fluorescent antibody. Cells would be analyzed by FACS and fluorescently-labeled cells would be sorted and collected. Plasmids would be rescued from sorted cells, amplified in bacteria and used for subsequent rounds of FACS enrichment until the plasmids that conferred HMPV F binding were identified based upon the strategy described previously (Barton et al., 2001). DNA sequencing would be required to identify the cellular protein(s) encoded on each plasmid.

These three approaches represent the first step in identifying a cellular protein that is required for HMPV F binding. Subsequent loss-of-function and gain-of-function experiments such as those described in Chapters II and IV would be required to confirm that an identified cellular protein was a functional receptor for HMPV.

What molecular events are required to trigger HMPV hemifusion?

The proverbial "black box" with respect to paramyxovirus entry is a lack of understanding of the fusion protein triggering process. For all paramyxoviruses, the process by which receptor binding triggers conformational changes in the F protein remains unclear. HMPV F interacts with both heparan sulfate and RGD-binding integrins during attachment. Whether binding to these receptors results in structural changes in F that drive fusion is not clear. Furthermore, whether HMPV binds receptors

simultaneously or sequentially is not known. Simultaneously binding to multiple receptors may induce conformational changes in multiple sites of the HMPV F extracellular domain, thereby promoting destabilization, protein refolding, and fusion. Alternatively, HMPV F binding to one receptor may expose the receptor binding site for another co-receptor, similar to the strategy utilized by HIV gp120/gp41 during fusion (Wilen et al., 2012). My data suggest that an F-integrin interaction is not sufficient to trigger conformational changes in the F protein that are important for the initiation of hemifusion. While Chang et al. demonstrated that HMPV F attaches to heparan sulfate these researchers did not determine whether heparan sulfate binding triggered hemifusion. The requirement for F binding to heparan sulfate should be tested with the R18-MPV fusion assay I have developed. If F binding to heparan sulfate was required to trigger hemifusion, then I would expect i) preincubation of R18-MPV with heparan sulfate to impair R18 dequenching kinetics, ii) addition of heparan sulfate to R18-MPV postbinding to enhance fusion kinetics or extent, and iii) R18-MPV fusion with cell lines deficient in heparan sulfate synthesis to be abolished. If heparan sulfate engagement is required to trigger HMPV hemifusion, then further studies are warranted to map the interaction between F and heparan sulfate to define how F engagement serves to drive HMPV fusion.

A more detailed knowledge of the regions of HMPV F that are important for fusion triggering is also needed. Others have implicated two distal regions with predicted charged residue clusters (located in domains II and III of HMPV F, shown in Fig. 1-5) to be important for HMPV F cell-cell fusion. These residues likely identify areas of the protein that undergo conformational changes during fusion. The idea that charged

residues drive electrostatic repulsions to trigger the HMPV F prefusion protein to spring into the postfusion conformation during the fusion process is logical. The HRA region of F must undergo a significant structural rearrangement during fusion, extending to form a long coiled-coil and moving a long distance to refold into a six-helix bundle with HRB coils near the TM domain (Lamb and Jardetzky, 2007). This structural change must also occur at the right time and place, as refolding of class I fusion proteins is irreversible. Thus, sensor residues could act as molecular switches that modulate electrostatic interactions, leading to repulsive forces that drive movement of structural elements within the F protein. Mutagenesis studies suggest that protonation of His_{435} in the HRB linker domain serves a critical role in HMPV cell-cell fusion, as does a predicted cluster of basic residues Lys_{295}, Arg_{396}, and Arg_{438} in domain I (Mas et al., 2011; Schowalter et al., 2009). Interestingly, a predicted cluster of positively charged residues in this same region of the AMPV-A F protein (a distantly related pneumovirus) are important for fusion activity (Wei et al., 2012). Another charged region in domain III of HMPV F contains three acidic residues Glu_{51}, Asp_{54}, and Glu_{56} that are important for fusion, but also appear to be critical for protein stability (Chang et al., 2012a). These residues are clustered in a charged region present in the F2 subunit of F in close proximity to two basic residues (Chang et al., 2012a). The specific acidic residues in the F2 subunit and basic residues in the HRA domain are highly conserved in all HMPV strains; therefore, others have predicted that salt bridges and/or electrostatic interactions in this region may contribute to F triggering during HMPV fusion (Chang et al., 2012a). This hypothesis is supported by another study that indicated that the F2 subunit from AMPV-C could confer a hyperfusogenic phenotype to HMPV F1 (de Graaf et al., 2009). I think these residues

(and other neighboring residues) warrant further investigation in a particle-cell fusion assay like the R18-VLP assay where fusion kinetics and extent can both be quantified.

AMPV-C F is more fusogenic than HMPV F in cell-cell fusion assays, and as noted the F2 subunit of AMPV-C confers a hyperfusogenic phenotype on the HMPV F1 subunit (de Graaf et al., 2009). AMPV-C F containing VLPs should be produced and tested in the R18-VLP fusion assay. If AMPV-C F is more fusogenic in the particle-cell fusion assay, then chimeric F proteins with regions of HMPV F inserted into AMPV-C F could be used to probe for areas of the protein that augment hemifusion kinetics or extent.

Finally, R18-MPV fusion in the presence of neutralizing mAbs should be tested to determine whether the antibodies inhibit fusion. Several HMPV F mAbs have been isolated and the epitopes defined. The R18-MPV binding and fusion assays provide methods to determine whether virus is neutralized during entry and at what step. Thus, these experiments would contribute to a better understanding of F epitopes that are required for fusion triggering.

Our understanding of HMPV F triggering is complicated by observations that some F proteins require exposure to low pH to drive syncytium formation. Typically, enveloped viruses either fuse at neutral pH or require exposure to low pH for fusion activity. I speculate that low pH treatment could result in histidine protonation events that serve to destabilize HMPV F in a similar manner to receptor engagement, although this hypothesis requires further investigation. This could explain why not all strains require low-pH exposure, but highly conserved charged regions of F are critical for function of all HMPV strains. The role of low pH in HMPV entry is still unclear. Inhibitors of endosomal acidification such as bafilomycin A1 and concanamycin A have been shown

to partially reduce HMPV infection of the low-pH sensitive CAN97-83 virus strain (Schowalter et al., 2009). Intriguingly, bafilomycin A1 and concanamycin A also partially inhibit infection by the pH-independent NL199 (B1) strain of HMPV, but not the NL1-00 (A1) strain which has been shown to be triggered by low pH exposure in syncytium assays (Mas et al., 2011). Because the low-pH-sensitive phenotype observed in cell-cell fusion assays does not necessarily correlate with inhibition of HMPV infection by endosomal acidification inhibitors, it is not clear that the ability to enhance fusogenicity with low pH pulses is correlated with a requirement for endosomal acidification during entry. Furthermore, whether particle-cell fusion requires exposure to low pH requires further investigation to determine whether low pH is an absolute requirement for triggering of F proteins from some HMPV strains. I have done experiments to test the requirement for endosomal acidification during fusion and infection, and found that ammonium chloride and bafilomycin treatment did not affect fusion kinetics, fusion extent, or infectivity (not shown). These data do not support a role for low pH in fusion triggering, but the R18-MPV fusion assay should be used to investigate whether low pH pulses affect fusion kinetics and extent.

What is the cellular pathway utilized by HMPV during entry?

The site of HMPV fusion requires further investigation. I have shown that chemical inhibitors of endocytosis pathways, e.g. chlorpromazine and dynasore, significantly impair HMPV fusion and infection. Further, my data indicate that HMPV particles are internalized before fusion, but other experiments are required to identify the precise mechanism of virus internalization. Viruses can be internalized by clathrin-

mediated endocytosis, caveolin-mediated endocytosis, non-clathrin, non-caveolin dependent endocytosis, or macropinocytosis. To gain a better understanding of which of these cellular mechanisms was required for HMPV infection, I have performed a preliminary screen using siRNAs to target genes involved in common entry pathways to identify cellular genes that are necessary for HMPV infection.

I transfected BEAS-2B cells with a non-targeting (Scramble) siRNA or siRNA pools targeting the genes listed in Table 1. After 72 hours, I infected cells with either HMPV or VSV. At 20 hours post virus inoculation, I harvested cells and measured HMPV and VSV infection rates by flow cytometry. VSV enters cells via clathrin-mediated endocytosis and requires endosomal acidification to trigger virus fusion during infection (Roche et al., 2008; Rucker et al., 2012; Superti et al., 1987). Along with the VSV infection control, I also tested whether siRNA treatment affected the uptake of fluorescently labeled transferrin. The transferrin protein is endocytosed by clathrin-mediated endocytosis in a dynamin-dependent mechanism (Dautry-Varsat, 1986).

I used western blots to determine the level of target protein expression at the time of infection or transferrin uptake (Fig. 6-2B-E). I was able to confirm reduced protein expression for four of the five target genes. Caveolin-1 expression was reduced by 99%, PKCα expression was reduced by 94%, and dynamin-2 expression was reduced by 92%. The efficiency of knockdown for these three proteins was consistent in replicate experiments. The ability to reduce clathrin heavy chain expression was more variable. On average, clathrin heavy chain expression was reduced by 84% but knockdown ranged from ~70% to >90% in replicate experiments. The western blot shown in Fig. 6-2C

represents average levels of clathrin heavy chain expression during the siRNA experiments.

The siRNAs targeting clathrin heavy chain and dynamin-2 significantly impaired HMPV infection (Fig. 6-2A, orange bars). The effect of reduced clathrin heavy chain expression on HMPV infection was modest (76% of control), but similar to what I observed for transferrin uptake (78% of control), which is mediated by clathrin-dependent endocytosis (Fig. 6-2A, green bars). Clathrin-mediated endocytosis depends upon dynamin, and both clathrin heavy chain and dyamin-2 siRNAs reduced HMPV infection to a similar level. The siRNAs targeting clathrin heavy chain and dynamin-2 impaired VSV infection (Fig. 6-2, blue bars) as expected. Again, the inhibitory effect of these siRNAs on VSV infection was not complete and for dynamin did not reach statistical significance due to variability in the effect during four independent experiments (CLTC, 53% of control; DNM2, 71% of control). This suggests to me that enough functional clathrin and dynamin proteins are still available to mediate VSV infection because the virus absolutely requires endocytosis for productive infection. The caveolin-1 siRNA significantly impaired VSV infection (CAV1, 61% of control), which was unexpected. A recent genome-wide siRNA screen for human kinases required for endocytosis found that siRNA targeting CAV1 did not affect VSV infection (Pelkmans et al., 2005). Currently, it is unclear what my result means because VSV is thought to enter cells strictly by a clathrin-dependent mechanism although I was not able to find other published studies that had tested the effect of CAV1-specific siRNAs on VSV infection.

The siRNAs targeting caveolin-1 and PKCα did not affect HMPV infection or transferrin uptake. These results argue against HMPV internalization by caveolin-

mediated endocytosis and macropinocytosis. Additional experiments are required to rule out these cellular pathways. For example, the effect of nystatin, which is a sterol-binding agent that disrupts cholesterol-mediated caveolae-containing membrane microdomains, should be performed to rule out caveolin-mediated endocytosis. Macropinocytosis is an actin-dependent process that is associated with plasma membrane ruffling. Experiments with known inhibitors of macropinocytosis such as genistein, calphostin C, bisindolyl-maleimide, and an N-terminally myristoylated pseudosubstrate of PKCα (PKC-myr) will be required to rule out macropinocytosis as an internalization mechanism. To determine whether HMPV internalization is an actin-dependent process, I would test the effect of cytochalasin D and jasplakinolide, inhibitors of F-actin polymerization, on HMPV entry. Actin could be required for HMPV internalization and/or vesicle trafficking. With the DiD-Red-MPV microscopy-based fusion assay, the effect of actin inhibitors on internalization, hemifusion, and fusion pore enlargement could all be determined. Live-cell imaging experiments to determine whether HMPV induces membrane ruffling during entry would also be informative.

Table 6-1. List of genes targeted by siRNA pools used in primary screen.

Primary function and name of gene[a]	Product name, function(s), and other characteristics
Clathrin-mediated endocytosis	
CLTC	Clathrin heavy chain; binds to clathrin light chain to form the clathrin triskelion
Caveolin-mediated endocytosis	
CAV1	Caveolin-1; coats the cytoplasmic face of caveolae, expressed in many cell types
Macropinocytosis	
PKCα	Protein kinase C alpha; serine/threonine kinase that associates with plasma membrane to promote ruffling and macropinosome formation
General endocytosis	
DNM2	Dynamin-2; involved in pinching off of endocytic vesicles from the plasma membrane; expressed in many cell types
Endosomal acidification	
ATP6V0C	V-type proton ATPase 16kDa proteolipid subunit; component of vacuolar ATPase (V-ATPase), a multisubunit enzyme that mediates endosome acidification

[a]All siRNA pools were siGENOME SMARTpool (ThermoScientific) and were kindly provided by Borden Lacy and Melissa Farrow.

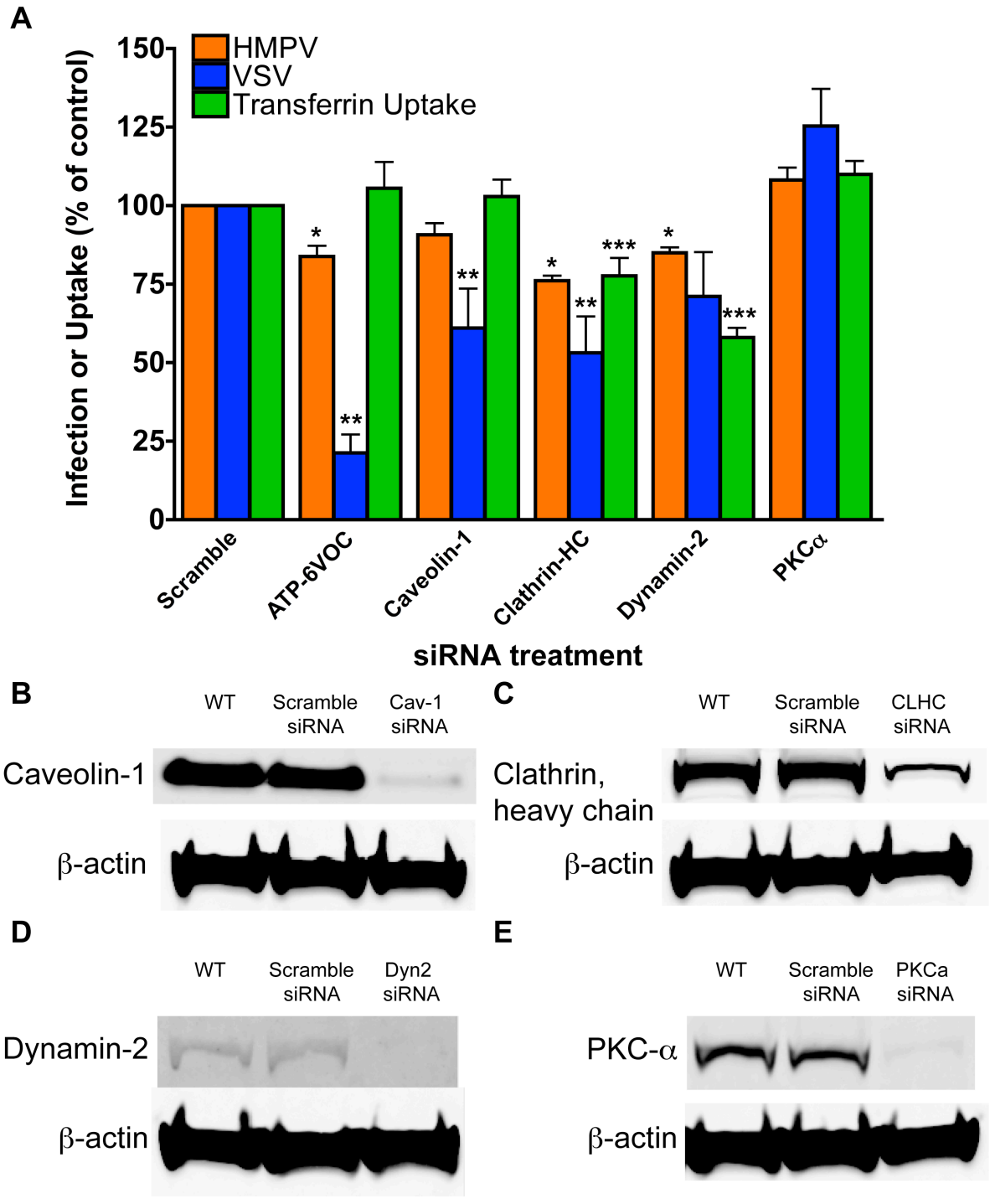
A
HMPV
VSV
Transferrin Uptake
Infection or Uptake (% of control)
150
125
100
75
50
25
0
Scramble
ATP-6VOC
Caveolin-1
Clathrin-HC
Dynamin-2
PKCα
siRNA treatment
B
WT
Scramble siRNA
Cav-1 siRNA
Caveolin-1
β-actin
C
WT
Scramble siRNA
CLHC siRNA
Clathrin, heavy chain
β-actin
D
WT
Scramble siRNA
Dyn2 siRNA
Dynamin-2
β-actin
E
WT
Scramble siRNA
PKCa siRNA
PKC-α
β-actin

Fig. 6-2. The impact of siRNAs targeting genes involved in endocytosis on HMPV infection, VSV infection, and transferrin uptake.
BEAS-2B cells (1 x 10^5) were transfected with siRNAs (1.5 pmol) using LipoRNAiMax reagent (1.5 µl) and plated in 24-well plates. After 72 h, cells were either infected or tested for transferrin uptake. Cells were infected with HMPV or VSV to achieve 15 to 20% infected cells (MOI ~ 0.5). After 20 h, infected cells were enumerated by flow cytometry analysis. For transferrin uptake experiments, cells were incubated with Alexa Fluor 488-transferrin (20 µg/mL) for 30 min at 37°C, washed with PBS, lifted from plates with trypsin, treated with citric acid wash (pH 4.5) for 2 min to remove surface-bound transferrin, washed, fixed in paraformaldehyde, and stored overnight at 4°C before flow cytometry analysis on the same day as infected cells. (A) HMPV infectivity (orange bars), VSV infectivity (blue bars), and transferrin uptake (green bars) were normalized to the average number of cells after treatment with the control siRNA (Scramble). Results represent means ± SEM for at least four independent experiments. Target gene names and a brief description of the protein function are provided in Table 1. Asterisks indicate $p < 0.05$ using ANOVA with Dunnett's test comparing specific siRNA to control siRNA. (B-E) Western blots were performed after siRNA treatment for 72 h. For each experiment, cell lysates were made from untreated cells (WT), cells transfected with the non-targeting control siRNA (Scramble), or cells transfected with siRNA targeting the indicated gene: caveolin-1 (B), clathrin heavy chain (C), dynamin-2 (D), or PKCα (E). Total protein concentrations of each lysate were measured and adjusted to ensure equal loading (50 to 100 µg), and membranes were probed with β-actin-specific antibody to ensure equivalent loading. Blots from a representative experiment are shown.

Surprisingly, the siRNA targeting ATP6V0C reduced HMPV infectivity (ATP6V0C; 84% of control), but the effect was not as potent as the reduction in VSV infectivity (ATP6V0C; 21% of control) (Fig. 6-2A, orange and blue bars, respectively). This was the expected result for VSV infection because VSV fusion requires an endosomal drop in pH. HMPV fusion occurs at neutral pH and chemical inhibitors of endosomal acidification do not significantly impair infection by all strains of HMPV, so I did not expect the ATP6V0C siRNA to affect HMPV infectivity. Other experiments are required to determine whether HMPV entry requires endosomal acidification. It is possible that disrupting ATP6V0C expression impaired endosomal trafficking, and the reduction in HMPV infectivity results from vesicles not arriving at the appropriate compartment for HMPV fusion to take place. This would explain why HMPV infection was modestly impaired compared to the potent inhibition of VSV infection. Other pH-independent virus controls such as hRSV, parainfluenza virus 5 (PIV5), and amphotropic murine leukemia virus (MLV) should be tested in parallel to HMPV to better interpret this result.

These preliminary results suggest that HMPV enters cells via clathrin-mediated endocytosis. However, more experiments specifically measuring virus entry are required to confirm the infection data. Specifically, I would test whether siRNAs targeting clathrin heavy chain, dynamin-2, or ATP6V0C impair HMPV fusion (using the R18-MPV fusion assay) and internalization (using the confocal fluorescence microscopy-based assays). I would additionally test siRNAs targeting clathrin light chain, dynamin-1, dynamin-3, Rab5, and Eps15. All of these cellular proteins may be required for clathrin-mediated endocytosis in BEAS-2B cells.

Finally, thin-section electron microscopy experiments to examine HMPV entry into cells would be very informative. I would expect to observe HMPV particles enclosed in clathrin-coated pits near the cell periphery after a 10 to 20 minute incubation of virus-bound cells at 37°C. If HMPV could fuse at the plasma membrane, I would expect to also observe HMPV particles in the process of fusing at the cell surface. Immunogold labeling using HMPV F-specific antibodies added to the cell surface at different times postbinding would determine whether virions fused at the cell membrane or escaped antibody recognition due to internalization. This is perhaps the best approach to determine whether HMPV fusion can occur at different sites.

Conclusions

My thesis provides a framework to investigate mechanisms of HMPV entry into target cells. I have developed new assays that will allow others to study viral and cellular determinants of HMPV attachment, internalization, and fusion. The future studies described in this chapter will enhance an understanding of how RGD-binding integrins mediate HMPV entry and may uncover novel aspects of integrin-mediated cellular processes involved in viral infections. Additionally, these studies may elucidate how the HMPV F protein is triggered to mediate fusion. Importantly, this work will clarify the cellular mechanism(s) required for HMPV internalization. Virus internalization before membrane fusion is a novel mechanism for paramyxovirus entry and the study of HMPV entry will provide insight into how viruses in *Paramyxoviridae* family may establish infection very differently. This work will improve our understanding of HMPV cell entry,

which may lead to the development of antiviral therapies that inhibit virus entry into target cells.

Broad Significance of Research Findings

Why is a pH-independent virus dependent on endocytosis?

Virus endocytosis during entry has historically been correlated with a requirement for low pH exposure. Indeed certain virus fusion proteins, e.g. influenza HA, undergo structural changes at low pH that are required for membrane fusion activity. Other virus fusion proteins, e.g. Ebola GP, require proteolytic cleavage by endosomal proteases that require low pH for optimal protease activity. In general, endosomal acidification inhibitors do not impair HMPV infection, and there is no current evidence to support a role for proteolytic cleavage of HMPV F for fusion activity, aside from the single cleavage event that activates the F0 precursor to the F1/F2 fusogenic form of the protein that can be mediated by trypsin prior to virus binding. Thus, it is currently unclear why a pH-independent virus, like HMPV, would be dependent on endocytosis.

Entrapment within an intracellular vesicle provides a unique environment for an HMPV virion, which is distinct from the extracellular milieu a particle encounters at the cell surface. While it is well understood that endosomal maturation leads to progressive acidification, recent findings indicate that ion flux across endosomal compartments is regulated and required for endosome function (Scott and Gruenberg, 2010). The ionic nature of endosomes varies considerably as endosomes mature along the endocytic pathway (Scott and Gruenberg, 2010). Nascent endocytic vesicles mature along a pathway into early endosomes, multivesicular bodies, late endosomes, and lysosomes.

During endosomal maturation, ion transporters mediate significant ion flux across the limited membrane of endosomes leading to changes in the ionic composition of the endosomal lumen (Scott and Gruenberg, 2010). An influx of H^+ ions leads to progressive acidification. The high Cl^- concentration (~130 mM) at the plasma membrane is not found in early endosomes (19 mM), but Cl^- concentrations increase as early endosomes mature (reviewed in (Scott and Gruenberg, 2010)). High Na^+ concentrations decrease during endosomal maturation, while the amounts of K^+ ions increase gradually (reviewed in (Scott and Gruenberg, 2010)). Ca^{2+} concentrations have been found to drop significantly from ~1 mM at the plasma membrane to ~5 μM in early endosomal compartments (Gerasimenko et al., 1998). Although monovalent cation (H^+, Na^+, and K^+) gradients are known to be more gradual, the dramatic changes in Cl^- and Ca^{2+} concentrations between the plasma membrane and early endosomes suggests that endosomal ion transporters can rapidly modify ion concentrations. Moreover, defects in calcium channels have been linked to several lysosomal-storage disorders in humans (Cheng et al., 2010) indicating that the transport of Ca^{2+} is critical for endosomal function. Thus, virus particles contained within endosomal compartments experience a changing ionic environment that could influence the structure and function of viral fusion and receptor proteins. Recent evidence suggests that changes in ionic strength can result in hRSV F protein triggering (Chaiwatpongsakorn et al., 2011). Perhaps HMPV fusion is triggered by changes in ion concentrations that occur during endosomal maturation. If changes in ionic strength are required for HMPV F triggering, this could explain why the virus needs to be internalized but does not require exposure to low pH.

Changes in divalent cation concentrations are known to lead to changes in integrin affinity, and it is tempting to speculate that integrin affinity may change after internalization due to the significant loss of Ca^{2+} as nascent endocytic vesicles mature into early endosomes. Cell migration involves integrin recycling and tight regulation of integrin affinity at the leading cell edge. This suggests that changes in integrin structural conformations may occur within endosomes as integrins are internalized and recycled back to the cell surface. Thus, it is possible that changes in integrin structure within an endosome could lead to changes in the HMPV F protein that drive the creation of a fusion pore for genome delivery. Alternatively, disassociation of HMPV F from RGD-binding integrins, rather than binding, may be required for F function during the fusion process.

The endocytic requirement for HMPV entry could also be linked to other surface proteins that are internalized from integrin-rich microdomains on the cell surface. Current evidence suggests that HMPV F binds multiple receptors at the cell surface, including some that have not yet been identified. If these receptors are sensitive to ionic changes or are susceptible to endosomal proteases, HMPV internalization may be required to change the receptor's structural conformation, which leads to HMPV F activation.

During HMPV fusion, the F protein must undergo a significant structural rearrangement to drive membrane fusion. The HRA region of F extends to form a long coiled-coil and moves a long distance to refold into a six-helix bundle with HRB coils near the TM domain (Lamb and Jardetzky, 2007). This structural change must also occur at the right time and place, as refolding of class I fusion proteins is irreversible. To better understand how the HMPV F protein functions alone to mediate fusion, recent studies have explored the requirements for fusion and investigated the importance of specific

residues within the extracellular domain of the protein for fusion activity. Mutational analyses suggest that specific charged residues in domain II of HMPV F impact the initiation of membrane fusion (Schowalter et al., 2009). Another charged region in the HMPV F extracellular head domain, located in domain III, includes several highly conserved acidic and basic residues that are important for F-mediated cell-cell fusion, but also appear to be critical for protein stability (Chang et al., 2012a). Others have predicted that salt bridges and/or electrostatic interactions in this region may contribute to F triggering during HMPV fusion (Chang et al., 2012a). Taking these studies together, it is clear that multiple regions in the HMPV F head domain are critical for fusion activity. Interestingly, two distal regions with predicted charged residue clusters have been implicated in fusion triggering (located in domains II and III). The idea that electrostatic repulsions can trigger the HMPV F prefusion protein to spring into the postfusion conformation during the fusion process is logical. Sensor residues could act as molecular switches that modulate electrostatic interactions, leading to repulsive forces that drive movement of structural elements within the F protein. Perhaps receptor interactions serve to augment local protein structure, driving electrostatic repulsion that can trigger fusion. Alternatively, changes in ionic strength inside an endosomal compartment may serve to destabilize electrostatic interactions within prefusion F providing a signal that the protein should refold and drive membrane fusion. Therefore, the changing ionic nature of endosomes could serve as a timing mechanism that induces F-mediated fusion at the appropriate compartment within a cell.

What benefit could endocytosis provide to pH-independent viruses?

Virus endocytosis may provide a common entry mechanism to evade immune response by allowing virus particles to rapidly escape neutralizing antibodies at the cell surface. Primary HMPV infection induces a strong neutralizing antibody response in animal models of infection. An endocytic mechanism of entry would allow HMPV particles to escape this neutralizing response in order to establish infection. With respect to evading virus-specific antibodies, any virus that is known to cause recurrent infections within a host would likely benefit from entry by endocytosis.

Virus endocytosis may also be a common strategy to optimize productive infection. It is possible that an endocytic entry mechanism could enhance HMPV infection by providing directed transport of viral particles to specific sites within the cell's cytoplasm. By hitching a ride through the dense cytoskeleton within endocytic vesicles, HMPV particles could concentrate at specific areas in the cell before fusion occurs. Thus, HMPV genomes would be concentrated at sites where viral transcription may be more likely to result in productive virus replication. It is reasonable to assume that delivering viral genomes to specific transcription/replication sites via fusion events would be more efficient than recruiting viral RNAs after random delivery into the cytoplasm. Moreover, other viruses, especially enveloped viruses that require nuclear import during the virus lifecycle, may benefit from virus fusion at endosomes in close proximity to the nucleus.

Finally, it is plausible that virus fusion, in general, is easier with an endosomal membrane than with the plasma membrane. Areas of high membrane curvature in a cell are thought to exist for limited periods of time (McMahon and Gallop, 2005). Tight

curvature on nascent endocytic vesicles is primarily achieved by cellular coat proteins (e.g. clathrin), which induce curvature by surrounding the lipid bilayer. The curvature is readily reversible when the coat proteins disassociate, which is thought to leave the vesicle more fusogenic due to the tension associated with high curvature (McMahon and Gallop, 2005). Indeed, nascent endosomes rapidly fuse into larger structures called early endosomes that serve as sorting stations for endocytic cargo. This indirectly suggests that endocytic vesicles are primed to undergo membrane fusion, which could reduce the energy required for viral fusogens to mediate membrane fusion. For example, the high membrane curvature of an endocytic membrane may be more easily disrupted by the insertion of viral fusion peptides (or loops in the case of class II and III fusion proteins) into the inner leaflet of the bilayer compared to insertion at the plasma membrane where curvature is less pronounced and stabilized by the actin cytoskeleton. Furthermore, the lipid composition of endosomes may help to facilitate virus fusion. Different lipids are known to influence positive and negative membrane curvature. Lipids in cell membranes are free to diffuse and mix in bilayer leaflets. Intuitively, endosomal membranes have a smaller surface area for free diffusion than the plasma membrane. Thus, if lipids need to be organized and tilted in specific ratios to induce membrane fusion, virus fusion would be expected to be more favorable in a membrane where free diffusion was limited.

Do other pH-independent viruses also use endocytic routes?

The realization that pH-independent fusion protein activity may not be sufficient to predict whether virus fusion occurs at the cell surface or within an endosome should direct us to revisit some long-held assumptions about virus entry. Paramyxovirus fusion at the cell surface has not been extensively studied, evidence for fusion at the cell surface is limited, and direct fusion at the plasma membrane has not been reported for all members of the paramyxovirus family. As I have discussed above, endosomes may provide an optimal site for membrane fusion that has little to do with the pH at which optimal fusion occurs. I think it is highly possible that other paramyxoviruses, and other pH-independent viruses in general, may use endocytic routes for entry into host cells.

The physiological trigger for paramyxovirus F proteins has not been identified for any member of the paramyxovirus family. Others have concluded that receptor binding is sufficient to trigger fusion because paramyxovirus F proteins can drive cell-cell fusion. However, overexpression of the VSV fusion protein, G, also drives cell-cell fusion at neutral pH even though VSV G fusion activity requires exposure to low pH within endosomes during virus entry. Once again, this suggests that the ability to mediate cell-cell fusion does not accurately predict whether virus fusion occurs at the cell surface or within endosomes. Perhaps the answer to how paramyxovirus F proteins are triggered to initiate fusion can be determined if we better understand where physiological virus fusion occurs. New techniques that enable virus particle tracking and methodologies such as the ones I have developed for HMPV should be used to revisit paramyxovirus entry. It is conceivable that other paramyxovirus F proteins fuse with intracellular vesicles. If this were true, then the key to understanding F triggering might be to understand the nature of

the compartment where fusion occurs. Endosomes are dynamic vesicles that could provide a variety of unique signals that might influence fusion protein structure and function. This argument could be made for not only paramyxoviruses but also for other enveloped viruses that fuse in a pH-independent manner. Thus, elucidating the site of membrane fusion for any virus could lead to novel discoveries about how viral fusion proteins drive membrane fusion.

REFERENCES

Aguilar, H. C., Ataman, Z. A., Aspericueta, V., Fang, A. Q., Stroud, M., Negrete, O. A., Kammerer, R. A., and Lee, B. (2009): A novel receptor-induced activation site in the Nipah virus attachment glycoprotein (G) involved in triggering the fusion glycoprotein (F). *J Biol Chem* **284**, 1628-35.

Akula, S. M., Pramod, N. P., Wang, F. Z., and Chandran, B. (2002): Integrin alpha3beta1 (CD 49c/29) is a cellular receptor for Kaposi's sarcoma-associated herpesvirus (KSHV/HHV-8) entry into the target cells. *Cell* **108**, 407-19.

Ali, S. A., Gern, J. E., Hartert, T. V., Edwards, K. M., Griffin, M. R., Miller, E. K., Gebretsadik, T., Pappas, T., Lee, W. M., and Williams, J. V. (2011): Real-world comparison of two molecular methods for detection of respiratory viruses. *Virol J* **8**, 332.

AppliedBiosystems (2001): User Bulletin #2: ABI PRISM 7700 Sequence Detection System.

Bagai, S., and Lamb, R. A. (1995): Quantitative measurement of paramyxovirus fusion: differences in requirements of glycoproteins between simian virus 5 and human parainfluenza virus 3 or Newcastle disease virus. *J Virol* **69**, 6712-9.

Barton, E. S., Forrest, J. C., Connolly, J. L., Chappell, J. D., Liu, Y., Schnell, F. J., Nusrat, A., Parkos, C. A., and Dermody, T. S. (2001): Junction adhesion molecule is a receptor for reovirus. *Cell* **104**, 441-51.

Bastien, N., Normand, S., Taylor, T., Ward, D., Peret, T. C., Boivin, G., Anderson, L. J., and Li, Y. (2003): Sequence analysis of the N, P, M and F genes of Canadian human metapneumovirus strains. *Virus Res* **93**, 51-62.

Bergelson, J. M., Chan, B. M., Finberg, R. W., and Hemler, M. E. (1993): The integrin VLA-2 binds echovirus 1 and extracellular matrix ligands by different mechanisms. *J Clin Invest* **92**, 232-9.

Berinstein, A., Roivainen, M., Hovi, T., Mason, P. W., and Baxt, B. (1995): Antibodies to the vitronectin receptor (integrin alpha V beta 3) inhibit binding and infection of foot-and-mouth disease virus to cultured cells. *J Virol* **69**, 2664-6.

Biacchesi, S., Pham, Q. N., Skiadopoulos, M. H., Murphy, B. R., Collins, P. L., and Buchholz, U. J. (2005): Infection of nonhuman primates with recombinant human metapneumovirus lacking the SH, G, or M2-2 protein categorizes each as a nonessential accessory protein and identifies vaccine candidates. *J Virol* **79**, 12608-13.

Biacchesi, S., Skiadopoulos, M. H., Boivin, G., Hanson, C. T., Murphy, B. R., Collins, P. L., and Buchholz, U. J. (2003): Genetic diversity between human metapneumovirus subgroups. *Virology* **315**, 1-9.

Biacchesi, S., Skiadopoulos, M. H., Yang, L., Lamirande, E. W., Tran, K. C., Murphy, B. R., Collins, P. L., and Buchholz, U. J. (2004): Recombinant human Metapneumovirus lacking the small hydrophobic SH and/or attachment G glycoprotein: deletion of G yields a promising vaccine candidate. *J Virol* **78**, 12877-87.

Bishop, K. A., Stantchev, T. S., Hickey, A. C., Khetawat, D., Bossart, K. N., Krasnoperov, V., Gill, P., Feng, Y. R., Wang, L., Eaton, B. T., Wang, L. F., and Broder, C. C. (2007): Identification of Hendra virus G glycoprotein residues that are critical for receptor binding. *J Virol* **81**, 5893-901.

Bissonnette, M. L., Connolly, S. A., Young, D. F., Randall, R. E., Paterson, R. G., and Lamb, R. A. (2006): Analysis of the pH requirement for membrane fusion of different isolates of the paramyxovirus parainfluenza virus 5. *J Virol* **80**, 3071-7.

Boivin, G., De Serres, G., Cote, S., Gilca, R., Abed, Y., Rochette, L., Bergeron, M. G., and Dery, P. (2003): Human metapneumovirus infections in hospitalized children. *Emerg Infect Dis* **9**, 634-40.

Boivin, G., Mackay, I., Sloots, T. P., Madhi, S., Freymuth, F., Wolf, D., Shemer-Avni, Y., Ludewick, H., Gray, G. C., and LeBlanc, E. (2004): Global genetic diversity of human metapneumovirus fusion gene. *Emerg Infect Dis* **10**, 1154-7.

Bonaparte, M. I., Dimitrov, A. S., Bossart, K. N., Crameri, G., Mungall, B. A., Bishop, K. A., Choudhry, V., Dimitrov, D. S., Wang, L. F., Eaton, B. T., and Broder, C. C. (2005): Ephrin-B2 ligand is a functional receptor for Hendra virus and Nipah virus. *Proc Natl Acad Sci U S A* **102**, 10652-7.

Bose, S., Welch, B. D., Kors, C. A., Yuan, P., Jardetzky, T. S., and Lamb, R. A. (2011): Structure and mutagenesis of the parainfluenza virus 5 hemagglutinin-neuraminidase stalk domain reveals a four-helix bundle and the role of the stalk in fusion promotion. *J Virol* **85**, 12855-66.

Bretscher, M. S. (1989): Endocytosis and recycling of the fibronectin receptor in CHO cells. *EMBO J* **8**, 1341-8.

Breuss, J. M., Gallo, J., DeLisser, H. M., Klimanskaya, I. V., Folkesson, H. G., Pittet, J. F., Nishimura, S. L., Aldape, K., Landers, D. V., Carpenter, W., and et al. (1995): Expression of the beta 6 integrin subunit in development, neoplasia and tissue repair suggests a role in epithelial remodeling. *J Cell Sci* **108 (Pt 6)**, 2241-51.

Brodzinski, H., and Ruddy, R. M. (2009): Review of new and newly discovered respiratory tract viruses in children. *Pediatr Emerg Care* **25**, 352-60; quiz 361-3.

Brown, P. J., and Juliano, R. L. (1988): Monoclonal antibodies to distinctive epitopes on the alpha and beta subunits of the fibronectin receptor. *Exp Cell Res* **177**, 303-18.

Buchholz, U. J., Finke, S., and Conzelmann, K. K. (1999): Generation of bovine respiratory syncytial virus (BRSV) from cDNA: BRSV NS2 is not essential for virus

replication in tissue culture, and the human RSV leader region acts as a functional BRSV genome promoter. *J Virol* **73**, 251-9.

Bullough, P. A., Hughson, F. M., Skehel, J. J., and Wiley, D. C. (1994): Structure of influenza haemagglutinin at the pH of membrane fusion. *Nature* **371**, 37-43.

Carr, C. M., and Kim, P. S. (1993): A spring-loaded mechanism for the conformational change of influenza hemagglutinin. *Cell* **73**, 823-32.

Chaiwatpongsakorn, S., Epand, R. F., Collins, P. L., Epand, R. M., and Peeples, M. E. (2011): Soluble respiratory syncytial virus fusion protein in the fully cleaved, pretriggered state is triggered by exposure to low-molarity buffer. *J Virol* **85**, 3968-77.

Chan, D. C., and Kim, P. S. (1998): HIV entry and its inhibition. *Cell* **93**, 681-4.

Chang, A., Hackett, B., Winter, C. C., Buchholz, U. J., and Dutch, R. E. (2012a): Potential electrostatic interactions in multiple regions affect HMPV F-mediated membrane fusion. *J Virol* **86**, 9843-53.

Chang, A., Masante, C., Buchholz, U. J., and Dutch, R. E. (2012b): Human metapneumovirus (HMPV) binding and infection are mediated by interactions between the HMPV fusion protein and heparan sulfate. *J Virol* **86**, 3230-43.

Chen, F. A., Repasky, E. A., and Bankert, R. B. (1991): Human lung tumor-associated antigen identified as an extracellular matrix adhesion molecule. *J Exp Med* **173**, 1111-9.

Cheng, X., Shen, D., Samie, M., and Xu, H. (2010): Mucolipins: Intracellular TRPML1-3 channels. *FEBS Lett* **584**, 2013-21.

Colman, P. M., and Lawrence, M. C. (2003): The structural biology of type I viral membrane fusion. *Nat Rev Mol Cell Biol* **4**, 309-19.

Connolly, S. A., and Lamb, R. A. (2006): Paramyxovirus fusion: real-time measurement of parainfluenza virus 5 virus-cell fusion. *Virology* **355**, 203-12.

Connolly, S. A., Leser, G. P., Jardetzky, T. S., and Lamb, R. A. (2009): Bimolecular complementation of paramyxovirus fusion and hemagglutinin-neuraminidase proteins enhances fusion: implications for the mechanism of fusion triggering. *J Virol* **83**, 10857-68.

Cook, J. K. (2000): Avian pneumovirus infections of turkeys and chickens. *Vet J* **160**, 118-25.

Cox, B. D., Natarajan, M., Stettner, M. R., and Gladson, C. L. (2006): New concepts regarding focal adhesion kinase promotion of cell migration and proliferation. *J Cell Biochem* **99**, 35-52.

Cox, R. G., Livesay, S. B., Johnson, M., Ohi, M. D., and Williams, J. V. (2012): The Human Metapneumovirus Fusion Protein Mediates Entry via an Interaction with RGD-Binding Integrins. *J Virol* **86**, 12148-60.

Cseke, G., Maginnis, M. S., Cox, R. G., Tollefson, S. J., Podsiad, A. B., Wright, D. W., Dermody, T. S., and Williams, J. V. (2009): Integrin alphavbeta1 promotes infection by human metapneumovirus. *Proc Natl Acad Sci U S A* **106**, 1566-71.

Cseke, G., Wright, D. W., Tollefson, S. J., Johnson, J. E., Crowe, J. E., Jr., and Williams, J. V. (2007): Human metapneumovirus fusion protein vaccines that are immunogenic and protective in cotton rats. *J Virol* **81**, 698-707.

Dautry-Varsat, A. (1986): Receptor-mediated endocytosis: the intracellular journey of transferrin and its receptor. *Biochimie* **68**, 375-81.

Davison, E., Kirby, I., Whitehouse, J., Hart, I., Marshall, J. F., and Santis, G. (2001): Adenovirus type 5 uptake by lung adenocarcinoma cells in culture correlates with Ad5 fibre binding is mediated by alpha(v)beta1 integrin and can be modulated by changes in beta1 integrin function. *J Gene Med* **3**, 550-9.

de Graaf, M., Osterhaus, A. D., Fouchier, R. A., and Holmes, E. C. (2008): Evolutionary dynamics of human and avian metapneumoviruses. *J Gen Virol* **89**, 2933-42.

de Graaf, M., Schrauwen, E. J., Herfst, S., van Amerongen, G., Osterhaus, A. D., and Fouchier, R. A. (2009): Fusion protein is the main determinant of metapneumovirus host tropism. *J Gen Virol* **90**, 1408-16.

Deffrasnes, C., Hamelin, M. E., Prince, G. A., and Boivin, G. (2008): Identification and evaluation of a highly effective fusion inhibitor for human metapneumovirus. *Antimicrob Agents Chemother* **52**, 279-87.

Dollner, H., Risnes, K., Radtke, A., and Nordbo, S. A. (2004): Outbreak of human metapneumovirus infection in norwegian children. *Pediatr Infect Dis J* **23**, 436-40.

Dorig, R. E., Marcil, A., Chopra, A., and Richardson, C. D. (1993): The human CD46 molecule is a receptor for measles virus (Edmonston strain). *Cell* **75**, 295-305.

Ebihara, T., Endo, R., Kikuta, H., Ishiguro, N., Ishiko, H., Hara, M., Takahashi, Y., and Kobayashi, K. (2004): Human metapneumovirus infection in Japanese children. *J Clin Microbiol* **42**, 126-32.

Englund, J. A., Boeckh, M., Kuypers, J., Nichols, W. G., Hackman, R. C., Morrow, R. A., Fredricks, D. N., and Corey, L. (2006): Brief communication: fatal human metapneumovirus infection in stem-cell transplant recipients. *Ann Intern Med* **144**, 344-9.

Esper, F., Martinello, R. A., Boucher, D., Weibel, C., Ferguson, D., Landry, M. L., and Kahn, J. S. (2004): A 1-year experience with human metapneumovirus in children aged <5 years. *J Infect Dis* **189**, 1388-96.

Feldman, S. A., Audet, S., and Beeler, J. A. (2000): The fusion glycoprotein of human respiratory syncytial virus facilitates virus attachment and infectivity via an interaction with cellular heparan sulfate. *J Virol* **74**, 6442-7.

Fitzgerald, L. A., Poncz, M., Steiner, B., Rall, S. C., Jr., Bennett, J. S., and Phillips, D. R. (1987): Comparison of cDNA-derived protein sequences of the human fibronectin and vitronectin receptor alpha-subunits and platelet glycoprotein IIb. *Biochemistry* **26**, 8158-65.

Foulongne, V., Guyon, G., Rodiere, M., and Segondy, M. (2006): Human metapneumovirus infection in young children hospitalized with respiratory tract disease. *Pediatr Infect Dis J* **25**, 354-9.

Gallo, S. A., Reeves, J. D., Garg, H., Foley, B., Doms, R. W., and Blumenthal, R. (2006): Kinetic studies of HIV-1 and HIV-2 envelope glycoprotein-mediated fusion. *Retrovirology* **3**, 90.

Gerasimenko, J. V., Tepikin, A. V., Petersen, O. H., and Gerasimenko, O. V. (1998): Calcium uptake via endocytosis with rapid release from acidifying endosomes. *Curr Biol* **8**, 1335-8.

Giancotti, F. G., and Ruoslahti, E. (1990): Elevated levels of the alpha 5 beta 1 fibronectin receptor suppress the transformed phenotype of Chinese hamster ovary cells. *Cell* **60**, 849-59.

Guerrero, C. A., Mendez, E., Zarate, S., Isa, P., Lopez, S., and Arias, C. F. (2000): Integrin alpha(v)beta(3) mediates rotavirus cell entry. *Proc Natl Acad Sci U S A* **97**, 14644-9.

Hallak, L. K., Collins, P. L., Knudson, W., and Peeples, M. E. (2000): Iduronic acid-containing glycosaminoglycans on target cells are required for efficient respiratory syncytial virus infection. *Virology* **271**, 264-75.

Hamelin, M. E., Prince, G. A., Gomez, A. M., Kinkead, R., and Boivin, G. (2006): Human metapneumovirus infection induces long-term pulmonary inflammation associated with airway obstruction and hyperresponsiveness in mice. *J Infect Dis* **193**, 1634-42.

Harrison, M. S., Sakaguchi, T., and Schmitt, A. P. (2010): Paramyxovirus assembly and budding: building particles that transmit infections. *Int J Biochem Cell Biol* **42**, 1416-29.

Herfst, S., de Graaf, M., Schickli, J. H., Tang, R. S., Kaur, J., Yang, C. F., Spaete, R. R., Haller, A. A., van den Hoogen, B. G., Osterhaus, A. D., and Fouchier, R. A. (2004): Recovery of human metapneumovirus genetic lineages a and B from cloned cDNA. *J Virol* **78**, 8264-70.

Herfst, S., Mas, V., Ver, L. S., Wierda, R. J., Osterhaus, A. D., Fouchier, R. A., and Melero, J. A. (2008): Low-pH-induced membrane fusion mediated by human metapneumovirus F protein is a rare, strain-dependent phenomenon. *J Virol* **82**, 8891-5.

Hernandez, L. D., Hoffman, L. R., Wolfsberg, T. G., and White, J. M. (1996): Virus-cell and cell-cell fusion. *Annu Rev Cell Dev Biol* **12**, 627-61.

Hoekstra, D., de Boer, T., Klappe, K., and Wilschut, J. (1984): Fluorescence method for measuring the kinetics of fusion between biological membranes. *Biochemistry* **23**, 5675-81.

Horvath, C. M., Paterson, R. G., Shaughnessy, M. A., Wood, R., and Lamb, R. A. (1992): Biological activity of paramyxovirus fusion proteins: factors influencing formation of syncytia. *J Virol* **66**, 4564-9.

Hynes, R. O. (2002): Integrins: bidirectional, allosteric signaling machines. *Cell* **110**, 673-87.

Iorio, R. M., and Mahon, P. J. (2008): Paramyxoviruses: different receptors - different mechanisms of fusion. *Trends Microbiol* **16**, 135-7.

Ishiguro, N., Ebihara, T., Endo, R., Ma, X., Kikuta, H., Ishiko, H., and Kobayashi, K. (2004): High genetic diversity of the attachment (G) protein of human metapneumovirus. *J Clin Microbiol* **42**, 3406-14.

Jackson, T., Mould, A. P., Sheppard, D., and King, A. M. (2002): Integrin alphavbeta1 is a receptor for foot-and-mouth disease virus. *J Virol* **76**, 935-41.

Jackson, T., Sheppard, D., Denyer, M., Blakemore, W., and King, A. M. (2000): The epithelial integrin alphavbeta6 is a receptor for foot-and-mouth disease virus. *J Virol* **74**, 4949-56.

Kahn, J. S., Schnell, M. J., Buonocore, L., and Rose, J. K. (1999): Recombinant vesicular stomatitis virus expressing respiratory syncytial virus (RSV) glycoproteins: RSV fusion protein can mediate infection and cell fusion. *Virology* **254**, 81-91.

Kallewaard, N. L., Bowen, A. L., and Crowe, J. E., Jr. (2005): Cooperativity of actin and microtubule elements during replication of respiratory syncytial virus. *Virology* **331**, 73-81.

Karron, R. A., Buonagurio, D. A., Georgiu, A. F., Whitehead, S. S., Adamus, J. E., Clements-Mann, M. L., Harris, D. O., Randolph, V. B., Udem, S. A., Murphy, B. R., and Sidhu, M. S. (1997): Respiratory syncytial virus (RSV) SH and G proteins are not essential for viral replication in vitro: clinical evaluation and molecular characterization of a cold-passaged, attenuated RSV subgroup B mutant. *Proc Natl Acad Sci U S A* **94**, 13961-6.

Koistinen, P., and Heino, J. (2002): The selective regulation of alpha Vbeta 1 integrin expression is based on the hierarchical formation of alpha V-containing heterodimers. *J Biol Chem* **277**, 24835-41.

Krishnan, A., Verma, S. K., Mani, P., Gupta, R., Kundu, S., and Sarkar, D. P. (2009): A histidine switch in hemagglutinin-neuraminidase triggers paramyxovirus-cell membrane fusion. *J Virol* **83**, 1727-41.

Krusat, T., and Streckert, H. J. (1997): Heparin-dependent attachment of respiratory syncytial virus (RSV) to host cells. *Arch Virol* **142**, 1247-54.

Kuiken, T., van den Hoogen, B. G., van Riel, D. A., Laman, J. D., van Amerongen, G., Sprong, L., Fouchier, R. A., and Osterhaus, A. D. (2004): Experimental human metapneumovirus infection of cynomolgus macaques (Macaca fascicularis) results in virus replication in ciliated epithelial cells and pneumocytes with associated lesions throughout the respiratory tract. *Am J Pathol* **164**, 1893-900.

Lamb, R. A. (1993): Paramyxovirus fusion: a hypothesis for changes. *Virology* **197**, 1-11.

Lamb, R. A., and Jardetzky, T. S. (2007): Structural basis of viral invasion: lessons from paramyxovirus F. *Curr Opin Struct Biol* **17**, 427-36.

Lamb, R. A., Parks, G.D. (2007): *Paramyxoviridae*: The viruses and their replication., pp. 1449-1646. In D. M. Knipe, P.M. Howley (Ed.): *Fields Virology, 5th edition*, Lippincott Williams & Wilkins, Philadelphia, PA.

Lamb, R. A., Paterson, R. G., and Jardetzky, T. S. (2006): Paramyxovirus membrane fusion: lessons from the F and HN atomic structures. *Virology* **344**, 30-7.

Larcher, C., Geltner, C., Fischer, H., Nachbaur, D., Muller, L. C., and Huemer, H. P. (2005): Human metapneumovirus infection in lung transplant recipients: clinical presentation and epidemiology. *J Heart Lung Transplant* **24**, 1891-901.

Lee, J. K., Prussia, A., Paal, T., White, L. K., Snyder, J. P., and Plemper, R. K. (2008): Functional interaction between paramyxovirus fusion and attachment proteins. *J Biol Chem* **283**, 16561-72.

Liu, L., Bastien, N., and Li, Y. (2007): Intracellular processing, glycosylation, and cell surface expression of human metapneumovirus attachment glycoprotein. *J Virol* **81**, 13435-43.

Liu, Y., Nusrat, A., Schnell, F. J., Reaves, T. A., Walsh, S., Pochet, M., and Parkos, C. A. (2000): Human junction adhesion molecule regulates tight junction resealing in epithelia. *J Cell Sci* **113 (Pt 13)**, 2363-74.

Livak, K. J., and Schmittgen, T. D. (2001): Analysis of relative gene expression data using real-time quantitative PCR and the 2(-Delta Delta C(T)) Method. *Methods* **25**, 402-8.

Loughlin, G. M., and Moscona, A. (2006): The cell biology of acute childhood respiratory disease: therapeutic implications. *Pediatr Clin North Am* **53**, 929-59, ix-x.

Macia, E., Ehrlich, M., Massol, R., Boucrot, E., Brunner, C., and Kirchhausen, T. (2006): Dynasore, a cell-permeable inhibitor of dynamin. *Dev Cell* **10**, 839-50.

Mackay, I. M., Bialasiewicz, S., Jacob, K. C., McQueen, E., Arden, K. E., Nissen, M. D., and Sloots, T. P. (2006): Genetic diversity of human metapneumovirus over 4 consecutive years in Australia. *J Infect Dis* **193**, 1630-3.

Madhi, S. A., Ludewick, H., Abed, Y., Klugman, K. P., and Boivin, G. (2003): Human metapneumovirus-associated lower respiratory tract infections among hospitalized human immunodeficiency virus type 1 (HIV-1)-infected and HIV-1-uninfected African infants. *Clin Infect Dis* **37**, 1705-10.

Mahon, P. J., Mirza, A. M., and Iorio, R. M. (2011): Role of the Two Sialic Acid Binding Sites on the Newcastle Disease Virus HN Protein in Triggering the Interaction with the F Protein Required for the Promotion of Fusion. *J Virol* **85**, 12079-82.

Markwell, M. A., Portner, A., and Schwartz, A. L. (1985): An alternative route of infection for viruses: entry by means of the asialoglycoprotein receptor of a Sendai virus mutant lacking its attachment protein. *Proc Natl Acad Sci U S A* **82**, 978-82.

Mas, V., Herfst, S., Osterhaus, A. D., Fouchier, R. A., and Melero, J. A. (2011): Residues of the human metapneumovirus fusion (F) protein critical for its strain-related fusion phenotype: implications for the virus replication cycle. *J Virol* **85**, 12650-61.

McAdam, A. J., Hasenbein, M. E., Feldman, H. A., Cole, S. E., Offermann, J. T., Riley, A. M., and Lieu, T. A. (2004): Human metapneumovirus in children tested at a tertiary-care hospital. *J Infect Dis* **190**, 20-6.

McGinnes, L. W., and Morrison, T. G. (2006): Inhibition of receptor binding stabilizes Newcastle disease virus HN and F protein-containing complexes. *J Virol* **80**, 2894-903.

McMahon, H. T., and Gallop, J. L. (2005): Membrane curvature and mechanisms of dynamic cell membrane remodelling. *Nature* **438**, 590-6.

Melanson, V. R., and Iorio, R. M. (2004): Amino acid substitutions in the F-specific domain in the stalk of the newcastle disease virus HN protein modulate fusion and interfere with its interaction with the F protein. *J Virol* **78**, 13053-61.

Melanson, V. R., and Iorio, R. M. (2006): Addition of N-glycans in the stalk of the Newcastle disease virus HN protein blocks its interaction with the F protein and prevents fusion. *J Virol* **80**, 623-33.

Miller, S. A., Tollefson, S., Crowe, J. E., Jr., Williams, J. V., and Wright, D. W. (2007): Examination of a fusogenic hexameric core from human metapneumovirus and

identification of a potent synthetic peptide inhibitor from the heptad repeat 1 region. *J Virol* **81**, 141-9.

Miyauchi, K., Kim, Y., Latinovic, O., Morozov, V., and Melikyan, G. B. (2009): HIV enters cells via endocytosis and dynamin-dependent fusion with endosomes. *Cell* **137**, 433-44.

Morgan, C., and Howe, C. (1968): Structure and development of viruses as observed in the electron microscope. IX. Entry of parainfluenza I (Sendai) virus. *J Virol* **2**, 1122-32.

Moscona, A. (2005): Entry of parainfluenza virus into cells as a target for interrupting childhood respiratory disease. *J Clin Invest* **115**, 1688-98.

Mullins, J. A., Erdman, D. D., Weinberg, G. A., Edwards, K., Hall, C. B., Walker, F. J., Iwane, M., and Anderson, L. J. (2004): Human metapneumovirus infection among children hospitalized with acute respiratory illness. *Emerg Infect Dis* **10**, 700-5.

Murakami, M., Towatari, T., Ohuchi, M., Shiota, M., Akao, M., Okumura, Y., Parry, M. A., and Kido, H. (2001): Mini-plasmin found in the epithelial cells of bronchioles triggers infection by broad-spectrum influenza A viruses and Sendai virus. *Eur J Biochem* **268**, 2847-55.

Navaratnarajah, C. K., Leonard, V. H., and Cattaneo, R. (2009): Measles virus glycoprotein complex assembly, receptor attachment, and cell entry. *Curr Top Microbiol Immunol* **329**, 59-76.

Negrete, O. A., Levroney, E. L., Aguilar, H. C., Bertolotti-Ciarlet, A., Nazarian, R., Tajyar, S., and Lee, B. (2005): EphrinB2 is the entry receptor for Nipah virus, an emergent deadly paramyxovirus. *Nature* **436**, 401-5.

Ohi, M., Li, Y., Cheng, Y., and Walz, T. (2004): Negative Staining and Image Classification - Powerful Tools in Modern Electron Microscopy. *Biol Proced Online* **6**, 23-34.

Paterson, R. G., Russell, C. J., and Lamb, R. A. (2000): Fusion protein of the paramyxovirus SV5: destabilizing and stabilizing mutants of fusion activation. *Virology* **270**, 17-30.

Pedroso de Lima, M. C., Ramalho-Santos, J., Martins, M. F., Pato de Carvalho, A., Bairos, V., and Nir, S. (1992): Kinetic modeling of Sendai virus fusion with PC-12 cells. Effect of pH and temperature on fusion and viral inactivation. *Eur J Biochem* **205**, 181-6.

Peiris, J. S., Tang, W. H., Chan, K. H., Khong, P. L., Guan, Y., Lau, Y. L., and Chiu, S. S. (2003): Children with respiratory disease associated with metapneumovirus in Hong Kong. *Emerg Infect Dis* **9**, 628-33.

Pelkmans, L., Fava, E., Grabner, H., Hannus, M., Habermann, B., Krausz, E., and Zerial, M. (2005): Genome-wide analysis of human kinases in clathrin- and caveolae/raft-mediated endocytosis. *Nature* **436**, 78-86.

Pelletier, G., Dery, P., Abed, Y., and Boivin, G. (2002): Respiratory tract reinfections by the new human Metapneumovirus in an immunocompromised child. *Emerg Infect Dis* **8**, 976-8.

Pfaffl, M. W. (2001): A new mathematical model for relative quantification in real-time RT-PCR. *Nucleic Acids Res* **29**, e45.

Pilewski, J. M., Latoche, J. D., Arcasoy, S. M., and Albelda, S. M. (1997): Expression of integrin cell adhesion receptors during human airway epithelial repair in vivo. *Am J Physiol* **273**, L256-63.

Plemper, R. K., Hammond, A. L., Gerlier, D., Fielding, A. K., and Cattaneo, R. (2002): Strength of envelope protein interaction modulates cytopathicity of measles virus. *J Virol* **76**, 5051-61.

Porotto, M., Fornabaio, M., Kellogg, G. E., and Moscona, A. (2007): A second receptor binding site on human parainfluenza virus type 3 hemagglutinin-neuraminidase contributes to activation of the fusion mechanism. *J Virol* **81**, 3216-28.

Porotto, M., Murrell, M., Greengard, O., and Moscona, A. (2003): Triggering of human parainfluenza virus 3 fusion protein (F) by the hemagglutinin-neuraminidase (HN) protein: an HN mutation diminishes the rate of F activation and fusion. *J Virol* **77**, 3647-54.

Pulli, T., Koivunen, E., and Hyypia, T. (1997): Cell-surface interactions of echovirus 22. *J Biol Chem* **272**, 21176-80.

Puri, A., Grimaldi, S., and Blumenthal, R. (1992): Role of viral envelope sialic acid in membrane fusion mediated by the vesicular stomatitis virus envelope glycoprotein. *Biochemistry* **31**, 10108-13.

Raymond, T., Gorbunova, E., Gavrilovskaya, I. N., and Mackow, E. R. (2005): Pathogenic hantaviruses bind plexin-semaphorin-integrin domains present at the apex of inactive, bent alphavbeta3 integrin conformers. *Proc Natl Acad Sci U S A* **102**, 1163-8.

Razinkov, V., Gazumyan, A., Nikitenko, A., Ellestad, G., and Krishnamurthy, G. (2001): RFI-641 inhibits entry of respiratory syncytial virus via interactions with fusion protein. *Chem Biol* **8**, 645-59.

Retta, S. F., Cassara, G., D'Amato, M., Alessandro, R., Pellegrino, M., Degani, S., De Leo, G., Silengo, L., and Tarone, G. (2001): Cross talk between beta(1) and alpha(V) integrins: beta(1) affects beta(3) mRNA stability. *Mol Biol Cell* **12**, 3126-38.

Roche, S., Albertini, A. A., Lepault, J., Bressanelli, S., and Gaudin, Y. (2008): Structures of vesicular stomatitis virus glycoprotein: membrane fusion revisited. *Cell Mol Life Sci* **65**, 1716-28.

Roger, P., Puchelle, E., Bajolet-Laudinat, O., Tournier, J. M., Debordeaux, C., Plotkowski, M. C., Cohen, J. H., Sheppard, D., and de Bentzmann, S. (1999): Fibronectin and alpha5beta1 integrin mediate binding of Pseudomonas aeruginosa to repairing airway epithelium. *Eur Respir J* **13**, 1301-9.

Rucker, P., Wieninger, S. A., Matthias Ullmann, G., and Sticht, H. (2012): Ph-dependent molecular dynamics of vesicular stomatitis virus glycoprotein G. *Proteins* **80**, 2601-13.

Russell, C. J., Jardetzky, T. S., and Lamb, R. A. (2001): Membrane fusion machines of paramyxoviruses: capture of intermediates of fusion. *EMBO J* **20**, 4024-34.

Russell, C. J., Kantor, K. L., Jardetzky, T. S., and Lamb, R. A. (2003): A dual-functional paramyxovirus F protein regulatory switch segment: activation and membrane fusion. *J Cell Biol* **163**, 363-74.

Ryder, A. B., Tollefson, S. J., Podsiad, A. B., Johnson, J. E., and Williams, J. V. (2010): Soluble recombinant human metapneumovirus G protein is immunogenic but not protective. *Vaccine* **28**, 4145-52.

Santangelo, P. J., Lifland, A. W., Curt, P., Sasaki, Y., Bassell, G. J., Lindquist, M. E., and Crowe, J. E., Jr. (2009): Single molecule-sensitive probes for imaging RNA in live cells. *Nat Methods* **6**, 347-9.

Schildgen, V., van den Hoogen, B., Fouchier, R., Tripp, R. A., Alvarez, R., Manoha, C., Williams, J., and Schildgen, O. (2011): Human Metapneumovirus: lessons learned over the first decade. *Clin Microbiol Rev* **24**, 734-54.

Schlender, J., Zimmer, G., Herrler, G., and Conzelmann, K. K. (2003): Respiratory syncytial virus (RSV) fusion protein subunit F2, not attachment protein G, determines the specificity of RSV infection. *J Virol* **77**, 4609-16.

Schowalter, R. M., Chang, A., Robach, J. G., Buchholz, U. J., and Dutch, R. E. (2009): Low-pH triggering of human metapneumovirus fusion: essential residues and importance in entry. *J Virol* **83**, 1511-22.

Schowalter, R. M., Smith, S. E., and Dutch, R. E. (2006): Characterization of human metapneumovirus F protein-promoted membrane fusion: critical roles for proteolytic processing and low pH. *J Virol* **80**, 10931-41.

Scott, C. C., and Gruenberg, J. (2010): Ion flux and the function of endosomes and lysosomes: pH is just the start: the flux of ions across endosomal membranes influences endosome function not only through regulation of the luminal pH. *Bioessays* **33**, 103-10.

Shaikh, F. Y., Cox, R. G., Lifland, A. W., Hotard, A. L., Williams, J. V., Moore, M. L., Santangelo, P. J., and Crowe, J. E., Jr. (2012): A critical phenylalanine residue in the respiratory syncytial virus fusion protein cytoplasmic tail mediates assembly of internal viral proteins into viral filaments and particles. *MBio* **3**.

Sheppard, D. (2003): Functions of pulmonary epithelial integrins: from development to disease. *Physiol Rev* **83**, 673-86.

Shirogane, Y., Takeda, M., Iwasaki, M., Ishiguro, N., Takeuchi, H., Nakatsu, Y., Tahara, M., Kikuta, H., and Yanagi, Y. (2008): Efficient multiplication of human metapneumovirus in Vero cells expressing the transmembrane serine protease TMPRSS2. *J Virol* **82**, 8942-6.

Smith, E. C., Popa, A., Chang, A., Masante, C., and Dutch, R. E. (2009): Viral entry mechanisms: the increasing diversity of paramyxovirus entry. *FEBS J* **276**, 7217-27.

Srinivasakumar, N., Ogra, P. L., and Flanagan, T. D. (1991): Characteristics of fusion of respiratory syncytial virus with HEp-2 cells as measured by R18 fluorescence dequenching assay. *J Virol* **65**, 4063-9.

Stewart, P. L., and Nemerow, G. R. (2007): Cell integrins: commonly used receptors for diverse viral pathogens. *Trends Microbiol* **15**, 500-7.

Summerford, C., Bartlett, J. S., and Samulski, R. J. (1999): AlphaVbeta5 integrin: a co-receptor for adeno-associated virus type 2 infection. *Nat Med* **5**, 78-82.

Superti, F., Seganti, L., Ruggeri, F. M., Tinari, A., Donelli, G., and Orsi, N. (1987): Entry pathway of vesicular stomatitis virus into different host cells. *J Gen Virol* **68 (Pt 2)**, 387-99.

Swanson, K. A., Settembre, E. C., Shaw, C. A., Dey, A. K., Rappuoli, R., Mandl, C. W., Dormitzer, P. R., and Carfi, A. (2011): Structural basis for immunization with postfusion respiratory syncytial virus fusion F glycoprotein (RSV F) to elicit high neutralizing antibody titers. *Proc Natl Acad Sci U S A* **108**, 9619-24.

Takimoto, T., Taylor, G. L., Connaris, H. C., Crennell, S. J., and Portner, A. (2002): Role of the hemagglutinin-neuraminidase protein in the mechanism of paramyxovirus-cell membrane fusion. *J Virol* **76**, 13028-33.

Tanabayashi, K., and Compans, R. W. (1996): Functional interaction of paramyxovirus glycoproteins: identification of a domain in Sendai virus HN which promotes cell fusion. *J Virol* **70**, 6112-8.

Tatsuo, H., Ono, N., Tanaka, K., and Yanagi, Y. (2000): SLAM (CDw150) is a cellular receptor for measles virus. *Nature* **406**, 893-7.

Techaarpornkul, S., Barretto, N., and Peeples, M. E. (2001): Functional analysis of recombinant respiratory syncytial virus deletion mutants lacking the small hydrophobic and/or attachment glycoprotein gene. *J Virol* **75**, 6825-34.

Techaarpornkul, S., Collins, P. L., and Peeples, M. E. (2002): Respiratory syncytial virus with the fusion protein as its only viral glycoprotein is less dependent on cellular glycosaminoglycans for attachment than complete virus. *Virology* **294**, 296-304.

Teng, M. N., Whitehead, S. S., and Collins, P. L. (2001): Contribution of the respiratory syncytial virus G glycoprotein and its secreted and membrane-bound forms to virus replication in vitro and in vivo. *Virology* **289**, 283-96.

Thammawat, S., Sadlon, T. A., Hallsworth, P. G., and Gordon, D. L. (2008): Role of cellular glycosaminoglycans and charged regions of viral G protein in human metapneumovirus infection. *J Virol* **82**, 11767-74.

Tio, P. H., Jong, W. W., and Cardosa, M. J. (2005): Two dimensional VOPBA reveals laminin receptor (LAMR1) interaction with dengue virus serotypes 1, 2 and 3. *Virol J* **2**, 25.

Tollefson, S. J., Cox, R. G., and Williams, J. V. (2010): Studies of culture conditions and environmental stability of human metapneumovirus. *Virus Res* **151**, 54-9.

Tsurudome, M., Kawano, M., Yuasa, T., Tabata, N., Nishio, M., Komada, H., and Ito, Y. (1995): Identification of regions on the hemagglutinin-neuraminidase protein of human parainfluenza virus type 2 important for promoting cell fusion. *Virology* **213**, 190-203.

Ulbrandt, N. D., Ji, H., Patel, N. K., Riggs, J. M., Brewah, Y. A., Ready, S., Donacki, N. E., Folliot, K., Barnes, A. S., Senthil, K., Wilson, S., Chen, M., Clarke, L., MacPhail, M., Li, J., Woods, R. M., Coelingh, K., Reed, J. L., McCarthy, M. P., Pfarr, D. S., Osterhaus, A. D., Fouchier, R. A., Kiener, P. A., and Suzich, J. A. (2006): Isolation and characterization of monoclonal antibodies which neutralize human metapneumovirus in vitro and in vivo. *J Virol* **80**, 7799-806.

van den Hoogen, B. G., Bestebroer, T. M., Osterhaus, A. D., and Fouchier, R. A. (2002): Analysis of the genomic sequence of a human metapneumovirus. *Virology* **295**, 119-32.

van den Hoogen, B. G., de Jong, J. C., Groen, J., Kuiken, T., de Groot, R., Fouchier, R. A., and Osterhaus, A. D. (2001): A newly discovered human pneumovirus isolated from young children with respiratory tract disease. *Nat Med* **7**, 719-24.

van den Hoogen, B. G., Herfst, S., Sprong, L., Cane, P. A., Forleo-Neto, E., de Swart, R. L., Osterhaus, A. D., and Fouchier, R. A. (2004): Antigenic and genetic variability of human metapneumoviruses. *Emerg Infect Dis* **10**, 658-66.

van den Hoogen, B. G., van Doornum, G. J., Fockens, J. C., Cornelissen, J. J., Beyer, W. E., de Groot, R., Osterhaus, A. D., and Fouchier, R. A. (2003): Prevalence and clinical

symptoms of human metapneumovirus infection in hospitalized patients. *J Infect Dis* **188**, 1571-7.

Vicente, D., Montes, M., Cilla, G., and Perez-Trallero, E. (2004): Human metapneumovirus and chronic obstructive pulmonary disease. *Emerg Infect Dis* **10**, 1338-9.

Villar, E., and Barroso, I. M. (2006): Role of sialic acid-containing molecules in paramyxovirus entry into the host cell: a minireview. *Glycoconj J* **23**, 5-17.

Wang, F. Z., Akula, S. M., Sharma-Walia, N., Zeng, L., and Chandran, B. (2003): Human herpesvirus 8 envelope glycoprotein B mediates cell adhesion via its RGD sequence. *J Virol* **77**, 3131-47.

Wang, L. H., Rothberg, K. G., and Anderson, R. G. (1993): Mis-assembly of clathrin lattices on endosomes reveals a regulatory switch for coated pit formation. *J Cell Biol* **123**, 1107-17.

Wang, X., and Bergelson, J. M. (1999): Coxsackievirus and adenovirus receptor cytoplasmic and transmembrane domains are not essential for coxsackievirus and adenovirus infection. *J Virol* **73**, 2559-62.

Wang, Z., Mirza, A. M., Li, J., Mahon, P. J., and Iorio, R. M. (2004): An oligosaccharide at the C-terminus of the F-specific domain in the stalk of the human parainfluenza virus 3 hemagglutinin-neuraminidase modulates fusion. *Virus Res* **99**, 177-85.

Wei, Y., Feng, K., Yao, X., Cai, H., Li, J., Mirza, A. M., and Iorio, R. M. (2012): Localization of a region in the fusion (F) protein of avian metapneumovirus that modulates cell-cell fusion. *J Virol* **86**, 11800-14.

Weinacker, A., Ferrando, R., Elliott, M., Hogg, J., Balmes, J., and Sheppard, D. (1995): Distribution of integrins alpha v beta 6 and alpha 9 beta 1 and their known ligands, fibronectin and tenascin, in human airways. *Am J Respir Cell Mol Biol* **12**, 547-56.

Wen, X., Krause, J. C., Leser, G. P., Cox, R. G., Lamb, R. A., Williams, J. V., Crowe, J. E., Jr., and Jardetzky, T. S. (2012): Structure of the human metapneumovirus fusion protein with neutralizing antibody identifies a pneumovirus antigenic site. *Nat Struct Mol Biol* **19**, 461-3.

Whitman, S. D., and Dutch, R. E. (2007): Surface density of the Hendra G protein modulates Hendra F protein-promoted membrane fusion: role for Hendra G protein trafficking and degradation. *Virology* **363**, 419-29.

Wickham, T. J., Mathias, P., Cheresh, D. A., and Nemerow, G. R. (1993): Integrins alpha v beta 3 and alpha v beta 5 promote adenovirus internalization but not virus attachment. *Cell* **73**, 309-19.

Widjojoatmodjo, M. N., Boes, J., van Bers, M., van Remmerden, Y., Roholl, P. J., and Luytjes, W. (2010): A highly attenuated recombinant human respiratory syncytial virus lacking the G protein induces long-lasting protection in cotton rats. *Virol J* **7**, 114.

Wild, T. F., Malvoisin, E., and Buckland, R. (1991): Measles virus: both the haemagglutinin and fusion glycoproteins are required for fusion. *J Gen Virol* **72 (Pt 2)**, 439-42.

Wilen, C. B., Tilton, J. C., and Doms, R. W. (2012): Molecular mechanisms of HIV entry. *Adv Exp Med Biol* **726**, 223-42.

Williams, C. H., Kajander, T., Hyypia, T., Jackson, T., Sheppard, D., and Stanway, G. (2004a): Integrin alpha v beta 6 is an RGD-dependent receptor for coxsackievirus A9. *J Virol* **78**, 6967-73.

Williams, J. V. (2005): Human Metapneumovirus: An Important Cause of Respiratory Disease in Children and Adults. *Curr Infect Dis Rep* **7**, 204-210.

Williams, J. V., Chen, Z., Cseke, G., Wright, D. W., Keefer, C. J., Tollefson, S. J., Hessell, A., Podsiad, A., Shepherd, B. E., Sanna, P. P., Burton, D. R., Crowe, J. E., Jr., and Williamson, R. A. (2007): A recombinant human monoclonal antibody to human metapneumovirus fusion protein that neutralizes virus in vitro and is effective therapeutically in vivo. *J Virol* **81**, 8315-24.

Williams, J. V., Crowe, J. E., Jr., Enriquez, R., Minton, P., Peebles, R. S., Jr., Hamilton, R. G., Higgins, S., Griffin, M., and Hartert, T. V. (2005a): Human metapneumovirus infection plays an etiologic role in acute asthma exacerbations requiring hospitalization in adults. *J Infect Dis* **192**, 1149-53.

Williams, J. V., Harris, P. A., Tollefson, S. J., Halburnt-Rush, L. L., Pingsterhaus, J. M., Edwards, K. M., Wright, P. F., and Crowe, J. E., Jr. (2004b): Human metapneumovirus and lower respiratory tract disease in otherwise healthy infants and children. *N Engl J Med* **350**, 443-50.

Williams, J. V., Tollefson, S. J., Johnson, J. E., and Crowe, J. E., Jr. (2005b): The cotton rat (Sigmodon hispidus) is a permissive small animal model of human metapneumovirus infection, pathogenesis, and protective immunity. *J Virol* **79**, 10944-51.

Williams, J. V., Wang, C. K., Yang, C. F., Tollefson, S. J., House, F. S., Heck, J. M., Chu, M., Brown, J. B., Lintao, L. D., Quinto, J. D., Chu, D., Spaete, R. R., Edwards, K. M., Wright, P. F., and Crowe, J. E., Jr. (2006): The role of human metapneumovirus in upper respiratory tract infections in children: a 20-year experience. *J Infect Dis* **193**, 387-95.

Wilson, I. A., Skehel, J. J., and Wiley, D. C. (1981): Structure of the haemagglutinin membrane glycoprotein of influenza virus at 3 A resolution. *Nature* **289**, 366-73.

Yanagi, Y. (2001): The cellular receptor for measles virus--elusive no more. *Rev Med Virol* **11**, 149-56.

Yang, C. F., Wang, C. K., Tollefson, S. J., Piyaratna, R., Lintao, L. D., Chu, M., Liem, A., Mark, M., Spaete, R. R., Crowe, J. E., Jr., and Williams, J. V. (2009): Genetic diversity and evolution of human metapneumovirus fusion protein over twenty years. *Virol J* **6**, 138.

Yao, Q., Hu, X., and Compans, R. W. (1997): Association of the parainfluenza virus fusion and hemagglutinin-neuraminidase glycoproteins on cell surfaces. *J Virol* **71**, 650-6.

Yin, H. S., Wen, X., Paterson, R. G., Lamb, R. A., and Jardetzky, T. S. (2006): Structure of the parainfluenza virus 5 F protein in its metastable, prefusion conformation. *Nature* **439**, 38-44.